University of Vermont
ScholarWorks @ UVM

Graduate College Dissertations and Theses | Dissertations and Theses

2015

Lidar Remote Sensing Of Forest Canopy Structure: An Assessment Of The Accuracy Of Lidar And Its Relationship To Higher Trophic Levels

Christopher Felix Hansen
University of Vermont

Follow this and additional works at: https://scholarworks.uvm.edu/graddis

Part of the Ecology and Evolutionary Biology Commons, Forest Sciences Commons, and the Natural Resources Management and Policy Commons

Recommended Citation
Hansen, Christopher Felix, "Lidar Remote Sensing Of Forest Canopy Structure: An Assessment Of The Accuracy Of Lidar And Its Relationship To Higher Trophic Levels" (2015). *Graduate College Dissertations and Theses*. 356.
https://scholarworks.uvm.edu/graddis/356

This Thesis is brought to you for free and open access by the Dissertations and Theses at ScholarWorks @ UVM. It has been accepted for inclusion in Graduate College Dissertations and Theses by an authorized administrator of ScholarWorks @ UVM. For more information, please contact donna.omalley@uvm.edu.

LIDAR REMOTE SENSING OF FOREST CANOPY STRUCTURE: AN ASSESSMENT OF THE ACCURACY OF LIDAR AND ITS RELATIONSHIP TO HIGHER TROPHIC LEVELS

A Thesis Presented

by

Christopher F. Hansen

to

The Faculty of the Graduate College

of

The University of Vermont

In Partial Fulfillment of the Requirements
for the Degree of Master of Science
Specializing in Natural Resources

May, 2015

Defense Date: December 12, 2014
Thesis Examination Committee:

Allan M. Strong, Ph.D., Advisor
Paul G. Schaberg, Ph.D., Co-Advisor
Shelly A. Rayback, Ph.D., Chairperson
Cynthia J. Forehand, Ph.D., Dean of the Graduate College

ABSTRACT

Light detection and ranging (LiDAR) data can provide detailed information about three-dimensional forest horizontal and vertical structure that is important to forest productivity and wildlife habitat. Indeed, LiDAR data have been shown to provide accurate estimates to forest structural parameters and measures of higher trophic levels (e.g., avian abundance and diversity). However, links between forest structure and tree function have not been evaluated using LiDAR. This study was designed and scaled to assess the relationship of LiDAR to multiple aspects of forest structure and higher trophic levels (arthropod and bird populations), which included the ground-based collection of percent crown and understory closure, as well as arthropod and avian abundance and diversity data. Additional plot-based measures were added to assess the relationship of LiDAR to forest health and productivity. High-resolution discrete-return LiDAR data (flown summer of 2009) were acquired for the Hubbard Brook Experimental Forest (HBEF) in New Hampshire, USA. LiDAR data were classified into four canopy structural categories: 1) high crown and high understory closure, 2) high crown and low understory closure, 3) low crown and high understory closure, and 4) low crown and low understory closure. Nearby plots from each of the four LiDAR categories were grouped into "blocks" to assess the spatial consistency of data. Ground-based measures of forest canopy structure, site, stand and individual tree measures were collected on nine 50 m-plots from each LiDAR category (36 plots total), during summer of 2012. Analysis of variance was used to assess the relationships between LiDAR and a suite of tree function measures. Our results show the novel ability of LiDAR to assess forest health and productivity at the stand and individual tree level. We found significant correspondence between LiDAR categories and our ground-based measures of tree function, including xylem increment growth, foliar nutrition, crown health, and stand mortality. Furthermore, we found consistent reductions in xylem increment growth, decreases in foliar nutrition and crown health, and increases in stand mortality related to high understory closure. This suggests that LiDAR measures can reflect competitive interactions, not just among overstory trees for light, but also interactions between overstory trees and understory vegetation for resources other than light (e.g., nutrients). High-resolution LiDAR data show promise in the assessment of forest health and productivity related to tree function.

Keywords: northern hardwood forest, tree function, active remote sensing, forest canopy structure

ACKNOWLEDGEMENTS

This research was supported through funds provided by the Northeastern States Research Cooperative (NSRC) and the USDA CSREES McIntire-Stennis Forest Research Program. I am grateful to all of those who provided technical assistance in the lab and in the field. They include, Sean MacFaden, Josh Halman, Paula Murakami, Ben Engel, Dan Hale, Gary Hawley, Ali Kosiba, Kindle Loomis, Allison Middleman, Allyson Makuch, Jarlath O'Neil-Dunne, Nick Rodenhouse, and Helen Yurchenco. I thank my committee members, Paul Schaberg, Allan Strong, and Shelly Rayback for their support and mentorship throughout this process. Finally, this research could not have been completed without assistance from the staff of the Hubbard Brook Experimental Forest, New Hampshire, USA - in particular Ian Halm.

TABLE OF CONTENTS

Page

LIST OF TABLES

Table Page

LIST OF FIGURES

Figure Page

CHAPTER 1. LITERATURE REVIEW

1.1. Introduction to light detection and ranging (LiDAR)

Light detection and ranging (LiDAR) is a remote sensing technique in which near-infrared laser pulses are emitted from a sensor on a fixed-wing aircraft. Based on the timing and intensity of the return signal and in conjunction with an inertial navigation system (INS), as well as a GPS fixed to the aircraft and referenced to another ground GPS, location data about canopy/vegetation vertical structure (including canopy height and ground elevation) can be determined with great accuracy (Schmid et al. 2008). LiDAR has the ability to create three-dimensional elevation surfaces, as well as record return signal intensity and therefore, can be utilized as a spatial and spectral segmentation tool (Antonarakis et al. 2008).

LiDAR instruments are able to produce greater than 150,000 laser pulses per second and record up to five return signals per pulse. The resulting product is a densely spaced and highly accurate collection of georeferenced elevation points, called point clouds (Schmid et al. 2008). Each point within a point cloud represents an individual return with a unique intensity value. Point clouds can be converted to digital elevation models (DEM), digital surface models (DSM), and canopy height models/normalized digital surface models (CHM/nDSM) for further analysis (Wehr and Lohr 1999, Lim et al. 2003, Evans et al. 2009, Swatantran et al. 2012).

LiDAR is classified into two types: discrete return and full waveform LiDAR. Both types record the timing and intensity of the return signal back to the sensor and the exact three-dimensional location of each point (X, Y, and Z coordinates). Discrete

return LiDAR records only individual (discrete) signal returns, whereas full waveform LiDAR records the entire outgoing and return signal (Lefsky et al. 2002, Evans et al. 2009). Advantages of discrete return LiDAR are its ability to record multiple returns at smaller footprint sizes. The circular sampling area created from the beam divergence from the LiDAR sensor is referred to as the footprint size (Lim et al. 2003). Most discrete return LiDAR footprint sizes now range from 20 to 80 cm in size, which is useful in studies where information on individual plots or even individual trees is desired. By contrast, full waveform LiDAR records the entire waveform over larger areas (large footprint sizes varying from 3 to 8 m and up to 70 m) (Lim et al. 2003, Evans et al. 2009). File sizes are much larger with waveform LiDAR due to the recording of the entire return signal and are therefore, more difficult to work with. Also, although waveform LiDAR may capture the full vertical profile better than discrete return LiDAR (Lim et al. 2003), it does not map three-dimensional vertical structure as accurately as discrete return LiDAR due to its larger footprint sizes and lower resolution (Lefsky et al. 2002). Swatantran et al. (2012) found that, although waveform LiDAR was not as accurate in representing vertical structure, it was more accurate in estimating canopy top elevation than discrete return LiDAR. Despite underestimating canopy top elevation, discrete return LiDAR was more accurate in estimations of ground elevation – so both types have utility Swatantran et al. (2012).

Studies involving mapping and classification of vegetation structure have traditionally been limited in the extent of the area assessed due to the costly and time-consuming nature of fieldwork. In addition, more traditional remotely sensed data has had the limitation of providing little or no information about canopy/vegetation vertical

structure. LiDAR is able to map vegetation structure three dimensionally, as well as record spectral intensity at landscape scales at relatively low costs compared to conventional remote sensing techniques (Lefsky et al. 2002, Schmid et al. 2008, Sherrill et al. 2008).

Three dimensional spatial patterns of vegetation have been shown to be important in ecological studies, especially those pertaining to wildlife habitat (MacArthur and MacArthur 1961). Until recently, conventional remote sensing has only been able to map forests in two dimensions (Lefsky et al. 2002). Recently, forest and wildlife habitat studies have used LiDAR to assess basic structural attributes such as canopy height, canopy cover and vertical profiles from which indirect measures (e.g., biomass, timber volume, basal area, crown closure, leaf area index, species diversity, etc.) have been derived (Lefsky et al. 2002, Jensen et al. 2008, Næsset and Gobakken 2008, Hollaus et al. 2009, Goetz et al. 2010, Swatantran et al. 2011).

Due to its ability to accurately depict forest canopy height, and potentially forest canopy structure and complexity, LiDAR has quickly become an indispensable tool for estimating forest-based metrics. Indices derived from LiDAR data have been demonstrated by many studies to be highly correlated with *in situ* measures of forest-height variables, biomass, basal area, and forest age (Lefsky et al. 2002, Lefsky et al. 2005, Hudak et al. 2006, Sherrill et al. 2008, Falkowski et al. 2009). Descriptors derived from LiDAR are now commonly used in a variety of forest-based applications, including forest inventory analyses (Gatziolis 2009, 2012), carbon stock estimation (Stephens et al. 2007, Asner 2009, Dubayah et al. 2010, Asner et al. 2012), and wildlife habitat modeling (Hyde et al. 2006, Goetz et al. 2010). LiDAR data have also been correlated to estimates

of forest vertical structure such as Leaf Area Index (LAI) (Sherrill et al. 2008). Surprisingly, few studies have assessed high resolution LiDAR estimates of forest canopy structure in deciduous hardwood forests and applications to higher trophic levels and/or biodiversity.

Coarse-scale resolution LiDAR data have been used to estimate forest canopy structure and complexity in deciduous hardwood forests and relate these to at least one important indicator of biodiversity: bird species richness (Goetz et al. 2007, Goetz et al. 2010). The use of high resolution LiDAR-derived data for habitat analyses and estimates of biodiversity have currently not been evaluated and might provide essential improvements to existing LiDAR-based models. In addition, relating LiDAR data to crown features that are significant components of forest health and productivity (e.g., crown vigor and dieback, and mechanical damage) is uncommon but shows promise (Leckie et al. 2003, Solberg et al. 2006). Lastly, the relationship between LiDAR estimates of forest structure and complexity, and arthropod abundance and diversity is nearly absent in the literature, despite being an important link between primary producers (i.e., trees) and secondary consumers (i.e., birds). Arthropod abundance and diversity has been shown to be directly influenced by forest canopy structure (Halaj et al. 2000, Jeffries et al. 2006) and indirectly influenced by forest canopy gaps via light availability, soil/leaf litter moisture, and foliar nutrition (Shure and Phillips 1991, Goßner 2009). As such, arthropod measures are important indicators of biodiversity that may potentially be assessed via LiDAR data.

1.2. Forest-based applications

Basal area, stand density and biomass estimation

The basic measurements made by LiDAR sensors are directly related to vegetation structure and function, and therefore, can be used in the estimation of many forest-based metrics (Lefsky et al. 2002). During the last decade, accurate estimates of basal area, stand density, biomass, and timber volume have all been obtained from LiDAR data. The direct retrieval of canopy height variables from LiDAR data has made this possible (Lim et al. 2003).

For example, Hudak et al. (2006) found that LiDAR had better utility in predicting basal area than other multispectral and remotely sensed data. They also noted that LiDAR canopy height and canopy cover variables were most useful in predicting basal area and tree density, respectively.

In addition, biomass estimates have been made with both waveform and discrete return LiDAR laser systems to varying degrees of success and in combination with other remotely sensed data. Using discrete return LiDAR, Næsset and Gobakken (2008) found that LiDAR metrics explained 88% of the variability of above ground estimates of biomass in boreal forests of Norway. Swatantran et al. (2011) found similar results in estimation of biomass using waveform LiDAR in the Sierra Nevada, with the exception of their estimates being refined by the fusion of hyperspectral data with LiDAR data. It is expected that with the attainment of higher spatial resolution LiDAR data, the accuracies of basal area, stand density, and biomass estimates (as well as other forest metrics) will only increase with time (Gatziolis and Andersen 2008).

Canopy/foliage density measures

Leaf area Index (LAI) has been defined as the total one-sided area of leaf tissue per unit ground surface area (Bréda 2003). Leaf area index is a key component of biogeochemical cycles in ecosystems by driving within- and below-canopy microclimate, determining and controlling canopy water interception, radiation extinction, and water and carbon gas exchange (Bréda 2003). Accurate measures of LAI have typically been difficult to quantify due to large spatial and temporal variability (Bréda 2003, Richardson et al. 2009). Conventional remote sensing techniques have partially solved the issues of spatial and temporal variability, but still show inaccuracies in high biomass ecosystems (Jensen et al. 2008). LiDAR has shown great promise in the estimation of LAI, as well as other crown density measures (e.g., dieback and mechanical damage and defoliation), while accounting for the spatial and temporal variability and inaccuracies of ground based and conventional remotely sensed LAI estimations (Reutebuch et al. 2005, Richardson et al. 2009).

LiDAR-based estimates of LAI have been obtained through various methods and models. In the context of insect defoliation on Scots pine (*Pinus sylvestris* L.), Solberg et al. (2006) compared laser pulse penetration through the canopy with stand density based on position and height of individual trees to obtain actual and expected LAI. Richardson et al. (2009) used a model-based approach (based on the Beer-Lambert Law – an equation relating the absorption of light to the properties of the material it is travelling through) to obtain LAI and found high correlations between LiDAR-based LAI estimates with LAI derived from hemispherical photography.

Succession, forest gaps, and object-oriented classification

Few studies have utilized LiDAR in evaluating forest gaps and subsequent forest succession. The heterogeneity of forests has made the utilization of LiDAR for gap analysis particularly difficult in the northeastern part of the United States. The few studies that have utilized LiDAR have taken place in the western United States in more homogeneous forests. These studies have focused on object-oriented classification with the inclusion of other remotely sensed data and GIS layers to identify polygons of varying gap sizes/successional stages (St-Onge and Vepakomma 2004, Pascual et al. 2008). Object-oriented classification (as opposed to pixel-based classification) is not a new technique, however. With increasing spatial resolution of remotely sensed data, object-oriented classification has become a more useful and powerful tool than the classification of pixels at coarser spatial scales (Blaschke 2010). Even with object-oriented classification, the majority of studies have focused on classifying land cover (forest and ground types), not forest gaps and successional stages (Antonarakis et al. 2008).

A recent study by Falkowski et al. (2009) is an example of LiDAR-based analysis of forest succession/gaps that does not use object-oriented classifiers. In this study, six categories of forest successional stages were classified using LiDAR-derived metrics in conjunction with an algorithmic modeling procedure (Random Forest algorithm), which obtained overall accuracies of higher than 90%. Random Forest algorithms have been show to be the most robust and flexible imputation methods in the simultaneous prediction of multiple response variables, while using predictor variables derived from LiDAR data (Hudak et al. 2008). LiDAR data, used in conjunction with Random Forest

algorithms, have also been utilized in studies predicting basal area and tree density (Hudak et al. 2008), as well as the prevalence of bird species (Swatantran et al. 2012).

1.3. Wildlife applications

Three dimensional spatial patterns and vertical structure of vegetation have been shown to be important for bird habitat (MacArthur and MacArthur 1961), and therefore, LiDAR-based metrics that predict bird presence/absence are similar, if not the same, as those used for classification of forest successional stages. A ground breaking study by MacArthur and MacArthur (1961) showed that the diversity of songbirds was positively associated with the vertical distribution of vegetation within forests. The utilization of LiDAR in wildlife studies is contingent on its ability to assess this vertical distribution, as well as the horizontal distribution of vegetation (Goetz et al. 2007, Clawges et al. 2008, Goetz et al. 2010, Swatantran et al. 2012).

Many LiDAR-based wildlife studies have focused on birds and have used LiDAR structural indices to predict species diversity (Clawges et al. 2008), species prevalence (Swatantran et al. 2012), and species richness (Goetz et al. 2007, Lesak et al. 2011). Breeding habitat of individual bird species has also been predicted using LiDAR-derived structural indices (Bradbury et al. 2005, Goetz et al. 2010). In addition, important forest structural features such as snags (and other coarse woody debris) and large residual trees have been mapped with LiDAR, and used as indicators of habitat quality for certain species (Pesonen et al. 2008, Martinuzzi et al. 2009, García-Feced et al. 2011).

The utilization of LiDAR to assess forest structure in relation to bird species and their habitat requirements is common in the literature. However, LiDAR is also utilized

in other ecosystem assessments, including the examination of mammalian habitat. For example, the Delmarva fox squirrel (*Sciurus niger cinereus*) in Delaware (Nelson et al. 2005). LiDAR has also been used to discriminate cluster zones of massive stony coral colonies on patch reefs of northern Florida, although this type of LiDAR differs from most of the above by being blue-green wavelength LiDAR (as opposed to near infrared) due to its application in or around water and not vegetation (Brock et al. 2006).

Finally, LiDAR has been used to assess arthropod abundance and diversity; however, it is uncommon in the literature despite being an important link between forest structure and higher trophic levels. For example, Müller and Brandl (2009) showed strong relationships between LiDAR variables of canopy height and forest beetle assemblages in the Bavarian Forest National Park in Germany. Similarly, Vierling et al. (2011), found strong predictive power of LiDAR variables in assessing spider distributions, also in the Bavarian Forest National Park in Germany. Arthropods are dependent on the form and associated function of forest systems, and therefore should be related to LiDAR variables. Further assessments of individual species and arthropod assembleges may provide further insight into the utility of LiDAR.

1.4. Data processing, software and deliverables of discrete return LiDAR

LiDAR data is most widely packaged in the .LAS file format, which contains both three-dimensional spatial and spectral intensity information. Once acquired, typical operations performed on LiDAR point cloud data include: visualization (which includes single point selection, measurements, primitive fitting, and generating cross sections), segmentation, classification, filtering, transformation (including rotations, cropping,

merging, and georeferencing), gridding, and mathematical operations (Fernandez et al. 2007).

There are many point cloud processing software packages available for the manipulation of LiDAR data, each of which has associated advantages and limitations. They include: Quick Terrain Modeler, Terrasolid Suite, MARS, Innovmetric Polyworks, Fledermaus, Matlab, LViz, and Surfer to name a few. Quick Terrain (QT) Modeler is the software package that will be used for this project. Originally developed by John Hopkins University's Applied Physics Lab, QT Modeler is capable of handling any LiDAR-generated dataset, as well as other three dimensional datasets such as those generated by Synthetic Aperture Radar (SAR). QT modeler has proven to be one of the best visualization software packages for LiDAR point cloud data (Fernandez et al. 2007).

As with other remotely sensed data (e.g., Landsat), LiDAR data are divided into five levels of processing (Evans et al. 2009). The first level (level zero) is the raw sensor data. It is of no interest to the vast majority of users, but should be archived for the development and testing of such things as GPS corrections. Level one processing consists of corrections performed by the vendor, including: geometric correction, sensor corrections, tiling, and converting to the appropriate data format (i.e., .LAS). Level two processing consists of products derived from basic post-processing procedures, which include classifying ground returns, digital elevation models (DEM), digital surface models (DSM), intensity information, and point height information. Level three processing derives products that are tailored for specific applications. These products - such as canopy height, canopy density, and stratified canopy density - are based on transformations, ratios, and simple calculations. Level four processing involves variables

from previous processing levels and is used for specific modeling applications such as stand density, basal area, and biomass estimates (Lim et al. 2003, Chen 2007, Schmid et al. 2008, Evans et al. 2009)

1.5. Conclusions

The literature described above illustrates LiDAR's ability to quantify forest-based measures directly (e.g., canopy height) and indirectly (e.g., basal area, LAI, etc.) and therefore, its ability to answer broader ecological questions related to forest structure and function and related wildlife. Previous research on LiDAR and forest structure has identified significant relationships between predicted LiDAR-based forest vertical structure and ground-based measures of forest vertical structure (Zimble et al. 2003, van Leeuwen and Nieuwenhuis 2010, Jones et al. 2011, Van Ewjik et al. 2011), as well as predicted LiDAR forest canopy gaps and ground-based assessments of forest canopy gaps (Koukoulas and Blackburn 2004, St-Onge and Vepakomma 2004, Gaulton and Malthus 2010, Van Ewjik et al. 2011). In addition, previous research has identified significant relationships between LiDAR-based forest vertical structure and forest canopy gap variables with bird prevalence and habitat (Goetz et al. 2007, Goetz et al. 2010, Swatantran et al. 2012), as well as bird species richness (Goetz et al. 2007, Lesak et al. 2011). Despite these promising results, connections between LiDAR metrics of forest vertical structure and forest canopy gaps and trophic level interactions have not been fully evaluated. The next chapter (and appendices) of this thesis describes a new study to further evaluate the potential utility of LiDAR data for identifying patterns of forest structure relevant to tree health and productivity and higher trophic levels.

1.6. References

Antonarakis, A. S., K. S. Richards, and J. Brasington. 2008. Object-based land cover classification using airborne LiDAR. Remote Sensing of Environment **112**:2988-2998.

Asner, G. P. 2009. Tropical forest carbon assessment: integrating satellite and airborne mapping approaches. Environmental Research Letters **4**:034009.

Asner, G. P., J. Mascaro, H. C. Muller-Landau, G. Vieilledent, R. Vaudry, M. Rasamoelina, J. S. Hall, and M. van Breugel. 2012. A universal airborne LiDAR approach for tropical forest carbon mapping. Oecologia **168**:1147-1160.

Blaschke, T. 2010. Object based image analysis for remote sensing. ISPRS Journal of Photogrammetry and Remote Sensing **65**:2-16.

Bradbury, R. B., R. A. Hill, D. C. Mason, S. A. Hinsley, J. D. Wilson, H. Balzter, G. Q. A. Anderson, M. J. Whittingham, I. J. Davenport, and P. E. Bellamy. 2005. Modelling relationships between birds and vegetation structure using airborne LiDAR data: a review with case studies from agricultural and woodland environments. Ibis **147**:443-452.

Bréda, N. J. J. 2003. Ground−based measurements of leaf area index: a review of methods, instruments and current controversies. Journal of Experimental Botany **54**:2403-2417.

Brock, J. C., C. W. Wright, I. B. Kuffner, R. Hernandez, and P. Thompson. 2006. Airborne lidar sensing of massive stony coral colonies on patch reefs in the northern Florida reef tract. Remote Sensing of Environment **104**:31-42.

Chen, Q. 2007. Airborne LiDAR data processing and information extraction. Photogrammetric Engineering and Remote Sensing **73**:91-95.

Clawges, R., K. Vierling, L. Vierling, and E. Rowell. 2008. The use of airborne lidar to assess avian species diversity, density, and occurrence in a pine/aspen forest. Remote Sensing of Environment **112**:2064-2073.

Dubayah, R., S. Sheldon, D. Clark, M. Hofton, J. Blair, G. Hurtt, and R. Chazdon. 2010. Estimation of tropical forest height and biomass dynamics using lidar remote sensing at La Selva, Costa Rica. Journal of Geophysical Research: Biogeosciences (2005–2012) **115**.

Evans, J., A. Hudak, R. Faux, and A. M. Smith. 2009. Discrete Return Lidar in Natural Resources: Recommendations for Project Planning, Data Processing, and Deliverables. Remote Sensing **1**:776-794.

Falkowski, M. J., J. S. Evans, S. Martinuzzi, P. E. Gessler, and A. T. Hudak. 2009. Characterizing forest succession with lidar data: An evaluation for the Inland Northwest, USA. Remote Sensing of Environment **113**:946-956.

Fernandez, J. C., S. A., J. Caceres, K. C. Slatton, M. Starek, and R. Kumar. 2007. An Overview of LiDAR Point Cloud Processing Software. Pages 1-27, Geosensing Engineering and Mapping (GEM), Civil and Coastal Engineering Department, University of Florida.

García-Feced, C., D. J. Tempel, and M. Kelly. 2011. LiDAR as a Tool to Characterize Wildlife Habitat: California Spotted Owl Nesting Habitat as an Example. Journal of Forestry **109**:436-443.

Gatziolis, D. 2009. Precise FIA plot registration using field and dense LIDAR data. Pages 243-249 Proceedings of the eigth annual forest inventory and analysis symposium. United States Dept. of Agriculture, Forest Service General Technical Report WO-79, Washington, D.C.

Gatziolis, D. 2012. Advancements in LiDAR-based registration of FIA field plots. Pages 432-437. United States Dept. of Agriculture, Forest Service General Technical Report NRS-P-105, Washington, D.C.

Gatziolis, D. and H.-E. Andersen. 2008. A Guide to LiDAR Data Acquisition and Processing for the Forests of the Pacific Northwest. Pages 1-32 *in* U. F. Service, editor. USDA Forest Service, Pacific Northwest Research Station.

Gaulton, R. and T. J. Malthus. 2010. LiDAR mapping of canopy gaps in continuous cover forests: A comparison of canopy height model and point cloud based techniques. International Journal of Remote Sensing **31**:1193-1211.

Goetz, S., D. Steinberg, R. Dubayah, and B. Blair. 2007. Laser remote sensing of canopy habitat heterogeneity as a predictor of bird species richness in an eastern temperate forest, USA. Remote Sensing of Environment **108**:254-263.

Goetz, S. J., D. Steinberg, M. G. Betts, R. T. Holmes, P. J. Doran, R. Dubayah, and M. Hofton. 2010. Lidar remote sensing variables predict breeding habitat of a Neotropical migrant bird. Ecology **91**:1569-1576.

Goßner, M. M. 2009. Light intensity affects spatial distribution of Heteroptera in deciduous forests. European Journal of Entomology **106**:241-252.

Halaj, J., D. W. Ross, and A. R. Moldenke. 2000. Importance of habitat structure to the arthropod food−web in Douglas−fir canopies. Oikos **90**:139-152.

Hollaus, M., W. Wagner, K. Schadauer, B. Maier, and K. Gabler. 2009. Growing stock estimation for alpine forests in Austria: a robust lidar-based approach. Canadian Journal of Forest Research **39**:1387-1400.

Hudak, A. T., N. L. Crookston, J. S. Evans, M. J. Falkowski, A. M. S. Smith, P. E. Gessler, and P. Morgan. 2006. Regression modeling and mapping of coniferous forest basal area and tree density from discrete-return lidar and multispectral satellite data. Canadian Journal of Remote Sensing **32**:126-138.

Hyde, P., R. Dubayah, W. Walker, J. B. Blair, M. Hofton, and C. Hunsaker. 2006. Mapping forest structure for wildlife habitat analysis using multi-sensor (LiDAR, SAR/InSAR, ETM+, Quickbird) synergy. Remote Sensing of Environment **102**:63-73.

Jeffries, J. M., R. J. Marquis, and R. E. Forkner. 2006. Forest age influences oak insect herbivore community structure, richness, and density. Ecological Applications **16**:901-912.

Jensen, J. L. R., K. S. Humes, L. A. Vierling, and A. T. Hudak. 2008. Discrete return lidar-based prediction of leaf area index in two conifer forests. Remote Sensing of Environment **112**:3947-3957.

Jones, T. G., N. C. Coops, and T. Sharma. 2011. Assessing the utility of LiDAR to differentiate among vegetation structural classes. Remote Sensing Letters **3**:231-238.

Koukoulas, S. and G. A. Blackburn. 2004. Quantifying the spatial properties of forest canopy gaps using LiDAR imagery and GIS. International Journal of Remote Sensing **25**:3049-3072.

Leckie, D., F. Gougeon, D. Hill, R. Quinn, L. Armstrong, and R. Shreenan. 2003. Combined high-density lidar and multispectral imagery for individual tree crown analysis. Canadian Journal of Remote Sensing **29**:633-649.

Lefsky, M., D. Turner, M. Guzy, and W. Cohen. 2005. Combining lidar estimates of aboveground biomass and Landsat estimates of stand age for spatially extensive validation of modeled forest productivity. Remote Sensing of Environment **95**:549-558.

Lefsky, M. A., W. B. Cohen, G. G. Parker, and D. J. Harding. 2002. Lidar Remote Sensing for Ecosystem Studies. BioScience **52**:19-30.

Lesak, A. A., V. C. Radeloff, T. J. Hawbaker, A. M. Pidgeon, T. Gobakken, and K. Contrucci. 2011. Modeling forest songbird species richness using LiDAR-derived measures of forest structure. Remote Sensing of Environment **115**:2823-2835.

Lim, K., P. Treitz, M. Wulder, B. St-Onge, and M. Flood. 2003. LiDAR remote sensing of forest structure. Progress in Physical Geography **27**:88-106.

MacArthur, R. H. and J. W. MacArthur. 1961. On Bird Species Diversity. Ecology **42**:594-598.

Martinuzzi, S., L. A. Vierling, W. A. Gould, M. J. Falkowski, J. S. Evans, A. T. Hudak, and K. T. Vierling. 2009. Mapping snags and understory shrubs for a LiDAR-based assessment of wildlife habitat suitability. Remote Sensing of Environment **113**:2533-2546.

Næsset, E. and T. Gobakken. 2008. Estimation of above- and below-ground biomass across regions of the boreal forest zone using airborne laser. Remote Sensing of Environment **112**:3079-3090.

Nelson, R., C. Keller, and M. Ratnaswamy. 2005. Locating and estimating the extent of Delmarva fox squirrel habitat using an airborne LiDAR profiler. Remote Sensing of Environment **96**:292-301.

Pascual, C., A. García-Abril, L. G. García-Montero, S. Martín-Fernández, and W. B. Cohen. 2008. Object-based semi-automatic approach for forest structure characterization using lidar data in heterogeneous Pinus sylvestris stands. Forest Ecology and Management **255**:3677-3685.

Pesonen, A., M. Maltamo, K. Eerikäinen, and P. Packalèn. 2008. Airborne laser scanning-based prediction of coarse woody debris volumes in a conservation area. Forest Ecology and Management **255**:3288-3296.

Reutebuch, S. E., H.-E. Andersen, and R. J. McGaughey. 2005. Light Detection and Ranging (LIDAR): An Emerging Tool for Multiple Resource Inventory. Journal of Forestry **103**:286-292.

Richardson, J. J., L. M. Moskal, and S.-H. Kim. 2009. Modeling approaches to estimate effective leaf area index from aerial discrete-return LIDAR. Agricultural and Forest Meteorology **149**:1152-1160.

Schmid, K., K. Waters, B. Dingerson, R. M. Hadley, J. Carter, J. Dare, and N. C. S. Center. 2008. LiDAR 101: an introduction to LiDAR technology, data, and applications. Charleston, SC: NOAA Coastal Services Center.

Sherrill, K. R., M. A. Lefsky, J. B. Bradford, and M. G. Ryan. 2008. Forest structure estimation and pattern exploration from discrete-return lidar in subalpine forests of the central Rockies. Canadian Journal of Forest Research **38**:2081-2096.

Shure, D. and D. Phillips. 1991. Patch size of forest openings and arthropod populations. Oecologia **86**:325-334.

Solberg, S., E. Næsset, K. H. Hanssen, and E. Christiansen. 2006. Mapping defoliation during a severe insect attack on Scots pine using airborne laser scanning. Remote Sensing of Environment **102**:364-376.

St-Onge, B. and U. Vepakomma. 2004. Assessing Forest Gap Dynamics and Growth Using Multi-temporal Laser Scanner Data. International Archives of Photogrammetry, Remote Sensing and Spatial Information Sciences **36**:173-178.

Stephens, P., P. Watt, D. Loubser, A. Haywood, and M. Kimberley. 2007. Estimation of carbon stocks in New Zealand planted forests using airborne scanning LiDAR. Pages 389-394 *in* ISPRS Workshop on Laser Scanning 2007 and SilviLaser 2007. Citeseer.

Swatantran, A., R. Dubayah, S. Goetz, M. Hofton, M. G. Betts, M. Sun, M. Simard, and R. Holmes. 2012. Mapping Migratory Bird Prevalence Using Remote Sensing Data Fusion. PLoS ONE **7**:e28922.

Swatantran, A., R. Dubayah, D. Roberts, M. Hofton, and J. B. Blair. 2011. Mapping biomass and stress in the Sierra Nevada using lidar and hyperspectral data fusion. Remote Sensing of Environment **115**:2917-2930.

Van Ewjik, K. Y., P. M. Treitz, and N. A. Scott. 2011. Characterizing forest succession in Central Ontario using LiDAR-derived indices. Photogrammetric Engineering and Remote Sensing **77**:261-269.

van Leeuwen, M. and M. Nieuwenhuis. 2010. Retrieval of forest structural parameters using LiDAR remote sensing. European Journal of Forest Research **129**:749-770.

Wehr, A. and U. Lohr. 1999. Airborne laser scanning—an introduction and overview. ISPRS Journal of Photogrammetry and Remote Sensing **54**:68-82.

Zimble, D. A., D. L. Evans, G. C. Carlson, R. C. Parker, S. C. Grado, and P. D. Gerard. 2003. Characterizing vertical forest structure using small-footprint airborne LiDAR. Remote Sensing of Environment **87**:171-182.

CHAPTER 2. LIDAR REMOTE SENSING OF FOREST HEALTH & PRODUCTIVITY

2.1. Abstract

Light detection and ranging (LiDAR) data can provide detailed information about three-dimensional forest horizontal and vertical structure that is important to forest productivity and wildlife habitat. Indeed, LiDAR data have been shown to provide accurate estimates to forest structural parameters and measures of higher trophic levels (e.g., avian abundance and diversity). However, links between forest structure and tree function have not been evaluated using LiDAR. This study was designed and scaled to assess the relationship of LiDAR to multiple aspects of forest structure and higher trophic levels (arthropod and bird populations). Additional plot-based measures were added to assess the relationship of LiDAR to forest health and productivity. High-resolution discrete-return LiDAR data (flown summer of 2009) were acquired for the Hubbard Brook Experimental Forest (HBEF) in New Hampshire, USA. LiDAR data were classified into four canopy structural categories: 1) high crown and high understory closure, 2) high crown and low understory closure, 3) low crown and high understory closure, and 4) low crown and low understory closure. Nearby plots from each of the four LiDAR categories were grouped into "blocks" to assess the spatial consistency of data. Ground-based measures of forest canopy structure, site, stand and individual tree measures were collected on nine 50 m-plots from each LiDAR category (36 plots total), during summer of 2012. Analysis of variance was used to assess the relationships between LiDAR and a suite of tree function measures. Our results show the novel ability

of LiDAR to assess forest health and productivity at the stand and individual tree level. We found significant correspondence between LiDAR categories and our ground-based measures of tree function, including xylem increment growth, foliar nutrition, crown health, and stand mortality. Furthermore, we found consistent reductions in xylem increment growth, decreases in foliar nutrition and crown health, and increases in stand mortality related to high understory closure. This suggests that LiDAR measures can reflect competitive interactions, not just among overstory trees for light, but also interactions between overstory trees and understory vegetation for resources other than light (e.g., nutrients). High-resolution LiDAR data show promise in the assessment of forest health and productivity related to tree function.

Keywords: northern hardwood forest, tree function, active remote sensing, forest canopy structure

2.2. Introduction

Managers and biologists must develop cost-effective techniques to evaluate fundamental habitat features (e.g., forest three-dimensional structure and complexity, and forest canopy closure) that influence forest health and productivity, especially in the face of global climate change that may alter the structure and function of forest systems. Light detection and ranging (LiDAR) remote sensing, is a relatively new technique that may have value toward evaluating such features. LiDAR is an active remote sensing technique in which near-infrared laser pulses are emitted from a sensor, conventionally mounted on a fixed-wing aircraft, and more recently onboard satellites (van Leeuwen and Nieuwenhuis 2010). LiDAR technology in combination with an inertial navigation system (INS), an aircraft-mounted global positioning system (GPS), and referenced to a ground GPS, can be used to determine forest canopy/vegetation vertical structure (in addition to and in conjunction with ground elevation and canopy height) with great accuracy (Schmid et al. 2008).

Studies involving the mapping and classification of vegetation structure have traditionally been limited in the areal extent assessed due to costly and time-consuming nature of fieldwork. In addition, more traditional (i.e., passive) remotely sensed data provide little or no information about canopy/vegetation three-dimensional vertical structure (Lefsky et al. 2002, Koukoulas and Blackburn 2004). LiDAR is able to map vegetation structure in three dimensions as well as record spectral intensity at landscape scales at relatively low costs compared to conventional remote sensing techniques (Lefsky et al. 2002, Schmid et al. 2008, Sherrill et al. 2008).

Three dimensional spatial patterns of vegetation (i.e., forest canopy vertical structure and canopy gaps) have been shown to be important in ecological studies, especially those pertaining to arthropod (Halaj et al. 2000, Jeffries et al. 2006) and avian (MacArthur and MacArthur 1961, Roth 1976, Robinson and Holmes 1982, 1984, DeGraaf et al. 1998, Whelan 2001, Smith et al. 2008) habitat. Until recently, conventional remote sensing systems have only been able to map forests in two dimensions (Lefsky et al. 2002, Koukoulas and Blackburn 2004). Now LiDAR is being employed in forest and wildlife habitat studies to assess basic structural attributes (e.g., canopy height, canopy cover, vertical profiles and gap size and structure) from which indirect measures (e.g., biomass, timber volume, basal area, crown closure, leaf area index, species diversity, etc.) have been derived (Lefsky et al. 2002, Koukoulas and Blackburn 2004, Jensen et al. 2008, Næsset and Gobakken 2008, Hollaus et al. 2009, Goetz et al. 2010, Swatantran et al. 2011).

Several studies have used LiDAR to assess forest structural attributes, however, comparisons were made using coarse-resolution LiDAR (Hofton et al. 2002, Hudak et al. 2002, Hyde et al. 2005). In addition, few studies have provided assessments of the relationship between LiDAR and broad measures of forest stocking and higher trophic levels (Goetz et al. 2007, Goetz et al. 2010, Swatantran et al. 2012). High-resolution LiDAR data may be a useful tool for making comparisons of forest canopy structure (vertical and horizontal) and canopy gaps to both biotic (e.g., abundance and diversity of arthropods and avifauna and tree/forest health and productivity) and abiotic (e.g., microsite soil moisture, temperature and humidity) factors.

Our research had two objectives: 1) to assess the accuracy of high-resolution discrete return LiDAR in quantifying forest structure, and 2) to determine the relationship of high-resolution LiDAR to higher trophic levels, in particular arthropod and avian abundance and diversity. Our study was designed and scaled based on these objectives. In addition, plot-based measures were included to assess something quite novel - the relationship of LiDAR to tree health and productivity. The analyses presented here focus on the relationship of LiDAR to forest health and productivity, with a particular emphasis on measures of tree function. Just as LiDAR measures of tree structure have been shown to be relevant to dependent arthropod and avian populations, we hypothesize that LiDAR can quantify forest structural characteristics that are either the cause of tree health and productivity issues (e.g., slow growth due to overcrowding) or their consequence (e.g., elevated crown thinning or tree mortality). The resulting analysis provides the first evaluation of high-resolution LiDAR data as an indicator of forest structure and the health and productivity of individual trees and forest plots.

2.3. Materials and methods

2.3.1. Study site description

Research was conducted at the Hubbard Brook Experimental Forest (HBEF) in New Hampshire, USA (43°56′N, 71°45′W; Figure 1). The HBEF is part of the Long Term Ecological Research Network (LTER) of research sites across North America, and is located in the White Mountain National Forest. It is the longest continuous ecosystem study in the United States and consists of 3,160 Hectares of National Forest land (Schwarz et al. 2001, Swatantran et al. 2012). The HBEF is an east-west oriented basin

with predominately north-facing and south-facing aspects. Elevations at HBEF range from 222 to 1015 m. HBEF is dominated by spruce-northern hardwood forests (composed primarily of sugar maple [*Acer saccharum* Marsh.], American beech [*Fagus grandifolia* Ehrh.], yellow birch [*Betula alleghaniensis* Britton], and red spruce [*Picea rubens* Sarg.]) in the lower elevations and spruce-fir-birch forests (red spruce, balsam fir [*Abies balsamea* L. Mill.], and paper birch [*Betula papyrifera* Marsh.]) at elevations above 750 m (Schwarz et al. 2003). The HBEF is a structurally diverse forest with individual stands in widely different seral stages of successional development (Schwarz et al. 2001), making it an ideal location to study LiDAR's utility in assessing tree function.

2.3.2. LiDAR processing and field plot selection

High-resolution discrete return LiDAR data (flown leaf-on, September 1, 2009) were acquired for HBEF. These data were originally collected by the Canaan Valley Institute, West Virginia, for the University of Maryland, Department of Geography using an Optech ALTM 3100 flown at an altitude of approximately 1,065 meters above ground level. This instrument emits up to 100,000 near-infrared laser pulses per second with at least one laser pulse per square meter and up to four vertical returns. It has a positional accuracy within 15 cm in the vertical axis. Collection parameters included a pulse rate frequency of 100 kHz, scan frequency of 30 Hz, and a scan angle of 18°.

These data were received in raw (.LAS 1.0) format with no associated deliverables (i.e., were not processed into surface models). Using Quick Terrain Modeler (Applied Imagery, Inc., Silver Spring, MD, USA) and ERDAS Imagine (Intergraph

Corporation, Inc., Madison, AL, USA), LiDAR data were processed into a normalized digital surface model (nDSM) to represent canopy height, a digital elevation model (DEM) to represent ground elevation, and a 0.5 – 10 m aboveground level (AGL) surface model to represent the presence or absence of vegetation within the canopy's understory vertical plane (Figure 1).

LiDAR-derived surface models were used in conjunction with pre-existing geospatial vector data (acquired from the HBEF data archives) to identify areas of deciduous and mixed deciduous forest types within an elevation threshold of roughly 400 – 800 m. A 200 m x 200 m grid was placed over the resultant area to represent potential 4 ha sampling blocks. This block size was chosen because it approximated the territory size of black-throated blue warblers (*Setophaga caerulescens*) (Holmes et al. 2005), as one component of the study was to relate LiDAR data to avian habitat. Un-adjustable variations in LiDAR data involving the overlap of adjacent flight lines necessitated the conversion of raw LiDAR point clouds into surface models from which canopy and understory closure categories were created. Through the use of eCognition (an object-oriented segmentation software – Trimble Geospatial, Inc., Westminster, CO, USA), the LiDAR-derived surface models were processed to identify two understory closure categories (high understory closure > 55% and low understory closure ≤ 55% vegetation closure in the 0.5 – 10 meter AGL class) and two crown closure categories (high crown closure > 94% and low crown closure ≤ 94%). Canopy and understory categories were operationally defined to create breakpoints that divided the forests assessed into two equal-sized groups per canopy strata. Plots locations were selected based on the distribution and combinations of these categories within the potential sampling blocks.

This resulted in a total of four combinations of understory and crown closure categories: 1) high crown closure and high understory closure, 2) high crown closure and low understory closure, 3) low crown closure and high understory closure, and 4) low crown closure and low understory closure (Figure 1). Locations were selected for inclusion in the study using a "blocked" design, with each of the four LiDAR categories in relatively close proximity to each other to account for any spatial clustering of parameters that might affect response variables evaluated in this study.

Using the distribution of understory and crown closure categories within the potential sampling blocks, nine replicates (i.e., blocks) of the four combined understory and crown closure categories were established throughout HBEF for a total of 36, 50 m fixed radius plots. Following the protocol of the Forest Inventory and Analysis (FIA) program, each plot consisted of four, 7.32 m radius sub-plots, one located at plot center, and three located 36.6 m from plot center at azimuths 360°, 120°, and 240° (Bechtold and Scott 2005) (Figure 2).

2.3.3. Field-based data collection

Crown health and mortality

On each subplot, an inventory following FIA protocols (Bechtold and Scott 2005) was conducted on all trees greater than 12.5 cm, with the following information recorded for each tally tree: species, diameter at breast height (DBH: 1.4 m), crown status (i.e., dominant, co-dominant, intermediate, suppressed, or dead), and canopy health. On each FIA micro-plot, an inventory of all trees 2.5 to 12.5 cm DBH was obtained with the same measures as collected for subplots. For plot-level inventories, canopy health was

assessed via crown vigor index and percent branch dieback, which were estimated according to the methods of the North America Maple Project (NAMP; Cooke et al. 1996). Crown vigor index employs a 1-5 scale, where (1) represents highly vigorous crowns with little or no major branch dieback and less than 10% branch or twig mortality, (2) light decline with branch or twig mortality present and between 10 – 25%, (3) moderate decline with 25 – 50% branch and twig mortality, (4) severe decline with > 50% branch and twig mortality, and (5) dead. Percent branch dieback was estimated using a 12-class system (for complete methods, see Cooke et al. 1996). Assessments of crown vigor index and percent branch dieback were performed on each tree by two observers, positioned 180° from each other to account for any potential errors due to observer bias. In addition, basal area (BA) per hectare was calculated on all trees, regardless of crown status, and for standing dead trees using the following formula:

$$\text{Subplot BA } (m^2/ha) = (\Sigma\ (((\pi * DBH/2)^2)/10{,}000))/\ 0.016833$$

where π is 3.14 and 0.016833 is the subplot area in hectares. Measures of BA for living and dead trees were calculated at the plot-level for trees greater than 12.5 cm.

Xylem increment growth

Also at the plot level, five dominant and co-dominant sugar maple and five dominant and co-dominant yellow birch trees were selected for intensive tree-based measures (e.g., xylem increment growth and foliar nutrition assessments) and tagged with a unique identifier. These species were selected as they are two of the three most abundant canopy species that make up the northern hardwood forest at HBEF – American beech being the third and not chosen due to the confounding influence beech bark disease

has had on its health and productivity (Halman et al. 2014). Diameter at breast height (DBH: 1.4 m) was measured and visual assessments of canopy health were obtained for each tree. Dominant and co-dominant sugar maple and yellow birch trees selected for intensive tree-based measures that also occurred on subplots were only counted once in subplot stand inventory summaries.

Two xylem increment cores (180° from one another and perpendicular to the dominant slope) were collected for each of the selected dominant and co-dominant sugar maple and yellow birch trees, to determine tree age and assess annual growth. Xylem increment cores were collected at DBH using a 5 mm increment borer. The methods of Stokes and Smiley (1968) were used to mount, sand, and microscopically measure (using a Velmex sliding stage unit [Velmex Inc., Bloomfield, NY, USA] with MeasureJ2X software [VoorTech Consulting, Holderness, NH, USA]) annual xylem increments to 0.001 mm resolution for each core collected. Increment cores were crossdated visually using the method of Yamaguchi (1991) and corrected for locally absent and false rings using the program COFECHA (Holmes 1983). In addition, dendrochronological statistics (i.e., series inter-correlation, average mean sensitivity, and autocorrelation; Appendix C, Table 16) were obtained from COFECHA on a plot basis and used to calculate the expressed population signal (EPS) based on the equation presented by Wigley et al. (1984). The EPS is a measure of the common variance in a chronology and is dependent on sample size. When EPS values fall below a predetermined value, typically 0.85, the chronology is a less reliable indicator of a stand wide signal (Speer 2010). Values for 2012 (i.e., the year of data collection) were below 0.85 for some of our plots, requiring the use of an EPS value of 0.80. For our dataset (both sugar maple and

yellow birch), the latest date at which EPS values were at or above 0.80 was the year 1950, resulting in each of our chronologies spanning from 1950 - 2012 (Appendix C, Table 16).

Mean annual increment (i.e., mean ring width) was calculated for each individual tree and converted to basal area increment (BAI – a standardized measure of growth relative to basal area) according to the methods of Cook and Kairiukstis (1990) and using the formula:

$$BAI_t = (R^2_t - R^2_{t-1})$$

where R is the tree radius and t is the year of tree-ring formation. In addition to the creation of a chronology spanning from 1950-2012, BAI measurements were evaluated for both sugar maple and yellow birch in relation to the LiDAR data for multiple time periods: mean BAI for 2009 (the year that LiDAR data were acquired), mean BAI for the 1970s (i.e., 1970-1979), 2000-2012, and the change in growth (% Δ BAI) from the 1970s to 2000-2012. Time periods prior to the year of LiDAR acquisition were evaluated to assess the robustness of LiDAR's ability to assess BAI growth. For example, the 1970s were an important turning point in the trajectory of sugar maple BAI growth (Drohan et al. 2002, Duchesne et al. 2002), and was characterized by peak acidic deposition in the northeastern United States prior to amendments to the United States Clean Air Act (Driscoll et al. 2001). The time period 2000-2012 was assessed to evaluate LiDAR's relationship to current BAI growth, post-amendments to the Clean Air Act. LiDAR assessments of overall growth trajectories for both species were evaluated through % Δ BAI growth from the 1970s to 2000-2012. In addition, 1988-1997 (10 years before the 1998 ice

storm - a severe ice storm that damaged tree crowns at HBEF), and 1999-2008 (10 years after the 1998 ice storm and pre-LiDAR acquisition) were evaluated to assess the potential influence of a natural disturbance on LiDAR's ability to assess BAI growth.

Foliar nutrition

Foliar nutrition was assessed by collecting sunlit/upper canopy foliage using shotguns to obtain samples in early August, as is standard for foliar sample collections (Huggett et al. 2007, Comerford et al. 2013). Samples were collected from each of the five dominant and co-dominant sugar maple and yellow birch trees, resulting in 360 foliar samples.

Foliar samples were oven-dried at 55°C for two weeks and ground using a Wiley mill with a 2 mm mesh. Ground foliage was then run through a series of nitric acid and hydrogen peroxide digestions according to the methods of Jones and Case (1990). Cation concentrations – calcium (Ca), aluminum (Al), potassium (K), phosphorous (P), manganese (Mn), and magnesium (Mg) – were measured from the digested foliage using inductively coupled plasma atomic emission spectrometry (ICPAES) (Perkin-Elmer Optima DV 3000; Perkin-Elmer, Norwalk, CT, USA) and expressed as mg/kg. Peach leaf standards from the National Institute of Standards and Technology (SRM 15547) and blanks were processed for analytical comparisons.

2.3.4. Statistical Analyses

Plot means were calculated for all continuous response variables and outlier analyses – to look for any potentially spurious values – and tests for homogeneity of variance (i.e., Bartlett, Levene, etc.) were conducted for all plot-based data. Analysis of variance (ANOVA) was used to test for differences between LiDAR categories among continuous response variables. In addition to LiDAR categories, ANOVA models also included "block" as a source of variation to assess the spatial consistency of response variables. ANOVA models originally included an interaction term (i.e., LiDAR category x block), however, this term was removed due to model failure and lost degrees of freedom (Montgomery 2008). When significant differences among response variable means existed between LiDAR categories, specific differences were assessed using Tukey HSD tests. All analyses were performed using the statistical package JMP (SAS Institute, Inc., Cary, NC), with results being considered significantly different if $P \leq 0.05$, unless otherwise noted.

Ground-based measures consisting of continuous values were statistically analyzed following the methods outlined above. For categorical values (i.e., crown vigor index, and percent branch dieback), data were converted from categorical to continuous values through the calculation of plot means.

Linear relationships among crown health, xylem increment growth, and foliar nutrition, regardless of LiDAR categories, were also assessed using the statistical package R (version 2.15.3; a programming environment for data analysis and graphics © 2013). Finally, differential growth trends for sugar maple and yellow birch, obtained from xylem increment growth (expressed as BAI), were assessed via slope analyses for

the years 1950 to 1980 and 1981 to 2012, regardless of LiDAR categories. These time periods were chosen to capture pre- and post-sugar maple growth decline (Houston 1999, Drohan et al. 2002, Duchesne et al. 2002), and extend to yellow birch growth trends. In addition, these time periods were also pre- and post-amendments to the Clean Air Act (Driscoll et al. 2001). Slope values were obtained for each time period and statistically assessed between species using a student's t-test. Differential growth among individual years and between the two species was assessed using orthogonal contrasts of BAI growth means.

2.4. Results

Crown health and mortality

Significant differences were seen among LiDAR categories for measures of crown vigor index and percent branch dieback. Crown vigor index was significantly different between the high crown and high understory closure category and the high crown and low understory closure category ($P \leq 0.10$), with an overall trend of LiDAR categories with high understory closure having a greater crown vigor index (higher crown vigor index values being indicative of trees in poorer condition) regardless of crown closure (Table 1). Crown vigor index was obtained only on dominant and co-dominant trees with higher ratings indicative of trees in poorer health (Cooke et al. 1996). In addition, percent branch dieback, also obtained only on dominant and co-dominant trees, was significantly different among LiDAR categories, with high crown and high understory closure and low crown and low understory closure categories exhibiting

significantly greater dieback than the high crown and low understory closure category (Table 1).

Standing-dead basal area quantified at the subplot level, was significantly different ($P \leq 0.10$) among the LiDAR categories. Specifically, LiDAR plots with high crown and high understory closure exhibited greater standing-dead basal area than LiDAR plots with high crown and low understory closure (Table 1). Although not significant among all LiDAR categories, the trend was for LiDAR plots with high understory closure to have greater standing-dead basal area, regardless of crown closure.

Xylem increment growth

Measures of BAI were found to be significantly different among LiDAR categories for sugar maple but not yellow birch trees (Table 2). Sugar maple BAI for 2009 was significantly lower in LiDAR plots with high crown and high understory closure as compared to LiDAR plots with low crown and low understory closure. Average sugar maple BAI growth for 2000 – 2012 was significantly lower ($P \leq 0.10$) for trees in the high crown and high understory closure category compared to the high crown and low understory closure category. In addition, an average measure of sugar maple BAI growth for the years 1999 – 2008 (pre-LiDAR acquisition and post-1998 ice storm disturbance), as well as for the years 1988 – 1997 (pre-1998 ice storm disturbance) were both significantly different among LiDAR categories. LiDAR plots with high crown and high understory closure had lower pre- and post-1998 ice storm BAI growth than those with high crown and low understory closure (Table 2).

Pre- and post-disturbance measures were assessed to account for any confounding affects in BAI growth that might be due to the 1998 region-wide ice storm. This ice storm negatively influenced forests throughout northern New York, New England, and southeastern Canada, with heavy ice loading resulting in broken branches and the collapse of trees (Jones and Mulherin 1998, Rhoads et al. 2002). The forests of the HBEF were considerably damaged by the 1998 ice storm (Jones and Mulherin 1998) and significant crown loss resulted in reduced woody growth (Huggett et al. 2007, Halman et al. 2014). BAI growth could differ among LiDAR categories pre- versus post-ice storm depending on localized levels of damage experienced in 1998. Further, differential damage in 1998 could have altered crown and understory canopies and helped create the LiDAR categories that we later evaluated. However, the similarity in LiDAR differences between BAI growth for pre- and post-disturbance indicates that the 1998 ice storm disturbance was not a confounding factor. All other measures of BAI growth, for both sugar maple and yellow birch, were not significantly different among LiDAR categories.

Linear relationships between percent crown dieback and all measures of sugar maple BAI (regardless of LiDAR) were statistically significant and negative ($P \leq 0.005$, R^2 values ranging from 0.33 – 0.48), except for the 1970s. In contrast, no significant relationships were found for linear assessments of percent crown dieback and measures of yellow birch BAI, except for the 1970s, which was statistically significant and negative ($P \leq 0.10$, $R^2 = 0.09$; Table 3). Similar results were found between crown vigor index and BAI for sugar maple and yellow birch (data not shown).

Foliar nutrition

Measures of foliar cations were only significantly different among LiDAR categories for yellow birch. Furthermore, only Ca and the molar ratio of Ca:Al were significant (Table 4); LiDAR categories with high crown and low understory closure exhibited significantly greater foliar Ca than LiDAR categories with high crown and high understory closure and low crown and low understory closure. Additionally, yellow birch in the high crown and low understory closure plots had significantly ($P \leq 0.10$) higher Ca:Al molar ratios than yellow birch in high crown and high understory closure plots. Although not significant for all categories, the general trend was for LiDAR categories with low understory to exhibit greater yellow birch foliar Ca and greater Ca:Al molar ratios.

Relationships between foliar nutrition and changes in BAI over time (1970s – 2000-2012) and foliar nutrition and percent crown dieback for sugar maple and yellow birch were also assessed regardless of their relationship to LiDAR. Relationships between foliar nutrition and sugar maple BAI from the 1970s to 2000-2012 were significant and negative for Mn and significant and positive for the molar ratios Ca:Mn and Mg:Mn ($P \leq 0.05$, R^2 values ranging from 0.14 – 0.21). Measures of yellow birch foliar Ca, Mg, Ca:Mn, Mg:Mn were all significant and negatively associated with changes in yellow birch BAI from the 1970s to 2000-2012 ($P \leq 0.05$, r^2 values ranging from 0.12 – 0.30). Additionally, linear relationships between percent branch dieback and measures of sugar maple foliar Mg, Ca:Mn, and Mg:Mn were significant, and negative and measures of sugar maple foliar Mn were significant and positive ($P \leq 0.05$, R^2 values ranging from 0.11 – 0.29).

2.5. Discussion

LiDAR assessments of forest stand relationships

We found significant differences among LiDAR crown and understory closure categories and measures of crown health: crown vigor index and percent branch dieback (Table 1). For both of these measures, differences were seen between high crown and high understory and high crown and low understory closure groups, with greater vigor and less branch dieback on plots with low understory closure. The remaining LiDAR crown and understory closure categories (i.e., low crown and high understory and low crown and low understory closure) were intermediate to and not significantly different from the other categories for crown vigor. However, the low crown and low understory closure category was significantly different from the high crown and low understory closure category for percent branch dieback.

Similar results were found for measures of subplot standing dead basal area. LiDAR plots with high crown and low understory closure had significantly greater standing dead basal area than LiDAR plots with high crown and low understory closure.

Measures of stand (standing dead basal area, crown vigor index, and percent dieback) health and productivity that were significantly different among LiDAR categories might partially be explained by competition among overstory and understory vegetation for resources other than light availability (e.g., nutrients and water). Our results showed that higher understory closure, as assessed by LiDAR, was associated with greater standing dead basal area, higher crown vigor index (i.e., poorer tree health), and greater percent dieback (Table 1). Competition between canopy and understory vegetation can have a meaningful influence on plant systems (Goff and West 1975,

Woods 1984), although mostly in relation to forest composition and population structure. Indeed, this concept of competitive interactions among overstory and understory vegetation is partially why managers use silvicultural practices such as thinning-from-below (Barnes et al. 1997). However, Marqus and Ernst (1991) showed that thinning-from-below had little significance on overstory productivity, suggesting little competitive interactions for resources other than light – at least in the forest they assessed. Despite this, our results suggest that higher densities of understory vegetation may have increased competition and contributed to the overall poorer health for overstory canopy trees. Further indication of this was evident in our measures of sugar maple BAI. Significant differences in various measures of sugar maple BAI between LiDAR categories suggest that competition between understory and overstory vegetation may be partially responsible for lower mean growth (Table 2).

LiDAR assessments of dendroecological trends in BAI

LiDAR showed utility in differentiating xylem increment growth, particularly certain measures of BAI for sugar maple, but not for yellow birch. The relative uniformity of BAI growth of yellow birch among LiDAR categories was not surprising because the dendrochronological record compiled for this study shows relatively consistent growth for this species over time (Figure 3). However, yellow birch is a species that has experienced demographic shifts at the HBEF, with a seven percent decline in live biomass recently reported and attributed to greater mortality as compared to recruitment of this species (van Doorn et al. 2011). Our plot basal area measurements are in agreement with those of van Doorn et al. (2011); yellow birch had the highest

mean percent basal area on sub-plots (trees > 12.5cm DBH) and the lowest percent basal area on micro-plots (trees 2.5 – 12.5cm DBH) regardless of LiDAR category (Table 6). Despite a lack of recruitment, BAI growth for living trees of this species has been more or less steady for the last 62 years (Figure 3).

In contrast, sugar maple is a species with reports of decline in the northeastern United States since at least the 1980s, most notably attributable to acid deposition and cation leaching (Kolb and McCormick 1993, Houston 1999, Horsley et al. 2000, Schaberg et al. 2006, Huggett et al. 2007, Halman et al. 2014), although insect defoliation (Bauce and Allen 1991, Kolb and McCormick 1993, Houston 1999) and drought (Bernier et al. 1989, Allen et al. 1992) have also been cited as important contributing factors. The dendrochronological record compiled for this study shows a significant decline in BAI growth for this species from the 1980s to the present, with relatively consistent, if not slightly increased growth prior to the 1980s (Figure 3). Increases in live biomass of four percent were reported for this species by van Doorn et al. (2011) at the HBEF. However, their results included estimates of mortality and recruitment, whereas our results consisted only of BAI growth for live dominant and co-dominant trees.

Linear relationships of BAI growth regardless of LiDAR category for this study corroborate previous findings on long-term declines for sugar maple and steady growth for yellow birch. We found greater percent branch dieback to be associated with lower sugar maple BAI growth for all time periods assessed, except for the 1970s. In contrast, no relationships were found between percent branch dieback and yellow birch BAI for any of the time periods assessed, except for the 1970s, which was only significant at $P \leq 0.10$. In the 1970s, sugar maple BAI increased temporarily before a sustained decline in

the 1980s at our site (Figure 3) and the region (Horsley et al. 2000). Synchronous to the short improvement in sugar maple growth, yellow birch growth declined in the 1970s, possibly due to increased competition with sugar maple.

Our dendrochronological record also suggests that some long-term stressor is responsible for the decline of sugar maple BAI observed over the last half-century (Figure 3). Bauce and Allen (1991) studied sugar maple decline in upstate New York and concluded that competition predisposed sugar maple to the adverse effects of other stressors (e.g., base soil cation depletion, soil acidification, insect defoliation, drought, etc.).

LiDAR assessments of foliar nutrition

Foliar cation concentrations for sugar maple were generally in the range considered to be healthy, as published by Kolb and McCormick (1993) (Appendix C, Table 10). Exceptions to this were Al and Mg; Al exhibited higher levels and Mg lower levels than those published by Kolb and McCormick (1993). Al is considered to be a phytotoxic element to which sugar maple is particularly sensitive (Kolb and McCormick 1993, Houston 1999, Horsley et al. 2000, Schaberg et al. 2006, Huggett et al. 2007, Halman et al. 2014). In the absence of base cations (e.g., Ca, Mg, K), due to soil acidification and leaching, Al is mobilized and taken up by sugar maple (Schaberg et al. 2006, Huggett et al. 2007, Comerford et al. 2013, Halman et al. 2014). It was not surprising to observe high levels of Al and low levels of Mg at the HBEF as acidic deposition and base cation depletion have been documented throughout the HBEF for several decades (Likens et al. 1996, Driscoll et al. 2001). Furthermore, Horsley et al.

(2000) found that levels of foliar Mg and Mn, in combination with insect defoliation, were the most important factors associated with sugar maple health in Pennsylvania forests. Measures of foliar Mn collected for this study were all within the ranges reported for healthy sugar maple trees (Kolb and McCormick 1993). In addition, Ca, which is a biologically essential element that influences forest structure and function, has declined in availability and is now at or below threshold levels at the HBEF (Likens et al. 1998, Juice et al. 2006).

Measures of sugar maple foliar Ca concentrations corroborate this for our plots, with LiDAR categories with high crown and high understory closure having Ca levels slightly below healthy levels and all other categories being slightly above healthy levels (overlapping standard errors suggest that all categories are right around threshold levels of 5000 $mg \cdot kg^{-1}$; Table 3). Furthermore, the molar ratios of Ca:Al for sugar maple (not significantly different among LiDAR categories) were well below those that are reported for vigorous trees (Table 3). Long et al. (1997) suggested that anything less than a Ca:Al molar ratio of 110 was indicative of declining sugar maple. Low Ca:Al may have predisposed sugar maple trees to declines in growth after 1980 as seen elsewhere (Horsley et al. 2000, Schaberg et al. 2006, Schaberg et al. 2010). Regression analyses of sugar maple growth over time prior to and after 1980 (Figure 3) show patterns consistent with the possibility that changes in Ca:Al availability influenced growth. Before 1980, sugar maple BAI showed a small but significant increase in growth over time (P = 0.0352). This growth increase coincided with measures of increased Ca availability as acid deposition mobilized soil stores at HBEF (Likens et al. 1996). However, with ongoing acid inputs, soil Ca stores were depleted and Al was mobilized, leading to

reductions in Ca:Al (Likens et al. 1998). Reductions in sugar maple growth after 1980 occurred during this period of declining Ca:Al. After 1988, it was not uncommon for yellow birch (a species thought to be less sensitive to acid deposition-induced cation imbalances) to experience greater growth than sympatric sugar maple (Figure 3). This may provide another example on changing species dynamics associated with acid-induced cation perturbations. Elsewhere at HBEF, American beech (*Fagus grandifolia* Ehrh.) have increased in growth as sugar maple trees have declined due to changing Ca:Al status (Halman et al. 2014). Increased American beech growth and changing species dynamics is reflected in this study, with American beech accounting for 63.1 percent of micro-plot BA (Table 6).

All other foliar cation concentrations for sugar maple were within ranges considered healthy (Kolb and McCormick 1993) (Appendix C, Table 10). To our knowledge, there are no published ranges for healthy foliar cation concentrations for yellow birch. Unlike sugar maple, there is little evidence to suggest that yellow birch is sensitive to soil acidification and base cation leaching.

Our results of the relationship of LiDAR to foliar nutrition (for yellow birch) suggests that canopies with less competition in the understory have greater access to Ca, which can be limiting at HBEF. This further supports the potential for LiDAR to assess competitive interactions between and among canopy trees with understory vegetation. Interestingly, no significant differences among LiDAR categories relative to Ca and the molar ratio of Ca:Al were found for sugar maple, despite the fact that this species is particularly sensitive to Ca and Al perturbations, especially at HBEF (Table 3; Schaberg et al. 2006, Huggett et al. 2007, Schaberg et al. 2010, Halman et al. 2014).

Horsley et al. (2000) concluded that in combination with insect defoliation, levels of foliar Mg and Mn were the most important factors associated with sugar maple health. Results from our linear assessments of foliar nutrition and sugar maple BAI are in agreement with Horsley et al. (2000), with Mn being particularly important (Table 5). However, results from our analysis of LiDAR and sugar maple foliar nutrition were not significant. Overall, our LiDAR results may indicate that, in addition to competition with understory vegetation, greater crown closure and potentially fuller crowns translates to greater transpirational uptake capacity of foliar cations, though this possibility requires more specific testing.

The results presented here illustrate the potential of using high-resolution LiDAR data to assess tree function and associated forest health and productivity. LiDAR has been shown to be a useful tool in assessing basic measures of forest structure, such as canopy height, basal area, leaf area index (Hudak et al. 2002, Næsset 2007, Jensen et al. 2008), as well as certain aspects of higher trophic levels (e.g., bird species richness and bird prevalence) that are dependent upon canopy structure (Goetz et al. 2007, Swatantran et al. 2012). However, the ability of LiDAR to bridge the gaps between forest canopy structure, tree health and productivity measures had not been previously evaluated. Our results show the novel ability of LiDAR data to remotely assess measures of tree function, in particular measures of crown health, tree mortality, xylem increment growth and foliar nutrition. The consistency of LiDAR in defining attributes in forest canopy and understory structure reflective of tree functional traits is somewhat surprising considering two limitations inherent to the current study. First, LiDAR categories were calculated for large areas (4 ha) deemed important to avian habitat. LiDAR categories

based on broad spatial averages could have masked 50 m plot-based patterns in tree health and productivity due to a mismatch in scale. Second, LiDAR continuous point cloud data had to be converted to categorical LiDAR classes, which undoubtedly simplified the informational content of estimated forest structure. Despite these limitations, LiDAR estimates were associated with a range of stand- and tree-based measures of health and productivity. The breadth and consistency of these relationships is likely testament to the strong predictive capacity of LiDAR-based measures of forest structure for elucidating associated patterns of tree and forest function.

2.6. Acknowledgements

I am grateful to all of those who provided technical assistance in the lab and in the field. They include, Sean MacFaden, Josh Halman, Paula Murakami, Ben Engel, Dan Hale, Gary Hawley, Ali Kosiba, Kindle Loomis, Allison Middleman, Allyson Makuch, Jarlath O'Neil-Dunne, Nick Rodenhouse, and Helen Yurchenco. In addition, I am thankful to my committee members, Paul Schaberg, Allan Strong, and Shelly Rayback, for their support and mentorship in completing this research. This research could not have been completed without the kind assistance from the staff of the Hubbard Brook Experimental Forest in New Hampshire, in particular, Ian Halm. This manuscript is a contribution of the Hubbard Brook Ecosystem Study. Hubbard Brook is part of the Long-Term Ecological Research (LTER) network, which is supported by the National Science Foundation. The Hubbard Brook Experimental Forest is operated and maintained by the USDA Forest Service, Northern Research Station, Newtown Square, PA. This research

was supported by funds provided by the Northeastern States Research Cooperative

(NSRC) and the USDA CSREES McIntire-Stennis Forest Research Program.

2.7. References

Allen, D. C., C. J. Barnett, I. Millers, and D. Lachance. 1992. Temporal change (1988-1990) in sugar maple health, and factors associated with crown condition. Canadian Journal of Forest Research **22**:1776-1784.

Barnes, B. V., D. R. Zak, S. R. Denton, and S. H. Spurr. 1997. Forest ecology. John Wiley and Sons.

Bauce, E. and D. C. Allen. 1991. Etiology of a sugar maple decline. Canadian Journal of Forest Research **21**:686-693.

Bechtold, W. A. and C. T. Scott. 2005. The forest inventory and analysis plot design. The enhanced forest inventory and analysis program-national sampling design and estimation procedures. US Department of Agriculture Forest Service, Asheville, NC:27-42.

Bernier, B., D. Paré, and M. Brazeauu. 1989. Natural stresses, nutrient imbalances and forest decline in southeastern Quebec. Water, Air, and Soil Pollution **48**:239-250.

Comerford, D. P., P. G. Schaberg, P. H. Templer, A. M. Socci, J. L. Campbell, and K. F. Wallin. 2013. Influence of experimental snow removal on root and canopy physiology of sugar maple trees in a northern hardwood forest. Oecologia **171**:261-269.

Cook, E. R. and L. A. Kairiukstis. 1990. Methods of dendrochronology: applications in the environmental sciences. Kluwer Academic Publishers, Dordrecht.

Cooke, R., B. Pendrel, C. Barnett, and D. Allen. 1996. North American Maple Project Cooperative Field Manual. USDA Forest Service Northwestern Area, State and Private Forestry, Durham, NH.

DeGraaf, R. M., J. B. Hestbeck, and M. Yamasaki. 1998. Associations between breeding bird abundance and stand structure in the White Mountains, New Hampshire and Maine, USA. Forest Ecology and Management **103**:217-233.

Driscoll, C. T., G. B. Lawrence, A. J. Bulger, T. J. Butler, C. S. Cronan, C. Eagar, K. F. Lambert, G. E. Likens, J. L. Stoddard, and K. C. Weathers. 2001. Acidic Deposition in the Northeastern United States: Sources and Inputs, Ecosystem Effects, and Management Strategies: The effects of acidic deposition in the northeastern United States include the acidification of soil and water, which stresses terrestrial and aquatic biota. BioScience **51**:180-198.

Drohan, P., S. Stout, and G. Petersen. 2002. Sugar maple (< i> Acer saccharum</i> Marsh.) decline during 1979–1989 in northern Pennsylvania. Forest Ecology and Management **170**:1-17.

Duchesne, L., R. Ouimet, and D. Houle. 2002. Basal area growth of sugar maple in relation to acid deposition, stand health, and soil nutrients. Journal of Environmental Quality **31**:1676-1683.

Goetz, S., D. Steinberg, R. Dubayah, and B. Blair. 2007. Laser remote sensing of canopy habitat heterogeneity as a predictor of bird species richness in an eastern temperate forest, USA. Remote Sensing of Environment **108**:254-263.

Goetz, S. J., D. Steinberg, M. G. Betts, R. T. Holmes, P. J. Doran, R. Dubayah, and M. Hofton. 2010. Lidar remote sensing variables predict breeding habitat of a Neotropical migrant bird. Ecology **91**:1569-1576.

Goff, F. G. and D. West. 1975. Canopy-understory interaction effects on forest population structure. Forest Science **21**:98-108.

Halaj, J., D. W. Ross, and A. R. Moldenke. 2000. Importance of habitat structure to the arthropod food‐web in Douglas‐fir canopies. Oikos **90**:139-152.

Halman, J. M., P. G. Schaberg, G. J. Hawley, C. F. Hansen, and T. Fahey. 2014. Differential impacts of calcium and aluminum treatments on sugar maple and American beech growth dynamics. Canadian Journal of Forest Research.

Hofton, M. A., L. Rocchio, J. B. Blair, and R. Dubayah. 2002. Validation of vegetation canopy lidar sub-canopy topography measurements for a dense tropical forest. Journal of Geodynamics **34**:491-502.

Hollaus, M., W. Wagner, K. Schadauer, B. Maier, and K. Gabler. 2009. Growing stock estimation for alpine forests in Austria: a robust lidar-based approach. Canadian Journal of Forest Research **39**:1387-1400.

Holmes, R. L. 1983. Computer-assisted quality control in tree-ring dating and measurement. Tree-ring bulletin **43**:69-78.

Holmes, R. T., N. L. Rodenhouse, and T. S. Sillett. 2005. Black-throated Blue Warbler (*Setophaga caerulescens*). The Birds of North America Online (A. Poole, Ed.). Retrieved from The Birds of North America Online: http://bna.birds.cornell.edu/bna/species/087, Ithaca: Cornell Lab of Ornithology.

Horsley, S. B., R. P. Long, S. W. Bailey, R. A. Hallett, and T. J. Hall. 2000. Factors associated with the decline disease of sugar maple on the Allegheny Plateau. Canadian Journal of Forest Research **30**:1365-1378.

Houston, D. R. 1999. History of sugar maple decline. Pages 19-26 *in* Sugar maple ecology and health: Proceedings of an International Symposium, Warren, Pa. Edited by SB Horsley and RP Long. US For. Serv. Gen. Tech. Rep. NE-261.

Hudak, A. T., M. A. Lefsky, W. B. Cohen, and M. Berterretche. 2002. Integration of lidar and Landsat ETM+ data for estimating and mapping forest canopy height. Remote Sensing of Environment **82**:397-416.

Huggett, B. A., P. G. Schaberg, G. J. Hawley, and C. Eagar. 2007. Long-term calcium addition increases growth release, wound closure, and health of sugar maple (Acer saccharum) trees at the Hubbard Brook Experimental Forest. Canadian Journal of Forest Research **37**:1692-1700.

Hyde, P., R. Dubayah, B. Peterson, J. B. Blair, M. Hofton, C. Hunsaker, R. Knox, and W. Walker. 2005. Mapping forest structure for wildlife habitat analysis using waveform lidar: Validation of montane ecosystems. Remote Sensing of Environment **96**:427-437.

Jeffries, J. M., R. J. Marquis, and R. E. Forkner. 2006. Forest age influences oak insect herbivore community structure, richness, and density. Ecological Applications **16**:901-912.

Jensen, J. L. R., K. S. Humes, L. A. Vierling, and A. T. Hudak. 2008. Discrete return lidar-based prediction of leaf area index in two conifer forests. Remote Sensing of Environment **112**:3947-3957.

Jones, J. B. and V. W. Case. 1990. Sampling, handling and analyzing plant tissue samples. Ed. 3 edition. Soil Science Society of America, Madison, WI.

Jones, K. F. and N. D. Mulherin. 1998. An evaluation of the severity of the January 1998 ice storm in northern New England. DTIC Document.

Juice, S. M., T. J. Fahey, T. G. Siccama, C. T. Driscoll, E. G. Denny, C. Eagar, N. L. Cleavitt, R. Minocha, and A. D. Richardson. 2006. Response of sugar maple to calcium addition to northern hardwood forest. Ecology **87**:1267-1280.

Kolb, T. and L. McCormick. 1993. Etiology of sugar maple decline in four Pennsylvania stands. Canadian Journal of Forest Research **23**:2395-2402.

Koukoulas, S. and G. A. Blackburn. 2004. Quantifying the spatial properties of forest canopy gaps using LiDAR imagery and GIS. International Journal of Remote Sensing **25**:3049-3072.

Lefsky, M. A., W. B. Cohen, G. G. Parker, and D. J. Harding. 2002. Lidar Remote Sensing for Ecosystem Studies. BioScience **52**:19-30.

Likens, G., C. Driscoll, D. Buso, T. Siccama, C. Johnson, G. Lovett, T. Fahey, W. Reiners, D. Ryan, and C. Martin. 1998. The biogeochemistry of calcium at Hubbard Brook. Biogeochemistry **41**:89-173.

Likens, G. E., C. T. Driscoll, and D. C. Buso. 1996. Long-term effects of acid rain: response and recovery of a forest ecosystem. Science-AAAS-Weekly Paper Edition **272**:244-245.

Long, R. P., S. B. Horsley, and P. R. Lilja. 1997. Impact of forest liming on growth and crown vigor of sugar maple and associated hardwoods. Canadian Journal of Forest Research **27**:1560-1573.

MacArthur, R. H. and J. W. MacArthur. 1961. On Bird Species Diversity. Ecology **42**:594-598.

Marqus, D. A. and R. L. Ernst. 1991. The effects of stand structure after thinning on the growth of an Allegheny hardwood stand. Forest Science **37**:1182-1200.

Montgomery, D. C. 2008. Design and analysis of experiments. Wiley, New York.

Næsset, E. 2007. Airborne laser scanning as a method in operational forest inventory: Status of accuracy assessments accomplished in Scandinavia. Scandinavian Journal of Forest Research **22**:433-442.

Næsset, E. and T. Gobakken. 2008. Estimation of above- and below-ground biomass across regions of the boreal forest zone using airborne laser. Remote Sensing of Environment **112**:3079-3090.

Rhoads, A. G., S. P. Hamburg, T. J. Fahey, T. G. Siccama, E. N. Hane, J. Battles, C. Cogbill, J. Randall, and G. Wilson. 2002. Effects of an intense ice storm on the structure of a northern hardwood forest. Canadian Journal of Forest Research **32**:1763-1775.

Robinson, S. K. and R. T. Holmes. 1982. Foraging Behavior of Forest Birds: The Relationships Among Search Tactics, Diet, and Habitat Structure. Ecology **63**:1918-1931.

Robinson, S. K. and R. T. Holmes. 1984. Effects of Plant Species and Foliage Structure on the Foraging Behavior of Forest Birds. The Auk **101**:672-684.

Roth, R. R. 1976. Spatial heterogeneity and bird species diversity. Ecology **57**:773-782.

Schaberg, P. G., E. K. Miller, and C. Eagar. 2010. Assessing the threat that anthropogenic calcium depletion poses to forest health and productivity. Advances in Threat Assessment and Their Application to Forest and Rangeland Management:37.

Schaberg, P. G., J. W. Tilley, G. J. Hawley, D. H. DeHayes, and S. W. Bailey. 2006. Associations of calcium and aluminum with the growth and health of sugar maple trees in Vermont. Forest Ecology and Management **223**:159-169.

Schmid, K., K. Waters, B. Dingerson, R. M. Hadley, J. Carter, J. Dare, and N. C. S. Center. 2008. LiDAR 101: an introduction to LiDAR technology, data, and applications. Charleston, SC: NOAA Coastal Services Center.

Schwarz, P. A., T. J. Fahey, C. W. Martin, T. G. Siccama, and A. Bailey. 2001. Structure and composition of three northern hardwood–conifer forests with differing disturbance histories. Forest Ecology and Management **144**:201-212.

Schwarz, P. A., T. J. Fahey, and C. E. McCulloch. 2003. Factors controlling spatial variation of tree species abundance in a forested landscape. Ecology **84**:1862-1878.

Sherrill, K. R., M. A. Lefsky, J. B. Bradford, and M. G. Ryan. 2008. Forest structure estimation and pattern exploration from discrete-return lidar in subalpine forests of the central Rockies. Canadian Journal of Forest Research **38**:2081-2096.

Smith, K. M., W. S. Keeton, T. M. Donovan, and B. Mitchell. 2008. Stand-level forest structure and avian habitat: scale dependencies in predicting occurrence in a heterogeneous forest. Forest Science **54**:36-46.

Speer, J. H. 2010. Fundamentals of tree ring research. University of Arizona Press.

Stokes, M. A. and T. L. Smiley. 1968. An introduction to tree-ring dating. University of Chicago Press, Chicago, IL.

Swatantran, A., R. Dubayah, S. Goetz, M. Hofton, M. G. Betts, M. Sun, M. Simard, and R. Holmes. 2012. Mapping Migratory Bird Prevalence Using Remote Sensing Data Fusion. PLoS ONE **7**:e28922.

Swatantran, A., R. Dubayah, D. Roberts, M. Hofton, and J. B. Blair. 2011. Mapping biomass and stress in the Sierra Nevada using lidar and hyperspectral data fusion. Remote Sensing of Environment **115**:2917-2930.

van Doorn, N. S., J. J. Battles, T. J. Fahey, T. G. Siccama, and P. A. Schwarz. 2011. Links between biomass and tree demography in a northern hardwood forest: a decade of stability and change in Hubbard Brook Valley, New Hampshire. Canadian Journal of Forest Research **41**:1369-1379.

van Leeuwen, M. and M. Nieuwenhuis. 2010. Retrieval of forest structural parameters using LiDAR remote sensing. European Journal of Forest Research **129**:749-770.

Whelan, C. J. 2001. Foliage structure influences foraging of insectivorous forest birds: an experimental study. Ecology **82**:219-231.

Wigley, T., K. Briffa, and P. Jones. 1984. On the average value of correlated time series, with applications in dendroclimatology and hydrometeorology. Journal of Climate and Applied Meteorology **23**:201-213.

Woods, K. D. 1984. Patterns of tree replacement: canopy effects on understory pattern in hemlock-northern hardwood forests. Vegetatio **56**:87-107.

Yamaguchi, D. K. 1991. A simple method for cross-dating increment cores from living trees. Canadian Journal of Forest Research **21**:414-416.

Table 1. Mean (± SE) subplot standing dead basal area, plot level crown vigor index and percent branch dieback by LiDAR category, collected during 2012 at the Hubbard Brook Experimental Forest, NH, USA.

Response variable	Significance	LiDAR crown & understory closure category			
		High crown High understory	High crown Low understory	Low crown High understory	Low crown Low understory
Basal area (m^2/ha)					
Subplot - standing dead	*	**6.26 ± 1.30^{a}**	**2.46 ± 0.50^{b}**	**5.13 ± 1.03^{ab}**	**4.86 ± 1.15^{ab}**
Decline					
Crown vigor index	*	**2.34 ± 0.09^{a}**	**1.97 ± 0.07^{b}**	**2.27 ± 0.16^{ab}**	**2.22 ± 0.10^{ab}**
% branch dieback	**	**31.60 ± 2.27^{a}**	**23.86 ± 1.48^{b}**	**30.52 ± 3.03^{ab}**	**31.17 ± 2.12^{a}**

* Significant at $P \leq 0.10$, ** Significant at $P \leq 0.05$

Means (± SE) with differing letters are statistically significantly different based on a Tukey HSD test

Table 2. Mean (± SE) basal area increment (cm^2) for sugar maple (*Acer saccharum*) and yellow birch (*Betula alleghaniensis*) trees by LiDAR category, collected during 2012 at the Hubbard Brook Experimental Forest, NH, USA. Significant differences among LiDAR category means are displayed in bold.

Response variable	Significance	LiDAR crown & understory closure category			
		High crown High understory	High crown Low understory	Low crown High understory	Low crown Low understory
Basal area increment (cm^2)					
Sugar Maple:					
2000-2012	**	**7.05 ± 1.58^{b}**	**11.09 ± 0.96^{a}**	**10.92 ± 1.58^{ab}**	**10.33 ± 1.99^{ab}**
2009 (year of LiDAR acquisition)	**	**7.73 ± 1.74^{b}**	**11.69 ± 0.98^{ab}**	**11.41 ± 1.42^{ab}**	**12.44 ± 2.66^{a}**
Post-ice storm/pre-LiDAR (1999-2008)	**	**7.05 ± 1.61^{b}**	**11.27 ± 1.00^{a}**	**10.99 ± 1.62^{ab}**	**10.11 ± 1.93^{ab}**
Pre-ice storm (1988-1997)	**	**7.61 ± 1.82^{b}**	**13.69 ± 1.32^{a}**	**11.77 ± 1.08^{ab}**	**11.33 ± 1.96^{ab}**
Yellow Birch:					
2000-2012	NS	10.93 ± 1.44	10.99 ± 1.42	12.01 ± 1.64	11.37 ± 0.59
2009 (year of LiDAR acquisition)	NS	15.13 ± 2.20	14.36 ± 1.38	15.56 ± 2.36	14.86 ± 0.93
Post-ice storm/pre-LiDAR (1999-2008)	NS	10.34 ± 1.34	10.63 ± 1.48	11.45 ± 1.53	10.87 ± 0.58
Pre-ice storm (1988-1997)	NS	12.22 ± 1.30	13.10 ± 2.14	12.80 ± 1.51	12.31 ± 0.99

* Significant at $P \leq 0.10$, ** Significant at $P \leq 0.05$, "NS" denotes no significance

Means (± SE) with differing letters are statistically significantly different based on a Tukey HSD test

Table 3. Linear relationships between percent crown dieback and basal area increment (BAI) for sugar maple (*Acer saccharum) and* yellow birch (*Betula alleghaniensis*) trees sampled during 2012 at Hubbard Brook Experimental Forest, NH, USA.

BAI response variable	Estimate	Standard error	P-value	R-squared
Sugar maple BAI:				
2009	-1.3649	0.2870	< 0.0001	0.3995
1970s	N/A	N/A	NS	N/A
2000-2012	-0.2737	0.0489	< 0.0001	0.4799
Δ BAI - 1970s - 2000-2012	-1.4156	0.3492	0.0003	0.3258
Post Ice Storm: 1999-2008	-0.2796	0.0507	< 0.0001	0.4723
Pre Ice Storm: 1988-1997	-0.2497	0.0594	0.0002	0.3424
Yellow birch BAI:				
2009	N/A	N/A	NS	N/A
1970s	-0.0887	0.0480	0.0737	0.0911
2000-2012	N/A	N/A	NS	N/A
Δ BAI - 1970s - 2000-2012	N/A	N/A	NS	N/A
Post Ice Storm: 1999-2008	N/A	N/A	NS	N/A
Pre Ice Storm: 1988-1997	N/A	N/A	NS	N/A

"NS" denotes not significant, "N/A" denotes not applicable due to no significance

Table 4. Mean (± SE) foliar Ca and Ca:Al nutrition ($mg \cdot kg^{-1}$) for sugar maple (*Acer saccharum) and* yellow birch (*Betula alleghaniensis*) trees by LiDAR category, collected during 2012 at Hubbard Brook Experimental Forest, NH, USA. Significant differences among LiDAR category means are displayed in bold.

Response variable	Significance	LiDAR crown & understory closure category			
		High crown High understory	High crown Low understory	Low crown High understory	Low crown Low understory
Foliar nutrition - sunlit/upper canopy ($mg \cdot kg^{-1}$)					
Sugar maple:					
Ca	NS	4965.89 ± 565.79	5534.03 ± 192.17	5650.07 ± 626.43	5214.28 ± 429.92
Ca:Al molar ratio	NS	55.71 ± 8.91	70.41 ± 11.09	70.14 ± 18.9	55.91 ± 8.49
Yellow birch:					
Ca	**	**7966.97 ± 489.31^{b}**	**10122.90 ± 667.88^{a}**	**7969.18 ± 384.25^{b}**	**8757.82 ± 472.02^{ab}**
Ca:Al molar ratio	*	**85.06 ± 8.35^{b}**	**132.98 ± 16.67^{a}**	**101.31 ± 13.83^{ab}**	**130.84 ± 18.4^{ab}**

* Significant at $P \leq 0.10$, ** Significant at $P \leq 0.05$, "NS" denotes no significance

Means (± SE) with differing letters are statistically significantly different based on a Tukey HSD test

Table 5. Linear relationships between Δ BAI (1970s – 2000-2012) and foliar nutrition, and percent branch dieback and foliar nutrition for sugar maple (*Acer saccharum*) and yellow birch (*Betula alleghaniensis*) trees sampled during 2012 at Hubbard Brook Experimental Forest, NH, USA

Foliar nutrition predictor variable	Estimate	Standard error	P-value	R-squared
Foliar nutrition & Δ BAI (1970s - 2000-2012)				
Sugar maple				
Ca	N/A	N/A	NS	N/A
Al	N/A	N/A	NS	N/A
Mg	N/A	N/A	NS	N/A
Mn	-0.0293	0.0099	0.0056	0.2049
Ca:Al	N/A	N/A	NS	N/A
Ca:Mn	347.8047	146.3510	0.0233	0.1425
Mg:Mn	1101.7360	437.3051	0.0166	0.1573
Yellow birch				
Ca	-0.0103	0.0034	0.0049	0.2101
Al	N/A	N/A	NS	N/A
Mg	-0.0573	0.0150	0.0006	0.2993
Mn	N/A	N/A	NS	N/A
Ca:Al	N/A	N/A	NS	N/A
Ca:Mn	-380.6834	173.4116	0.0351	0.1241
Mg:Mn	-764.7613	362.2354	0.0422	0.1159
Foliar nutrition & percent crown dieback				
Sugar maple				
Ca	-0.0027	0.0014	0.0573	0.1023
Al	N/A	N/A	NS	N/A
Mg	-0.0149	0.0072	0.0476	0.1105
Mn	0.0134	0.0039	0.0014	0.2627
Ca:Al	-14.1240	4.9795	0.0076	0.1914
Ca:Mn	-201.5113	53.5372	0.0006	0.2941
Mg:Mn	-567.4133	165.6044	0.0016	0.2567
Yellow birch				
Ca	N/A	N/A	NS	N/A
Al	N/A	N/A	NS	N/A
Mg	-0.0152	0.0079	0.0633	0.0978
Mn	N/A	N/A	NS	N/A
Ca:Al	N/A	N/A	NS	N/A
Ca:Mn	N/A	N/A	NS	N/A
Mg:Mn	N/A	N/A	NS	N/A

"NS" denotes not significant, "N/A" denotes not applicable due to no significance

Table 6. Sub-plot and micro-plot basal area (m^2/ha) by tree species at Hubbard Brook Experimental Forest, NH, USA.

Sub-plot (trees > 12.5 cm)			Micro-plot (trees 2.5 - 12.5 cm)		
Species	Total BA	Percent	Species	Total BA	Percent
Betula alleghaniesis	428.9	35.5	*Fagus grandifolia*	64.8	63.1
Acer saccharum	394.8	32.6	*Acer saccharum*	15	14.6
Fagus grandifolia	203.5	16.8	*Acer pensylvanicum*	8.1	7.9
Fraxinus americana	74.7	6.2	*Picea rubens*	7	6.8
Acer rubrum	46.1	3.8	*Tsuga Canadensis*	5	4.8
Picea rubens	36.3	3	*Abies balsamea*	2.5	2.4
Abies balsamea	10	0.8	*Acer spicatum*	0.2	0.2
Tsuga canadensis	5.7	0.5	*Betula alleghaniesis*	0.1	0.1
Betula papyrifera	4.9	0.4	*Acer rubrum*	0	0
Acer pensylvanicum	4.6	0.4	*Betula papyrifera*	0	0
Unknown	0.3	0	*Fraxinus americana*	0	0
Conifer	52	4.3	Conifer	14.5	11.6
Deciduous	1157.9	95.7	Deciduous	88.3	88.4
Total BA	1209.8	100	Total BA	102.7	100

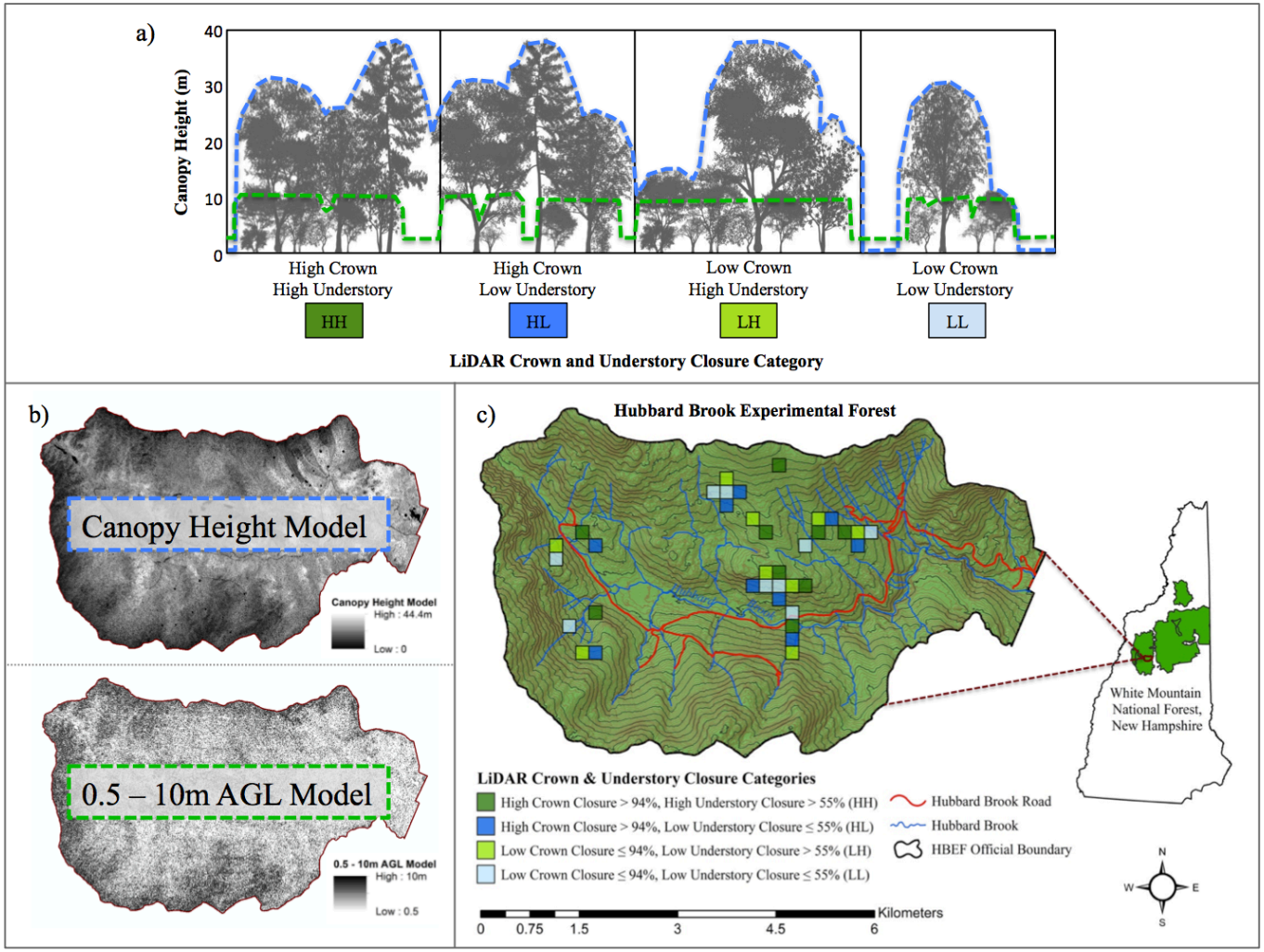

Figure 1. Study site and plot selection: a) LiDAR crown and understory closure categories, b) canopy height (nDSM) and 0.5-10 m AGL surface models, and c) Hubbard Brook Experimental Forest, NH, USA – showing the 36 4 ha blocks.

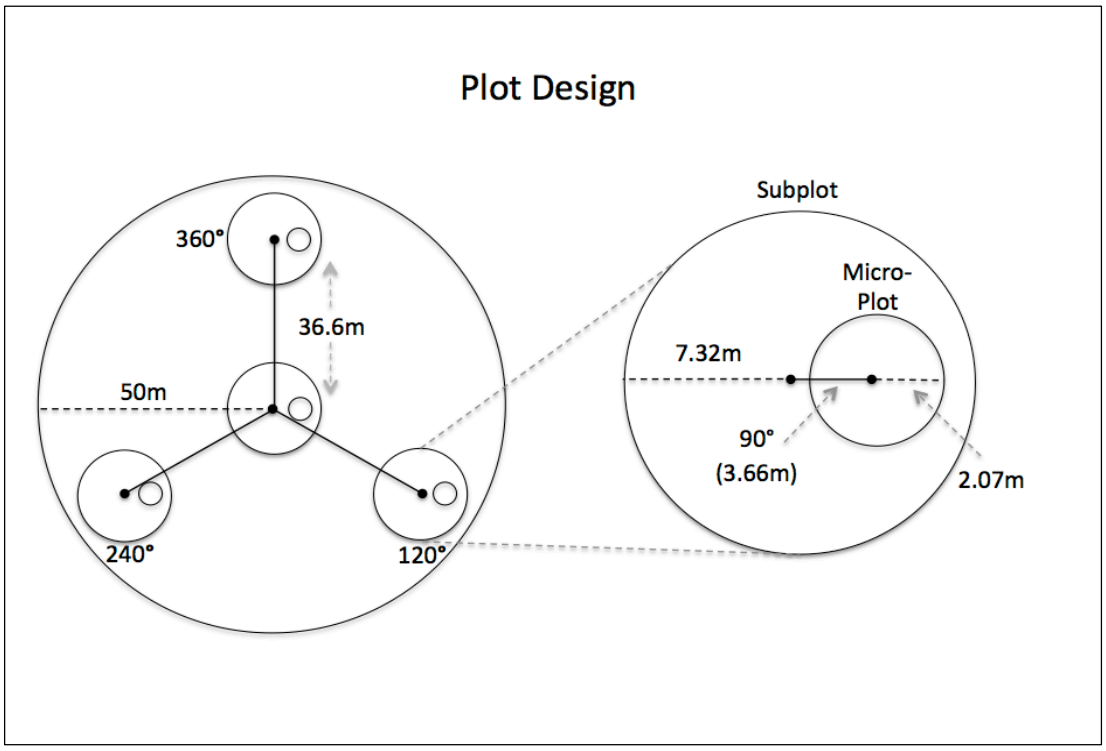

Figure 2. Diagram of the basic plot design, which was based on FIA protocols (Bechtold 2005).

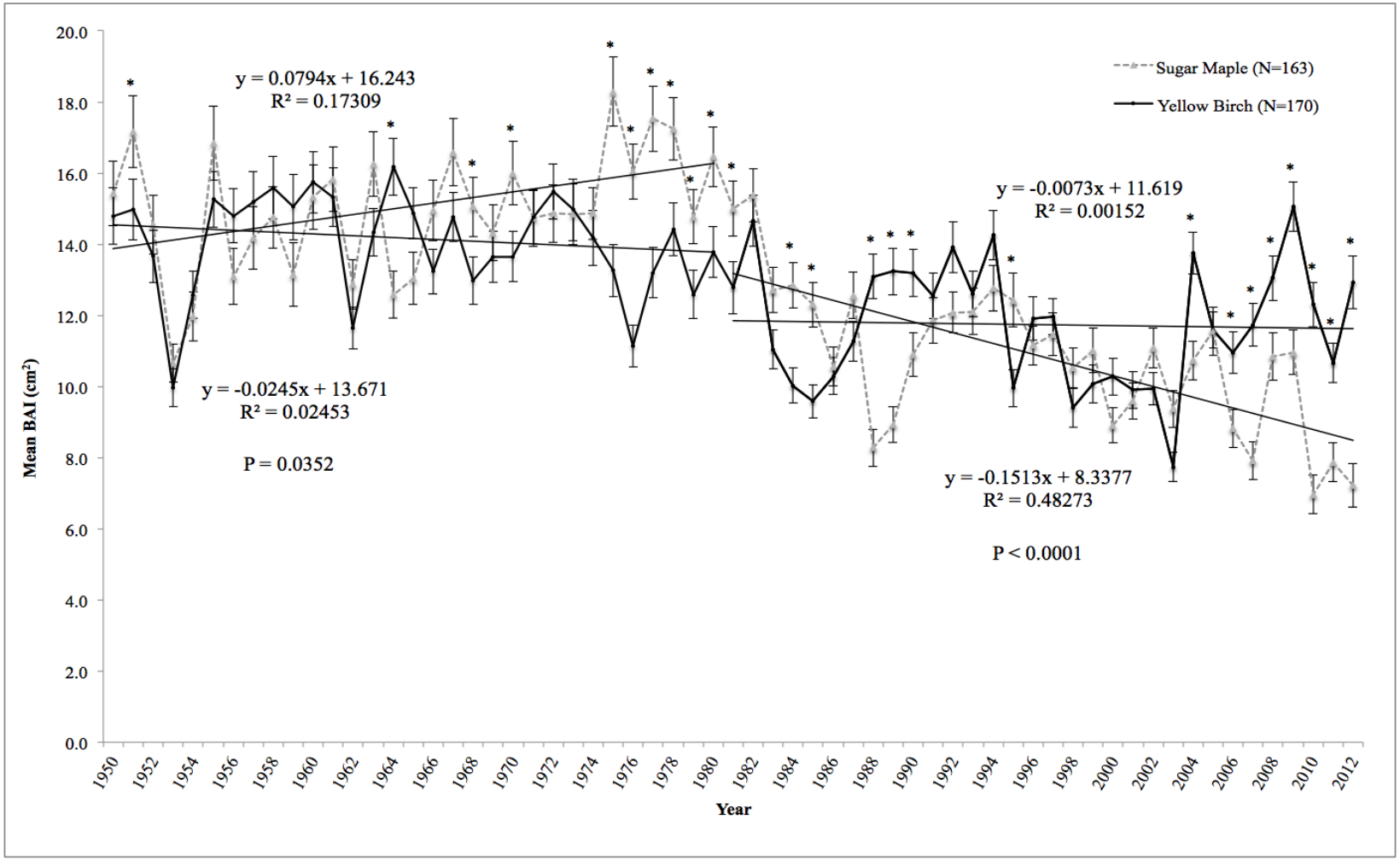

Figure 3. Mean basal area increment (BAI; ± SE) for sugar maple and yellow birch trees from 1950 – 2012 at Hubbard Brook Experimental Forest, NH, USA. Individual years that are significantly different between species are indicated by an asterisk (based on an orthogonal contrast between species with $P \leq 0.05$). Slope analyses indicate different linear growth trajectories for each species and its significance between species for the years 1950 – 1980 and 1981 – 2012.

COMPREHENSIVE BIBLIOGRAPHY

Allen, D. C., C. J. Barnett, I. Millers, and D. Lachance. 1992. Temporal change (1988-1990) in sugar maple health, and factors associated with crown condition. Canadian Journal of Forest Research 22:1776-1784.

Antonarakis, A. S., K. S. Richards, and J. Brasington. 2008. Object-based land cover classification using airborne LiDAR. Remote Sensing of Environment 112:2988-2998.

Asner, G. P. 2009. Tropical forest carbon assessment: integrating satellite and airborne mapping approaches. Environmental Research Letters 4:034009.

Asner, G. P., J. Mascaro, H. C. Muller-Landau, G. Vieilledent, R. Vaudry, M. Rasamoelina, J. S. Hall, and M. van Breugel. 2012. A universal airborne LiDAR approach for tropical forest carbon mapping. Oecologia 168:1147-1160.

Barnes, B. V., D. R. Zak, S. R. Denton, and S. H. Spurr. 1997. Forest ecology. John Wiley and Sons.

Bauce, E. and D. C. Allen. 1991. Etiology of a sugar maple decline. Canadian Journal of Forest Research 21:686-693.

Bechtold, W. A. and C. T. Scott. 2005. The forest inventory and analysis plot design. The enhanced forest inventory and analysis program-national sampling design and estimation procedures. US Department of Agriculture Forest Service, Asheville, NC:27-42.

Bechtold, W. A., Scott, C.T. 2005. The forest inventory and analysis plot design. Pages 37-52 *in* F. S. Department of Agriculture, editor. Department of Agriculture, Forest Service, Southern Research Station.

Bernier, B., D. Paré, and M. Brazeauu. 1989. Natural stresses, nutrient imbalances and forest decline in southeastern Quebec. Water, Air, and Soil Pollution 48:239-250.

Blaschke, T. 2010. Object based image analysis for remote sensing. ISPRS Journal of Photogrammetry and Remote Sensing 65:2-16.

Bormann, F. H. and G. E. Likens. 1979. Pattern and process in a forested ecosystem. Springer-Verlag.

Bradbury, R. B., R. A. Hill, D. C. Mason, S. A. Hinsley, J. D. Wilson, H. Balzter, G. Q. A. Anderson, M. J. Whittingham, I. J. Davenport, and P. E. Bellamy. 2005. Modelling relationships between birds and vegetation structure using airborne LiDAR data: a review with case studies from agricultural and woodland environments. Ibis 147:443-452.

Bréda, N. J. J. 2003. Ground−based measurements of leaf area index: a review of methods, instruments and current controversies. Journal of Experimental Botany 54:2403-2417.

Brennan, R. and T. Webster. 2006. Object-oriented land cover classification of lidar-derived surfaces. Canadian Journal of Remote Sensing 32:162-172.

Brock, J. C., C. W. Wright, I. B. Kuffner, R. Hernandez, and P. Thompson. 2006. Airborne lidar sensing of massive stony coral colonies on patch reefs in the northern Florida reef tract. Remote Sensing of Environment 104:31-42.

Chen, Q. 2007. Airborne LiDAR data processing and information extraction. Photogrammetric Engineering and Remote Sensing 73:91-95.

Clawges, R., K. Vierling, L. Vierling, and E. Rowell. 2008. The use of airborne lidar to assess avian species diversity, density, and occurrence in a pine/aspen forest. Remote Sensing of Environment 112:2064-2073.

Comerford, D. P., P. G. Schaberg, P. H. Templer, A. M. Socci, J. L. Campbell, and K. F. Wallin. 2013. Influence of experimental snow removal on root and canopy physiology of sugar maple trees in a northern hardwood forest. Oecologia 171:261-269.

Cook, E. R. and L. A. Kairiukstis. 1990. Methods of dendrochronology: applications in the environmental sciences. Kluwer Academic Publishers, Dordrecht.

Cooke, R., B. Pendrel, C. Barnett, and D. Allen. 1996. North American Maple Project Cooperative Field Manual. USDA Forest Service Northwestern Area, State and Private Forestry, Durham, NH.

DeGraaf, R. M., J. B. Hestbeck, and M. Yamasaki. 1998. Associations between breeding bird abundance and stand structure in the White Mountains, New Hampshire and Maine, USA. Forest Ecology and Management 103:217-233.

Denno, R. F., C. Gratton, M. A. Peterson, G. A. Langellotto, D. L. Finke, and A. F. Huberty. 2002. Bottom-up forces mediate natural-enemy impact in a phytophagous insect community. Ecology 83:1443-1458.

Driscoll, C. T., G. B. Lawrence, A. J. Bulger, T. J. Butler, C. S. Cronan, C. Eagar, K. F. Lambert, G. E. Likens, J. L. Stoddard, and K. C. Weathers. 2001. Acidic Deposition in the Northeastern United States: Sources and Inputs, Ecosystem Effects, and Management Strategies: The effects of acidic deposition in the northeastern United States include the acidification of soil and water, which stresses terrestrial and aquatic biota. BioScience 51:180-198.

Dubayah, R., S. Sheldon, D. Clark, M. Hofton, J. Blair, G. Hurtt, and R. Chazdon. 2010. Estimation of tropical forest height and biomass dynamics using lidar remote sensing at La Selva, Costa Rica. Journal of Geophysical Research: Biogeosciences (2005–2012) 115.

Evans, J., A. Hudak, R. Faux, and A. M. Smith. 2009. Discrete Return Lidar in Natural Resources: Recommendations for Project Planning, Data Processing, and Deliverables. Remote Sensing 1:776-794.

Falkowski, M. J., J. S. Evans, S. Martinuzzi, P. E. Gessler, and A. T. Hudak. 2009. Characterizing forest succession with lidar data: An evaluation for the Inland Northwest, USA. Remote Sensing of Environment 113:946-956.

Fernandez, J. C., S. A., J. Caceres, K. C. Slatton, M. Starek, and R. Kumar. 2007. An Overview of LiDAR Point Cloud Processing Software. Pages 1-27, Geosensing Engineering and Mapping (GEM), Civil and Coastal Engineering Department, University of Florida.

Finke, D. L. and R. F. Denno. 2004. Predator diversity dampens trophic cascades. Nature 429:407-410.

García-Feced, C., D. J. Tempel, and M. Kelly. 2011. LiDAR as a Tool to Characterize Wildlife Habitat: California Spotted Owl Nesting Habitat as an Example. Journal of Forestry 109:436-443.

Gatziolis, D. 2009. Precise FIA plot registration using field and dense LIDAR data. Pages 243-249 Proceedings of the eigth annual forest inventory and analysis symposium. United States Dept. of Agriculture, Forest Service General Technical Report WO-79, Washington, D.C.

Gatziolis, D. 2012. Advancements in LiDAR-based registration of FIA field plots. Pages 432-437. United States Dept. of Agriculture, Forest Service General Technical Report NRS-P-105, Washington, D.C.

Gatziolis, D. and H.-E. Andersen. 2008. A Guide to LiDAR Data Acquisition and Processing for the Forests of the Pacific Northwest. Pages 1-32 *in* U. F. Service, editor. USDA Forest Service, Pacific Northwest Research Station.

Gaulton, R. and T. J. Malthus. 2010. LiDAR mapping of canopy gaps in continuous cover forests: A comparison of canopy height model and point cloud based techniques. International Journal of Remote Sensing 31:1193-1211.

Goetz, S., D. Steinberg, R. Dubayah, and B. Blair. 2007. Laser remote sensing of canopy habitat heterogeneity as a predictor of bird species richness in an eastern temperate forest, USA. Remote Sensing of Environment 108:254-263.

Goetz, S. J., D. Steinberg, M. G. Betts, R. T. Holmes, P. J. Doran, R. Dubayah, and M. Hofton. 2010. Lidar remote sensing variables predict breeding habitat of a Neotropical migrant bird. Ecology 91:1569-1576.

Goff, F. G. and D. West. 1975. Canopy-understory interaction effects on forest population structure. Forest Science 21:98-108.

Goßner, M. M. 2009. Light intensity affects spatial distribution of Heteroptera in deciduous forests. European Journal of Entomology 106:241-252.

Halaj, J., D. W. Ross, and A. R. Moldenke. 2000. Importance of habitat structure to the arthropod food−web in Douglas−fir canopies. Oikos 90:139-152.

Halman, J. M., P. G. Schaberg, G. J. Hawley, C. F. Hansen, and T. Fahey. 2014. Differential impacts of calcium and aluminum treatments on sugar maple and American beech growth dynamics. Canadian Journal of Forest Research.

Herms, D. A. and W. J. Mattson. 1992. The dilemma of plants: to grow or defend. Quarterly Review of Biology:283-335.

Hofton, M. A., L. Rocchio, J. B. Blair, and R. Dubayah. 2002. Validation of vegetation canopy lidar sub-canopy topography measurements for a dense tropical forest. Journal of Geodynamics 34:491-502.

Hollaus, M., W. Wagner, K. Schadauer, B. Maier, and K. Gabler. 2009. Growing stock estimation for alpine forests in Austria: a robust lidar-based approach. Canadian Journal of Forest Research 39:1387-1400.

Holmes, R. L. 1983. Computer-assisted quality control in tree-ring dating and measurement. Tree-ring bulletin 43:69-78.

Holmes, R. T. and S. K. Robinson. 1981. Tree Species Preferences of Foraging Insectivorous Birds in a Northern Hardwoods Forest. Oecologia 48:31-35.

Holmes, R. T., N. L. Rodenhouse, and T. S. Sillett. 2005. Black-throated Blue Warbler (*Setophaga caerulescens*). The Birds of North America Online (A. Poole, Ed.). Retrieved from The Birds of North America Online: http://bna.birds.cornell.edu/bna/species/087, Ithaca: Cornell Lab of Ornithology.

Holmes, R. T., J. C. Schultz, and P. Nothnagle. 1979. Bird predation on forest insects: an exclosure experiment. Science 206:462-463.

Horsley, S. B., R. P. Long, S. W. Bailey, R. A. Hallett, and T. J. Hall. 2000. Factors associated with the decline disease of sugar maple on the Allegheny Plateau. Canadian Journal of Forest Research 30:1365-1378.

Houston, D. R. 1999. History of sugar maple decline. Pages 19-26 *in* Sugar maple ecology and health: Proceedings of an International Symposium, Warren, Pa. Edited by SB Horsley and RP Long. US For. Serv. Gen. Tech. Rep. NE-261.

Hudak, A. T., N. L. Crookston, J. S. Evans, M. J. Falkowski, A. M. S. Smith, P. E. Gessler, and P. Morgan. 2006. Regression modeling and mapping of coniferous forest basal area and tree density from discrete-return lidar and multispectral satellite data. Canadian Journal of Remote Sensing 32:126-138.

Hudak, A. T., N. L. Crookston, J. S. Evans, D. E. Hall, and M. J. Falkowski. 2008. Nearest neighbor imputation of species-level, plot-scale forest structure attributes from LiDAR data. Remote Sensing of Environment 112:2232-2245.

Hudak, A. T., M. A. Lefsky, W. B. Cohen, and M. Berterretche. 2002. Integration of lidar and Landsat ETM+ data for estimating and mapping forest canopy height. Remote Sensing of Environment 82:397-416.

Huggett, B. A., P. G. Schaberg, G. J. Hawley, and C. Eagar. 2007. Long-term calcium addition increases growth release, wound closure, and health of sugar maple (Acer saccharum) trees at the Hubbard Brook Experimental Forest. Canadian Journal of Forest Research 37:1692-1700.

Hyde, P., R. Dubayah, B. Peterson, J. B. Blair, M. Hofton, C. Hunsaker, R. Knox, and W. Walker. 2005. Mapping forest structure for wildlife habitat analysis using waveform lidar: Validation of montane ecosystems. Remote Sensing of Environment 96:427-437.

Hyde, P., R. Dubayah, W. Walker, J. B. Blair, M. Hofton, and C. Hunsaker. 2006. Mapping forest structure for wildlife habitat analysis using multi-sensor (LiDAR, SAR/InSAR, ETM+, Quickbird) synergy. Remote Sensing of Environment 102:63-73.

Jeffries, J. M., R. J. Marquis, and R. E. Forkner. 2006. Forest age influences oak insect herbivore community structure, richness, and density. Ecological Applications 16:901-912.

Jensen, J. L. R., K. S. Humes, L. A. Vierling, and A. T. Hudak. 2008. Discrete return lidar-based prediction of leaf area index in two conifer forests. Remote Sensing of Environment 112:3947-3957.

Johnson, M. D. 2000. Evaluation of an Arthropod Sampling Technique for Measuring Food Availability for Forest Insectivorous Birds (Evaluación de una Técnica para Muestrear Artrópodos para Medir la Disponibilidad de Alimento para Aves de Bosque Insectívoras). Journal of Field Ornithology 71:88-109.

Jones, J. B. and V. W. Case. 1990. Sampling, handling and analyzing plant tissue samples. Ed. 3 edition. Soil Science Society of America, Madison, WI.

Jones, K. F. and N. D. Mulherin. 1998. An evaluation of the severity of the January 1998 ice storm in northern New England. DTIC Document.

Jones, T. G., N. C. Coops, and T. Sharma. 2011. Assessing the utility of LiDAR to differentiate among vegetation structural classes. Remote Sensing Letters 3:231-238.

Juice, S. M., T. J. Fahey, T. G. Siccama, C. T. Driscoll, E. G. Denny, C. Eagar, N. L. Cleavitt, R. Minocha, and A. D. Richardson. 2006. Response of sugar maple to calcium addition to northern hardwood forest. Ecology 87:1267-1280.

Kolb, T. and L. McCormick. 1993. Etiology of sugar maple decline in four Pennsylvania stands. Canadian Journal of Forest Research 23:2395-2402.

Koricheva, J., S. Larsson, and E. Haukioja. 1998. Insect performance on experimentally stressed woody plants: a meta-analysis. Annual review of entomology 43:195-216.

Koukoulas, S. and G. A. Blackburn. 2004. Quantifying the spatial properties of forest canopy gaps using LiDAR imagery and GIS. International Journal of Remote Sensing 25:3049-3072.

Leckie, D., F. Gougeon, D. Hill, R. Quinn, L. Armstrong, and R. Shreenan. 2003. Combined high-density lidar and multispectral imagery for individual tree crown analysis. Canadian Journal of Remote Sensing 29:633-649.

Lefsky, M., D. Turner, M. Guzy, and W. Cohen. 2005. Combining lidar estimates of aboveground biomass and Landsat estimates of stand age for spatially extensive validation of modeled forest productivity. Remote Sensing of Environment 95:549-558.

Lefsky, M. A., W. B. Cohen, G. G. Parker, and D. J. Harding. 2002. Lidar Remote Sensing for Ecosystem Studies. BioScience 52:19-30.

Lesak, A. A., V. C. Radeloff, T. J. Hawbaker, A. M. Pidgeon, T. Gobakken, and K. Contrucci. 2011. Modeling forest songbird species richness using LiDAR-derived measures of forest structure. Remote Sensing of Environment 115:2823-2835.

Likens, G., C. Driscoll, D. Buso, T. Siccama, C. Johnson, G. Lovett, T. Fahey, W. Reiners, D. Ryan, and C. Martin. 1998. The biogeochemistry of calcium at Hubbard Brook. Biogeochemistry 41:89-173.

Likens, G. E., C. T. Driscoll, and D. C. Buso. 1996. Long-term effects of acid rain: response and recovery of a forest ecosystem. Science-AAAS-Weekly Paper Edition 272:244-245.

Lim, K., P. Treitz, M. Wulder, B. St-Onge, and M. Flood. 2003. LiDAR remote sensing of forest structure. Progress in Physical Geography 27:88-106.

Long, R. P., S. B. Horsley, and P. R. Lilja. 1997. Impact of forest liming on growth and crown vigor of sugar maple and associated hardwoods. Canadian Journal of Forest Research 27:1560-1573.

MacArthur, R. H. 1958. Population ecology of some warblers of northeastern coniferous forests. Ecology 39:599-619.

MacArthur, R. H. and H. S. Horn. 1969. Foliage Profile by Vertical Measurements. Ecology 50:802-804.

MacArthur, R. H. and J. W. MacArthur. 1961. On Bird Species Diversity. Ecology 42:594-598.

Marquis, R. J. and C. J. Whelan. 1994. Insectivorous birds increase growth of white oak through consumption of leaf-chewing insects. Ecology 75:2007-2014.

Marqus, D. A. and R. L. Ernst. 1991. The effects of stand structure after thinning on the growth of an Allegheny hardwood stand. Forest Science 37:1182-1200.

Martinuzzi, S., L. A. Vierling, W. A. Gould, M. J. Falkowski, J. S. Evans, A. T. Hudak, and K. T. Vierling. 2009. Mapping snags and understory shrubs for a LiDAR-based assessment of wildlife habitat suitability. Remote Sensing of Environment 113:2533-2546.

Montgomery, D. C. 2008. Design and analysis of experiments. Wiley, New York.

Müller, J. and R. Brandl. 2009. Assessing biodiversity by remote sensing in mountainous terrain: the potential of LiDAR to predict forest beetle assemblages. Journal of Applied Ecology 46:897-905.

Næsset, E. 2007. Airborne laser scanning as a method in operational forest inventory: Status of accuracy assessments accomplished in Scandinavia. Scandinavian Journal of Forest Research 22:433-442.

Næsset, E. and T. Gobakken. 2008. Estimation of above- and below-ground biomass across regions of the boreal forest zone using airborne laser. Remote Sensing of Environment 112:3079-3090.

Nelson, R., C. Keller, and M. Ratnaswamy. 2005. Locating and estimating the extent of Delmarva fox squirrel habitat using an airborne LiDAR profiler. Remote Sensing of Environment 96:292-301.

Nur, N., S. L. Jones, and G. R. Geupel. 1999. Statistical guide to data analysis of avian monitoring programs. US Fish and Wildlife Service.

Pascual, C., A. García-Abril, L. G. García-Montero, S. Martín-Fernández, and W. B. Cohen. 2008. Object-based semi-automatic approach for forest structure characterization using lidar data in heterogeneous Pinus sylvestris stands. Forest Ecology and Management 255:3677-3685.

Pesonen, A., M. Maltamo, K. Eerikäinen, and P. Packalèn. 2008. Airborne laser scanning-based prediction of coarse woody debris volumes in a conservation area. Forest Ecology and Management 255:3288-3296.

Polis, G. A. 1999. Why are parts of the world green? Multiple factors control productivity and the distribution of biomass. Oikos:3-15.

Ralph, C. J., S. Droege, and J. R. Sauer. 1995. Managing and Monitoring Birds Using Point Counts: Standards and Applications. General Technical Report, USDA Forest Service, Albany, CA.

Reutebuch, S. E., H.-E. Andersen, and R. J. McGaughey. 2005. Light Detection and Ranging (LIDAR): An Emerging Tool for Multiple Resource Inventory. Journal of Forestry 103:286-292.

Rhoads, A. G., S. P. Hamburg, T. J. Fahey, T. G. Siccama, E. N. Hane, J. Battles, C. Cogbill, J. Randall, and G. Wilson. 2002. Effects of an intense ice storm on the structure of a northern hardwood forest. Canadian Journal of Forest Research 32:1763-1775.

Riaño, D., F. Valladares, S. Condés, and E. Chuvieco. 2004. Estimation of leaf area index and covered ground from airborne laser scanner (Lidar) in two contrasting forests. Agricultural and Forest Meteorology 124:269-275.

Richardson, J. J., L. M. Moskal, and S.-H. Kim. 2009. Modeling approaches to estimate effective leaf area index from aerial discrete-return LIDAR. Agricultural and Forest Meteorology 149:1152-1160.

Robinson, S. K. and R. T. Holmes. 1982. Foraging Behavior of Forest Birds: The Relationships Among Search Tactics, Diet, and Habitat Structure. Ecology 63:1918-1931.

Robinson, S. K. and R. T. Holmes. 1984. Effects of Plant Species and Foliage Structure on the Foraging Behavior of Forest Birds. The Auk 101:672-684.

Roth, R. R. 1976. Spatial heterogeneity and bird species diversity. Ecology 57:773-782.

Schaberg, P. G., E. K. Miller, and C. Eagar. 2010. Assessing the threat that anthropogenic calcium depletion poses to forest health and productivity. Advances in Threat Assessment and Their Application to Forest and Rangeland Management:37.

Schaberg, P. G., J. W. Tilley, G. J. Hawley, D. H. DeHayes, and S. W. Bailey. 2006. Associations of calcium and aluminum with the growth and health of sugar maple trees in Vermont. Forest Ecology and Management 223:159-169.

Schmid, K., K. Waters, B. Dingerson, R. M. Hadley, J. Carter, J. Dare, and N. C. S. Center. 2008. LiDAR 101: an introduction to LiDAR technology, data, and applications. Charleston, SC: NOAA Coastal Services Center.

Schwarz, P. A., T. J. Fahey, C. W. Martin, T. G. Siccama, and A. Bailey. 2001. Structure and composition of three northern hardwood–conifer forests with differing disturbance histories. Forest Ecology and Management 144:201-212.

Schwarz, P. A., T. J. Fahey, and C. E. McCulloch. 2003. Factors controlling spatial variation of tree species abundance in a forested landscape. Ecology 84:1862-1878.

Sherrill, K. R., M. A. Lefsky, J. B. Bradford, and M. G. Ryan. 2008. Forest structure estimation and pattern exploration from discrete-return lidar in subalpine forests of the central Rockies. Canadian Journal of Forest Research 38:2081-2096.

Sherry, T. W. 1979. Competitive Interactions and Adaptive Strategies of American Redstarts and Least Flycatchers in a Northern Hardwoods Forest. The Auk 96:265-283.

Sherry, T. W. and R. T. Holmes. 1988. Habitat selection by breeding American Redstarts in response to a dominant competitor, the Least Flycatcher. The Auk:350-364.

Shure, D. and D. Phillips. 1991. Patch size of forest openings and arthropod populations. Oecologia 86:325-334.

Smith, K. M., W. S. Keeton, T. M. Donovan, and B. Mitchell. 2008. Stand-level forest structure and avian habitat: scale dependencies in predicting occurrence in a heterogeneous forest. Forest Science 54:36-46.

Solberg, S., E. Næsset, K. H. Hanssen, and E. Christiansen. 2006. Mapping defoliation during a severe insect attack on Scots pine using airborne laser scanning. Remote Sensing of Environment 102:364-376.

Speer, J. H. 2010. Fundamentals of tree ring research. University of Arizona Press.

St-Onge, B. and U. Vepakomma. 2004. Assessing Forest Gap Dynamics and Growth Using Multi-temporal Laser Scanner Data. International Archives of Photogrammetry, Remote Sensing and Spatial Information Sciences 36:173-178.

Stephens, P., P. Watt, D. Loubser, A. Haywood, and M. Kimberley. 2007. Estimation of carbon stocks in New Zealand planted forests using airborne scanning LiDAR. Pages 389-394 *in* ISPRS Workshop on Laser Scanning 2007 and SilviLaser 2007. Citeseer.

Stiling, P. and D. C. Moon. 2005. Quality or quantity: the direct and indirect effects of host plants on herbivores and their natural enemies. Oecologia 142:413-420.

Stokes, M. A. and T. L. Smiley. 1968. An introduction to tree-ring dating. University of Chicago Press, Chicago, IL.

Strengbom, J., J. Witzell, A. Nordin, and L. Ericson. 2005. Do multitrophic interactions override N fertilization effects on Operophtera larvae? Oecologia 143:241-250.

Swatantran, A., R. Dubayah, S. Goetz, M. Hofton, M. G. Betts, M. Sun, M. Simard, and R. Holmes. 2012. Mapping Migratory Bird Prevalence Using Remote Sensing Data Fusion. PLoS ONE 7:e28922.

Swatantran, A., R. Dubayah, D. Roberts, M. Hofton, and J. B. Blair. 2011. Mapping biomass and stress in the Sierra Nevada using lidar and hyperspectral data fusion. Remote Sensing of Environment 115:2917-2930.

van Aardt, J. A. N., R. H. Wynne, and R. G. Oderwald. 2006. Forest Volume and Biomass Estimation Using Small-Footprint Lidar-Distributional Parameters on a Per-Segment Basis. Forest Science 52:636-649.

Van Bael, S. A., J. D. Brawn, and S. K. Robinson. 2003. Birds defend trees from herbivores in a Neotropical forest canopy. Proceedings of the National Academy of Sciences 100:8304-8307.

van Doorn, N. S., J. J. Battles, T. J. Fahey, T. G. Siccama, and P. A. Schwarz. 2011. Links between biomass and tree demography in a northern hardwood forest: a decade of stability and change in Hubbard Brook Valley, New Hampshire. Canadian Journal of Forest Research 41:1369-1379.

Van Ewjik, K. Y., P. M. Treitz, and N. A. Scott. 2011. Characterizing forest succession in Central Ontario using LiDAR-derived indices. Photogrammetric Engineering and Remote Sensing 77:261-269.

van Leeuwen, M. and M. Nieuwenhuis. 2010. Retrieval of forest structural parameters using LiDAR remote sensing. European Journal of Forest Research 129:749-770.

Vierling, K., C. Bässler, R. Brandl, L. Vierling, I. Weiß, and J. Müller. 2011. Spinning a laser web: predicting spider distributions using LiDAR. Ecological Applications 21:577-588.

Vierling, K. T., C. E. Swift, A. T. Hudak, J. C. Vogeler, and L. A. Vierling. 2014. How much does the time lag between wildlife field-data collection and LiDAR-data acquisition matter for studies of animal distributions? A case study using bird communities. Remote Sensing Letters 5:185-193.

Wehr, A. and U. Lohr. 1999. Airborne laser scanning—an introduction and overview. ISPRS Journal of Photogrammetry and Remote Sensing 54:68-82.

Whelan, C. J. 2001. Foliage structure influences foraging of insectivorous forest birds: an experimental study. Ecology 82:219-231.

White, T. 1984. The abundance of invertebrate herbivores in relation to the availability of nitrogen in stressed food plants. Oecologia 63:90-105.

Wigley, T., K. Briffa, and P. Jones. 1984. On the average value of correlated time series, with applications in dendroclimatology and hydrometeorology. Journal of Climate and Applied Meteorology 23:201-213.

Woods, K. D. 1984. Patterns of tree replacement: canopy effects on understory pattern in hemlock-northern hardwood forests. Vegetatio 56:87-107.

Yamaguchi, D. K. 1991. A simple method for cross-dating increment cores from living trees. Canadian Journal of Forest Research 21:414-416.

Zimble, D. A., D. L. Evans, G. C. Carlson, R. C. Parker, S. C. Grado, and P. D. Gerard. 2003. Characterizing vertical forest structure using small-footprint airborne LiDAR. Remote Sensing of Environment 87:171-182.

APPENDIX A – Original Study-design

Introduction

The study presented in Chapter 2 was originally designed and scaled to assess the relationship of LiDAR to multiple aspects of forest structure, forest stand and individual tree health and productivity, as well as to higher trophic levels (arthropod and bird populations). The following appendix outlines the methods, results, discussion and conclusions from this original study design.

Methods

Forest structural metrics – LiDAR "ground truthing"

To quantify the ability of LiDAR to accurately represent forest canopy structure, ground-based forest canopy data were collected on each of the 36 plots. Measures of understory and crown closure were collected at five meter intervals along three 50 m transects (located at azimuths 360°, 120°, and 240° from plot center and a total of 31 points) on each plot. To quantify crown and understory closure, a 4.0 m measuring staff was employed along each transect and interval, and a binary presence/absence of vegetation > 10 m and from 0.5 – 10 m in height was recorded. Presence/absence data were converted to a continuous percentage value for both crown and understory closure per plot.

Abiotic site metrics

A soil moisture meter (Field Scout TDR 100, Spectrum Technologies, Inc., Aurora, IL, USA) was used to take an average of three readings at five meter intervals

along the three transects (mentioned above) within each of the 36 plots. Air temperature (°C) and relative humidity (%) readings were obtained by placing HOBO data loggers (HOBO U23 Pro v2, Onset Computer Corporation, Inc., Bourne, MA, USA) 2.0 m above ground level and within 10.0 m of plot center. Readings were taken every 15 minutes from June 18th to October 5th.

Plot means for temperature and relative humidity measures were summarized (i.e., mean, median, minimum, and maximum) by month, by the quarter of the year with the greatest amount of sunshine (i.e., solar temperature/relative humidity – typically early May to early August, but here as June 18 to August 7 due to limitations in instrument availability), by the quarter of the year with the warmest temperatures (i.e., meteorological temperature/relative humidity – June 18th to September 18th), and by astronomical temperature/relative humidity (i.e., the summer solstice – June 20th, through the fall equinox – September 21st).

Forest inventory metrics

On each subplot, an inventory following FIA protocols (Bechtold and Scott 2005) was conducted on all trees greater than 12.5 cm, with the following information recorded for each tally tree: species, diameter at breast height (DBH: 1.4 m), crown status (i.e., dominant, co-dominant, intermediate, suppressed, or dead), and canopy health. On each FIA micro-plot, an inventory of all trees 2.5 to 12.5 cm DBH was obtained with the same measures as collected for subplots. For plot-level inventories, canopy health was assessed via crown vigor index and percent branch dieback, which were estimated according to the methods of the North America Maple Project – NAMP; Cooke et al.

(1996). Crown vigor index employs a 1-5 scale, where (1) represents highly vigorous crowns with little or no major branch dieback and less than 10% branch or twig mortality, (2) light decline with branch or twig mortality present and between 10 – 25%, (3) moderate decline with 25 – 50% branch and twig mortality, (4) severe decline with > 50% branch and twig mortality, and (5) dead. Percent branch dieback was estimated using a 12-class system – for complete methods, see Cooke et al. (1996). Assessments of crown vigor index and percent branch dieback were performed on each tree by two observers, 180° from each other to account for any potential errors due to observer bias. In addition, basal area (BA) per hectare was calculated on all trees, regardless of crown status, and for standing dead trees using the following formula:

$$\text{Subplot BA } (m^2/ha) = (\Sigma\ (((DBH/2)^2)/10{,}000))/\ 0.016833$$

where π is 3.14 and 0.016833 is the subplot area in hectares. Measures of BA for living and dead trees were calculated at the plot-level for trees greater than 12.5 cm.

Arthropod and avian-based metrics

To quantify arthropod abundance and diversity, understory and mid-story branch clippings were obtained during mid to late June, 2012 according to the methods of Johnson (2000). Two sugar maple and two yellow birch trees per plot were sampled from the five selected sugar maple and yellow birch trees (mentioned above) when possible. Alternative trees were selected when a sufficient amount of lower foliage (maximum height of ~10 m) was not obtainable. Pole pruners were used to collect branches due to the explosive impact that would have resulted from using a shotgun. Foliar samples collected from the arthropod branch clippings were generally from shaded

foliage due to the ~10 m maximum collection height obtainable using this method. Arthropod samples were counted and identified to order in the field (Johnson 2000) and branch clippings were saved and used for foliar cation analysis of mid-canopy foliage (mentioned above). Foliar carbon (C) and nitrogen (N) were also assessed on mid-canopy foliage; C and N concentrations of dried and ground foliage were analyzed using a CHN – CE440 elemental analyzer (Exeter Analytical, Inc., North Chelmsford, MA, USA).

Avian abundance and diversity were quantified via 50 m fixed-radius bird point count surveys, that were conducted at plot center on all 36 plots and repeated four times during the height of the breeding season (late May through mid June). To avoid observer bias, two observers visited each plot twice during the breeding season. Standard ten-minute point counts were divided into three 3-min 20-sec intervals to provide estimates of detection probability (Ralph et al. 1995). Point count surveys began by 05:30, concluded by 10:30, and were only conducted on days with little or no rain or wind. Avian species presence/absence data were summarized into total and mean number of individuals, cumulative species richness (i.e., the total number of species detected across all four surveys), evenness (i.e., a measure of the relative abundance of each species within a community), Shannon-diversity index (H′; a diversity index that reflects both species richness and evenness of distribution among species present), and ecological species diversity ($e^{H'}$; a transformation of the Shannon-diversity index that expresses diversity in terms of species) according to the methods of Nur et al. (1999). To calculate Shannon diversity index, the following formula was used:

$$H' = \sum_{i=1}^{i=S} (p_i)(\ln p),\ i=1, 2,\ldots S$$

where S is the species count, and p_i is the proportion of S made up of the *i*th species.

Results and discussion

LiDAR ground truthing

To our knowledge, there are no studies quantifying direct measures of forest structure to assess the accuracy of LiDAR. There are, however, many studies using indirect measures (e.g., basal area, LAI, and above ground biomass) to essentially "ground truth" LiDAR. One objective of our study was to assess the accuracy of LiDAR by comparing ground-based measures of forest structure (i.e., direct measures) to LiDAR-derived measures of forest structure. Ground-based crown and understory closure were quantified in order to do so.

No significant differences were found in ground-based percent crown closure among our LiDAR crown and understory closure categories. Although not significant, LiDAR categories with low understory closure tended to have greater ground-based percent crown closure, suggesting that competition with understory vegetation for some resource other than light (e.g., nutrients and/or water) affected growth and therefore crown closure in the overstory at HBEF (Table 7). By contrast ground-based percent understory closure did differ among LiDAR categories. LiDAR categories with high understory closure had significantly higher ground-based percent understory closure than LiDAR categories with low understory closure (Table 7).

At lower elevations (i.e., below 800 m), the HBEF is predominately a closed canopy northern hardwood forest. By the nature of selecting plots within 400 – 800 m in elevation, we reduced variation in crown closure by eliminating other forest types within the HBEF valley (e.g., higher elevation red spruce-balsam fir forests, and lower elevation mixed deciduous-coniferous forests). In addition, large canopy openings (> 173 m^2; 30,000 pixels) were eliminated due to the potentially confounding influences of saturated soils, beaver ponds, the Hubbard Brook, roads, and other sources of larger canopy openings. Small canopy gaps (< 20 m^2; 400 pixels) were also eliminated as they were initially considered to be ecologically insignificant. Consequently, our ground-based measures of crown closure may have been quantified at a finer resolution than our LiDAR categories, resulting in a potential inability of LiDAR to accurately quantify crown closure. Moreover, because the scale at which the LiDAR categories were created (4 ha blocks) was much larger than those used for ground-based measures (50 m plots), LiDAR estimates likely included greater variations in crown characteristics than ground-based metrics.

To assess whether scale and/or the refinement of canopy openings consistently influenced the ability of LiDAR to accurately quantify forest crown and understory closure measures, LiDAR data were also reclassified three additional ways: 1) according to the 50 m radius scale of the ground based measures, 2) with no crown refinement, by including small canopy gaps that were originally deemed ecologically insignificant, and 3) at the 50 m radius plot scale and with no crown refinement (Appendix C, Figure 4). Ground-based percent understory closure remained significant in each additional LiDAR classification, with significance improving *($P \leq 0.05$)* with the reclassification of the

LiDAR categories to the 50 m radius scale. However, reclassification had no effect on ground-based percent crown closure (Appendix C, Table 14). Interestingly, ground-based percent crown closure differed significantly among block groups for all LiDAR classifications (two of the nine blocks where different than each other based on a Tukey HSD test), whereas ground-based percent understory closure did not differ among blocks. This suggests that ground-based crown closure was somewhat influenced by some moderate scale site factor(s) associated with "block" (e.g., windthrow, seeps, etc.).

Almost all previous work looking at the relationship of LiDAR to various forest structural parameters has used LiDAR derived surface models for further analysis, whether to derive indirect structural-based indices from these models (Goetz et al. 2007, Goetz et al. 2010), or to use surface-based models directly by comparing them to ground-based measures of forest structure (e.g., basal area, LAI, tree height, above ground biomass, etc.)(Riaño et al. 2004, Lefsky et al. 2005, Hudak et al. 2006, van Aardt et al. 2006, Næsset 2007, Jensen et al. 2008, Næsset and Gobakken 2008). In addition, previous work using object-oriented classifiers (e.g., eCognition) has been done by first creating surface models from the raw LiDAR data, and then segmenting objects from the surface models in conjunction with other spatially explicit data (e.g., passive satellite imagery; (Brennan and Webster 2006, Antonarakis et al. 2008). However, an ideal approach would be an object-oriented classification of the raw LiDAR point cloud to look at the density of points in the horizontal and vertical planes. Unfortunately, and at least for this study, individual LiDAR points were not tagged with their flight line number. Typically, LiDAR data are acquired with 50 % overlap of parallel flight lines and with individual points tagged with their flight line number (Evans et al. 2009). This

was not the case for the LiDAR data acquired for this study, thus resulting in an arbitrarily high density of points where flight lines overlapped, which could not be processed for further analyses of point density. Consequently, further analyses of HBEF LiDAR data consisted of the creation of surface models (i.e., nDSM and AGL; Figure 2b). This methodology simplifies the three-dimensionality of the LiDAR data into two dimensions, reducing some of the power of the LiDAR data, and potentially resulting in discrepancies between LiDAR-derived measures and ground-based measures of crown closure.

Another possible explanation for why there were discrepancies between LiDAR-derived and ground-based measures of crown closure might be the disparity between when the LiDAR data were acquired versus when ground-based data were collected. The LiDAR data were acquired in September 2009, whereas the ground based data were collected throughout the summer of 2012. It would be expected that crown closure would change over time more so than understory closure, particularly in the short term (e.g., < 5 years) and especially in a predominantly closed canopy forest. Competition for resources, as well as small-scale disturbances (e.g., windthrow, ice storms, insect outbreaks, etc.) have been shown to change canopy dynamics while leaving understory vegetation relatively unaffected in the short term (Barnes et al. 1997). Furthermore, shade tolerant understory vegetation might remain more or less constant while putting on relatively little annual growth and waiting for larger canopy gaps to open up (Barnes et al. 1997). For example, American beech, which can reproduce asexually through root and stump sprouting and is highly shade tolerant (Barnes et al. 1997), is common

throughout the understory at the HBEF (Schwarz et al. 2001) and accounted for 63.1 percent of the basal area of trees 2.5 – 12.5 cm DBH in this study (Table 6).

Site factors

Percent volumetric soil moisture showed no significant differences among LiDAR categories. There was a slight trend for LiDAR categories with high understory closure to have lower percent volumetric soil moisture (Appendix C, Table 7), which could hint at a greater utilization of groundwater on sites with high understory closure than sites with low understory closure and regardless of crown closure.

Most measures of temperature and relative humidity also showed no significant differences among LiDAR categories (Appendix C, Table 8). However, minimum solar temperature was significantly greater on LiDAR plots with high crown closure and low understory closure as compared to LiDAR plots with high crown and high understory. Although not significant among all LiDAR categories, the general trend was for LiDAR plots with low understory closure to have greater minimum solar temperatures regardless of crown closure (Appendix C, Table 7). This potentially illustrates an insulating (shade-induced cooling) effect of forest understory vegetation that LiDAR can assess, although detectable differences, both significant and non-significant, were < 1°C and might not be ecologically significant.

Minimum solar relative humidity also showed significant differences among LiDAR categories, with low crown and high understory closure plots having greater minimum relative humidity than plots with high crown and high understory closure (Appendix C, Table 7). This suggests that relative humidity is influenced by crown

closure more so than understory closure. This trend is inconsistent among the other LiDAR categories, however, and therefore inconclusive. For both temperature and relative humidity, HOBO data loggers, which were placed only at plot center, were probably not representative of the plot as a whole. A greater number of data loggers placed randomly throughout plots would potentially help decipher the ability of LiDAR to better assess microsite factors such as temperature and relative humidity.

Results presented here suggest that canopy cover, in particular understory closure, was associated with differences in microsite conditions (i.e., site factors: soil moisture, temperature, and relative humidity) that differ among LiDAR categories. However, greater sampling resolution would be needed to distinguish the full nature and consistency of differences associated with LiDAR-based estimates. Other confounding factors previously mentioned (i.e., scale, classification refinement, LiDAR acquisition vs. ground-based data collection, etc.), would also need to be considered when assessing the ability of LiDAR to quantify site factors.

Forest inventory factors

Basal area quantified at the micro-plot level (i.e., trees 2.5 – 12.5 cm DBH and represented by suppressed, intermediate, and co-dominant crown positions) was also significantly different among LiDAR categories, with high crown and high understory closure significantly different from all other LiDAR categories (data not shown). Furthermore, the trend was for LiDAR plots with high understory closure to exhibit greater micro-plot basal area regardless of crown closure. No other measures of basal area were significantly different among LiDAR categories. However, number of stems

per hectare (i.e., woody stems 2.5 – 12.5 cm DBH) also showed significant differences among LiDAR categories. LiDAR plots with high crown and high understory closure were significantly different from those with high crown and low understory closure, as well as from plots with low crown and low understory closure, with the general trend being a greater number of stems per hectare on LiDAR plots with high understory closure as compared to plots with low understory closure. In a sense, measures of micro-plot basal area and stems per hectare were measures of understory structure. These measures further confirmed, in addition to the ground-truthing of LiDAR understory closure, the ability of LiDAR to accurately quantify understory closure. Given the discrepancies observed between LiDAR and ground-based measures of crown closure, the poor correspondence between LiDAR categories and measures of basal area containing dominant and co-dominant trees (see Appendix C, Table 15), is not surprising.

Arthropod and avian factors

In addition to foliar cation concentrations of sunlit/upper canopy foliage, we also analyzed the nutrition of foliage collected via branch clippings (i.e., mid-canopy foliage) for arthropod sampling. We hypothesized that arthropod abundance would be related to foliar nutrition, which in turn would be related to forest health and productivity. Furthermore, forest structure influences forest health and productivity and therefore, LiDAR might potentially provide useful insights into mid-canopy foliar nutrition and arthropod abundance and diversity (i.e., the ability of LiDAR to assess trophic level interactions). Previous studies have shown relationships between LiDAR and arthropod populations (Müller and Brandl 2009, Vierling et al. 2011); however, assessments of

whether foliar nutrition was the intermediate connection between forest health and productivity and arthropod abundance and diversity has not been evaluated within the context of LiDAR data.

Measures of arthropod abundance, in particular and most notably, total arthropod mass and Lepidopteran mass (both larval and adult mass), were not significantly different among LiDAR categories (Apendix E, Table 11). Canopy arthropod abundance and diversity have been shown to be influenced by levels of N, P, and K in plants (Polis 1999). In particular, plants with high concentrations of N and low concentrations of C-based defenses have been shown to be a better food source for arthropod herbivores, with increases in plant N concentrations improving insect performance (White 1984). N concentration is particularly important because developing arthropods in early instar stages are particularly sensitive to nutrient deficiencies (Herms and Mattson 1992, Polis 1999). Strengbom et al. (2005) found higher survival probability and larger adult body mass among Lepidopteran larvae that were reared on plants fertilized with N. Other studies have reported similar results (White 1984, Stiling and Moon 2005). The lack of significant differences for arthropod abundance among LiDAR categories presented here are not surprising because measures of mid-canopy foliar N, P, and K often associated with arthropod abundance were also not significantly different among LiDAR categories. In contrast, linear relationships comparing sugar maple mid-canopy foliar N and P to total arthropod mass and Lepidopteran larval mass were significant and positive, with N having a considerably greater effect size (i.e., beta values) than P (Appendix C, Table 12). Similarly, N also had a significant and positive linear relationship with total arthropod mass and Lepidopteran larval mass on mid-canopy yellow birch foliage, with a

similar effect size. These findings are in agreement with previous findings on the association of N and P with arthropod abundance and performance.

In addition to foliar nutrition and arthropod abundance, we also hypothesized that avian abundance and diversity would be related to LiDAR categories, either directly through relationships of forest structure and foraging and nesting behavior/niche partitioning or indirectly through relationships of forest health and productivity to foliar nutrition and arthropod abundance. Trophic level interactions have been shown to occur among primary producers, primary consumers, and secondary consumers (e.g., trees, arthropod herbivores, and birds respectively) in many ecological systems (Holmes et al. 1979, Marquis and Whelan 1994, Koricheva et al. 1998, Denno et al. 2002, Van Bael et al. 2003, Finke and Denno 2004, Strengbom et al. 2005). Additionally, secondary consumers such as birds, have been shown to partition foraging and nesting space among congeners in both the horizontal and vertical planes (MacArthur 1958, MacArthur and MacArthur 1961, MacArthur and Horn 1969, Sherry 1979, Holmes and Robinson 1981, Robinson and Holmes 1982, 1984, Sherry and Holmes 1988, DeGraaf et al. 1998). Indeed, this was the basis for assessing avian abundance and diversity in relation to LiDAR. However, none of the measures of avian abundance and diversity varied among the LiDAR categories (Appendix C, Table 11). Furthermore, linear relationships between avian abundance and diversity with arthropod abundance were also not significant, regardless of LiDAR categories (data not shown).

Previous studies examining the ability of LiDAR to assess bird prevalence, occurrence, diversity, and species richness have shown significant and positive relationships (Goetz et al. 2007, Clawges et al. 2008, Lesak et al. 2011, Swatantran et al.

2012). One possible explanation for the lack of significant association here might be the scale at which bird surveys were conducted and recorded (50 m) relative to the scale at which LiDAR crown and understory closure categories were classified (4 ha). However, reclassification of the LiDAR data to the 50 m plot scale showed no improvement in the relationship of our estimates of bird abundance and diversity to LiDAR-derived measures of forest crown and understory closure (Appendix C, Table 15). Classification of forest vertical structure at more meaningful scales and shapes (e.g., bird territories; perhaps through the use of eCognition) might provide more accurate assessments of LiDAR-derived metrics to avian abundance and diversity overall.

Conclusions

Despite finding significant results among LiDAR categories for some (mostly stand and tree-based) response variables, our results suggest that a simplified classification approach to using high-resolution LiDAR data may produce categorical data that is too coarse when assessing forest structure and especially higher trophic levels. In addition, the utility and accuracy of high-resolution LiDAR data can be affected by many important factors. For example, in some circumstances disparity in scale was an important factor that helped explain the lack of statistical differentiation among response variables. All ground-based data were collected at the 50 m radius plot scale, whereas LiDAR categories were classified at the 4 ha scale. In addition, refinement of LiDAR categories to include all canopy gap sizes, also helped explain some variation among certain response variables. However, reclassification of LiDAR categories according to

scale and refinement did not help elucidate all patterns seen in response variables among LiDAR categories (Appendix C, Tables 14 & 15).

Additionally, although not assessed, disparities among LiDAR classification break points of crown and understory closure and ground-based measures of crown and understory closure, may also partially explain the low statistical power to differentiate among LiDAR categories for response variables, most notably ground-based crown and understory closure. Based on the break points used for LiDAR crown (high > 94% and low ≤ 94%) and understory (high >55% and low ≤ 55%) closure categories in this study, it is not surprising that many response variables typically varied by LiDAR understory closure or an interaction between understory and crown closure and not crown closure alone. The continuous values used to create LiDAR categories had greater variation among understory closure categories than among crown closure categories, and were more comparable to the variation seen in ground-based measures of understory closure (Appendix C, Table 13).

Temporal scale was also a potential issue because the time of LiDAR acquisition (2009) and that of ground-based data collection (2012) had a three-year lag. Recent research by Vierling et al. (2014) has explored this issue and concluded that a six year lag between field data collection and LiDAR acquisition had little effect on avian patterns in undisturbed coniferous forests of Idaho. However, the authors did note that this was just one example in one ecosystem and that further research is needed on this issue. HBEF has a complex history of disturbance, from selective logging in the late 18th century, to the broad-scale disturbance from the1938 hurricane (Bormann and Likens 1979), and more limited crown damage from the 1998 ice storm (Rhoads et al. 2002). However, in

the time frame of our study, HBEF has been undisturbed. The time lag between field data and LiDAR acquisition in our study might help explain the lack of relationships with LiDAR in some of our response variables, in particular the arthropod and avian data. In contrast, other response variables more directly related to forest structure (i.e., crown closure, basal area) would be expected to be less influenced by a time lag, especially in a largely undisturbed forest such as HBEF.

Lastly, simplified classification of raw LiDAR point clouds into surface models (i.e., DEM, nDSM, AGL, etc.) for further analysis may prove to be useful when assessing basic forest structural attributes (e.g., basal area, above ground biomass, canopy height, etc.). However, these classifications may be too coarse when assessing higher trophic levels (e.g., arthropods and avifauna) and their connections to forest structure. Limitations with the LiDAR data acquired for this study necessitated the processing of the raw LiDAR data into surface models. Further assessments of LiDAR to higher trophic levels should consider using the raw LiDAR point cloud to fully utilize the powerful three-dimensional nature of LiDAR.

These factors should be considered when utilizing LiDAR in ecological research and for further management and conservation of forested ecosystems. Despite these factors, LiDAR has been shown to be a powerful tool that is able to provide useful information about the three-dimensional structure of forest ecosystems and its complex relationship to higher trophic levels. Although our research partially supports this, additional study is needed to fully evaluate the utility of high-resolution LiDAR data in assessing forest structure and higher trophic levels.

APPENDIX B – Original study-design – references

Allen, D. C., C. J. Barnett, I. Millers, and D. Lachance. 1992. Temporal change (1988-1990) in sugar maple health, and factors associated with crown condition. Canadian Journal of Forest Research **22**:1776-1784.

Antonarakis, A. S., K. S. Richards, and J. Brasington. 2008. Object-based land cover classification using airborne LiDAR. Remote Sensing of Environment **112**:2988-2998.

Asner, G. P. 2009. Tropical forest carbon assessment: integrating satellite and airborne mapping approaches. Environmental Research Letters **4**:034009.

Asner, G. P., J. Mascaro, H. C. Muller-Landau, G. Vieilledent, R. Vaudry, M. Rasamoelina, J. S. Hall, and M. van Breugel. 2012. A universal airborne LiDAR approach for tropical forest carbon mapping. Oecologia **168**:1147-1160.

Barnes, B. V., D. R. Zak, S. R. Denton, and S. H. Spurr. 1997. Forest ecology. John Wiley and Sons.

Bauce, E. and D. C. Allen. 1991. Etiology of a sugar maple decline. Canadian Journal of Forest Research **21**:686-693.

Bechtold, W. A. and C. T. Scott. 2005. The forest inventory and analysis plot design. The enhanced forest inventory and analysis program-national sampling design and estimation procedures. US Department of Agriculture Forest Service, Asheville, NC:27-42.

Bechtold, W. A., Scott, C.T. 2005. The forest inventory and analysis plot design. Pages 37-52 *in* F. S. Department of Agriculture, editor. Department of Agriculture, Forest Service, Southern Research Station.

Bernier, B., D. Paré, and M. Brazeauu. 1989. Natural stresses, nutrient imbalances and forest decline in southeastern Quebec. Water, Air, and Soil Pollution **48**:239-250.

Blaschke, T. 2010. Object based image analysis for remote sensing. ISPRS Journal of Photogrammetry and Remote Sensing **65**:2-16.

Bormann, F. H. and G. E. Likens. 1979. Pattern and process in a forested ecosystem. Springer-Verlag.

Bradbury, R. B., R. A. Hill, D. C. Mason, S. A. Hinsley, J. D. Wilson, H. Balzter, G. Q. A. Anderson, M. J. Whittingham, I. J. Davenport, and P. E. Bellamy. 2005. Modelling relationships between birds and vegetation structure using airborne LiDAR data: a review with case studies from agricultural and woodland environments. Ibis **147**:443-452.

Bréda, N. J. J. 2003. Ground−based measurements of leaf area index: a review of methods, instruments and current controversies. Journal of Experimental Botany **54**:2403-2417.

Brennan, R. and T. Webster. 2006. Object-oriented land cover classification of lidar-derived surfaces. Canadian Journal of Remote Sensing **32**:162-172.

Brock, J. C., C. W. Wright, I. B. Kuffner, R. Hernandez, and P. Thompson. 2006. Airborne lidar sensing of massive stony coral colonies on patch reefs in the northern Florida reef tract. Remote Sensing of Environment **104**:31-42.

Chen, Q. 2007. Airborne LiDAR data processing and information extraction. Photogrammetric Engineering and Remote Sensing **73**:91-95.

Clawges, R., K. Vierling, L. Vierling, and E. Rowell. 2008. The use of airborne lidar to assess avian species diversity, density, and occurrence in a pine/aspen forest. Remote Sensing of Environment **112**:2064-2073.

Comerford, D. P., P. G. Schaberg, P. H. Templer, A. M. Socci, J. L. Campbell, and K. F. Wallin. 2013. Influence of experimental snow removal on root and canopy physiology of sugar maple trees in a northern hardwood forest. Oecologia **171**:261-269.

Cook, E. R. and L. A. Kairiukstis. 1990. Methods of dendrochronology: applications in the environmental sciences. Kluwer Academic Publishers, Dordrecht.

Cooke, R., B. Pendrel, C. Barnett, and D. Allen. 1996. North American Maple Project Cooperative Field Manual. USDA Forest Service Northwestern Area, State and Private Forestry, Durham, NH.

DeGraaf, R. M., J. B. Hestbeck, and M. Yamasaki. 1998. Associations between breeding bird abundance and stand structure in the White Mountains, New Hampshire and Maine, USA. Forest Ecology and Management **103**:217-233.

Denno, R. F., C. Gratton, M. A. Peterson, G. A. Langellotto, D. L. Finke, and A. F. Huberty. 2002. Bottom-up forces mediate natural-enemy impact in a phytophagous insect community. Ecology **83**:1443-1458.

Driscoll, C. T., G. B. Lawrence, A. J. Bulger, T. J. Butler, C. S. Cronan, C. Eagar, K. F. Lambert, G. E. Likens, J. L. Stoddard, and K. C. Weathers. 2001. Acidic Deposition in the Northeastern United States: Sources and Inputs, Ecosystem Effects, and Management Strategies: The effects of acidic deposition in the northeastern United States include the acidification of soil and water, which stresses terrestrial and aquatic biota. BioScience **51**:180-198.

Drohan, P., S. Stout, and G. Petersen. 2002. Sugar maple (< i> Acer saccharum</i> Marsh.) decline during 1979–1989 in northern Pennsylvania. Forest Ecology and Management **170**:1-17.

Dubayah, R., S. Sheldon, D. Clark, M. Hofton, J. Blair, G. Hurtt, and R. Chazdon. 2010. Estimation of tropical forest height and biomass dynamics using lidar remote sensing at La Selva, Costa Rica. Journal of Geophysical Research: Biogeosciences (2005–2012) **115**.

Duchesne, L., R. Ouimet, and D. Houle. 2002. Basal area growth of sugar maple in relation to acid deposition, stand health, and soil nutrients. Journal of Environmental Quality **31**:1676-1683.

Evans, J., A. Hudak, R. Faux, and A. M. Smith. 2009. Discrete Return Lidar in Natural Resources: Recommendations for Project Planning, Data Processing, and Deliverables. Remote Sensing **1**:776-794.

Falkowski, M. J., J. S. Evans, S. Martinuzzi, P. E. Gessler, and A. T. Hudak. 2009. Characterizing forest succession with lidar data: An evaluation for the Inland Northwest, USA. Remote Sensing of Environment **113**:946-956.

Fernandez, J. C., S. A., J. Caceres, K. C. Slatton, M. Starek, and R. Kumar. 2007. An Overview of LiDAR Point Cloud Processing Software. Pages 1-27, Geosensing Engineering and Mapping (GEM), Civil and Coastal Engineering Department, University of Florida.

Finke, D. L. and R. F. Denno. 2004. Predator diversity dampens trophic cascades. Nature **429**:407-410.

García-Feced, C., D. J. Tempel, and M. Kelly. 2011. LiDAR as a Tool to Characterize Wildlife Habitat: California Spotted Owl Nesting Habitat as an Example. Journal of Forestry **109**:436-443.

Gatziolis, D. 2009. Precise FIA plot registration using field and dense LIDAR data. Pages 243-249 Proceedings of the eigth annual forest inventory and analysis symposium. United States Dept. of Agriculture, Forest Service General Technical Report WO-79, Washington, D.C.

Gatziolis, D. 2012. Advancements in LiDAR-based registration of FIA field plots. Pages 432-437. United States Dept. of Agriculture, Forest Service General Technical Report NRS-P-105, Washington, D.C.

Gatziolis, D. and H.-E. Andersen. 2008. A Guide to LiDAR Data Acquisition and Processing for the Forests of the Pacific Northwest. Pages 1-32 *in* U. F. Service, editor. USDA Forest Service, Pacific Northwest Research Station.

Gaulton, R. and T. J. Malthus. 2010. LiDAR mapping of canopy gaps in continuous cover forests: A comparison of canopy height model and point cloud based techniques. International Journal of Remote Sensing **31**:1193-1211.

Goetz, S., D. Steinberg, R. Dubayah, and B. Blair. 2007. Laser remote sensing of canopy habitat heterogeneity as a predictor of bird species richness in an eastern temperate forest, USA. Remote Sensing of Environment **108**:254-263.

Goetz, S. J., D. Steinberg, M. G. Betts, R. T. Holmes, P. J. Doran, R. Dubayah, and M. Hofton. 2010. Lidar remote sensing variables predict breeding habitat of a Neotropical migrant bird. Ecology **91**:1569-1576.

Goff, F. G. and D. West. 1975. Canopy-understory interaction effects on forest population structure. Forest Science **21**:98-108.

Goßner, M. M. 2009. Light intensity affects spatial distribution of Heteroptera in deciduous forests. European Journal of Entomology **106**:241-252.

Halaj, J., D. W. Ross, and A. R. Moldenke. 2000. Importance of habitat structure to the arthropod food−web in Douglas−fir canopies. Oikos **90**:139-152.

Halman, J. M., P. G. Schaberg, G. J. Hawley, C. F. Hansen, and T. Fahey. 2014. Differential impacts of calcium and aluminum treatments on sugar maple and American beech growth dynamics. Canadian Journal of Forest Research.

Herms, D. A. and W. J. Mattson. 1992. The dilemma of plants: to grow or defend. Quarterly Review of Biology:283-335.

Hofton, M. A., L. Rocchio, J. B. Blair, and R. Dubayah. 2002. Validation of vegetation canopy lidar sub-canopy topography measurements for a dense tropical forest. Journal of Geodynamics **34**:491-502.

Hollaus, M., W. Wagner, K. Schadauer, B. Maier, and K. Gabler. 2009. Growing stock estimation for alpine forests in Austria: a robust lidar-based approach. Canadian Journal of Forest Research **39**:1387-1400.

Holmes, R. L. 1983. Computer-assisted quality control in tree-ring dating and measurement. Tree-ring bulletin **43**:69-78.

Holmes, R. T. and S. K. Robinson. 1981. Tree Species Preferences of Foraging Insectivorous Birds in a Northern Hardwoods Forest. Oecologia **48**:31-35.

Holmes, R. T., N. L. Rodenhouse, and T. S. Sillett. 2005. Black-throated Blue Warbler (*Setophaga caerulescens*). The Birds of North America Online (A. Poole, Ed.). Retrieved from The Birds of North America Online: http://bna.birds.cornell.edu/bna/species/087, Ithaca: Cornell Lab of Ornithology.

Holmes, R. T., J. C. Schultz, and P. Nothnagle. 1979. Bird predation on forest insects: an exclosure experiment. Science **206**:462-463.

Horsley, S. B., R. P. Long, S. W. Bailey, R. A. Hallett, and T. J. Hall. 2000. Factors associated with the decline disease of sugar maple on the Allegheny Plateau. Canadian Journal of Forest Research **30**:1365-1378.

Houston, D. R. 1999. History of sugar maple decline. Pages 19-26 *in* Sugar maple ecology and health: Proceedings of an International Symposium, Warren, Pa. Edited by SB Horsley and RP Long. US For. Serv. Gen. Tech. Rep. NE-261.

Hudak, A. T., N. L. Crookston, J. S. Evans, M. J. Falkowski, A. M. S. Smith, P. E. Gessler, and P. Morgan. 2006. Regression modeling and mapping of coniferous forest basal area and tree density from discrete-return lidar and multispectral satellite data. Canadian Journal of Remote Sensing **32**:126-138.

Hudak, A. T., N. L. Crookston, J. S. Evans, D. E. Hall, and M. J. Falkowski. 2008. Nearest neighbor imputation of species-level, plot-scale forest structure attributes from LiDAR data. Remote Sensing of Environment **112**:2232-2245.

Hudak, A. T., M. A. Lefsky, W. B. Cohen, and M. Berterretche. 2002. Integration of lidar and Landsat ETM+ data for estimating and mapping forest canopy height. Remote Sensing of Environment **82**:397-416.

Huggett, B. A., P. G. Schaberg, G. J. Hawley, and C. Eagar. 2007. Long-term calcium addition increases growth release, wound closure, and health of sugar maple (Acer saccharum) trees at the Hubbard Brook Experimental Forest. Canadian Journal of Forest Research **37**:1692-1700.

Hyde, P., R. Dubayah, B. Peterson, J. B. Blair, M. Hofton, C. Hunsaker, R. Knox, and W. Walker. 2005. Mapping forest structure for wildlife habitat analysis using waveform lidar: Validation of montane ecosystems. Remote Sensing of Environment **96**:427-437.

Hyde, P., R. Dubayah, W. Walker, J. B. Blair, M. Hofton, and C. Hunsaker. 2006. Mapping forest structure for wildlife habitat analysis using multi-sensor (LiDAR, SAR/InSAR, ETM+, Quickbird) synergy. Remote Sensing of Environment **102**:63-73.

Jeffries, J. M., R. J. Marquis, and R. E. Forkner. 2006. Forest age influences oak insect herbivore community structure, richness, and density. Ecological Applications **16**:901-912.

Jensen, J. L. R., K. S. Humes, L. A. Vierling, and A. T. Hudak. 2008. Discrete return lidar-based prediction of leaf area index in two conifer forests. Remote Sensing of Environment **112**:3947-3957.

Johnson, M. D. 2000. Evaluation of an Arthropod Sampling Technique for Measuring Food Availability for Forest Insectivorous Birds (Evaluación de una Técnica para Muestrear Artrópodos para Medir la Disponibilidad de Alimento para Aves de Bosque Insectívoras). Journal of Field Ornithology **71**:88-109.

Jones, J. B. and V. W. Case. 1990. Sampling, handling and analyzing plant tissue samples. Ed. 3 edition. Soil Science Society of America, Madison, WI.

Jones, K. F. and N. D. Mulherin. 1998. An evaluation of the severity of the January 1998 ice storm in northern New England. DTIC Document.

Jones, T. G., N. C. Coops, and T. Sharma. 2011. Assessing the utility of LiDAR to differentiate among vegetation structural classes. Remote Sensing Letters **3**:231-238.

Juice, S. M., T. J. Fahey, T. G. Siccama, C. T. Driscoll, E. G. Denny, C. Eagar, N. L. Cleavitt, R. Minocha, and A. D. Richardson. 2006. Response of sugar maple to calcium addition to northern hardwood forest. Ecology **87**:1267-1280.

Kolb, T. and L. McCormick. 1993. Etiology of sugar maple decline in four Pennsylvania stands. Canadian Journal of Forest Research **23**:2395-2402.

Koricheva, J., S. Larsson, and E. Haukioja. 1998. Insect performance on experimentally stressed woody plants: a meta-analysis. Annual review of entomology **43**:195-216.

Koukoulas, S. and G. A. Blackburn. 2004. Quantifying the spatial properties of forest canopy gaps using LiDAR imagery and GIS. International Journal of Remote Sensing **25**:3049-3072.

Leckie, D., F. Gougeon, D. Hill, R. Quinn, L. Armstrong, and R. Shreenan. 2003. Combined high-density lidar and multispectral imagery for individual tree crown analysis. Canadian Journal of Remote Sensing **29**:633-649.

Lefsky, M., D. Turner, M. Guzy, and W. Cohen. 2005. Combining lidar estimates of aboveground biomass and Landsat estimates of stand age for spatially extensive validation of modeled forest productivity. Remote Sensing of Environment **95**:549-558.

Lefsky, M. A., W. B. Cohen, G. G. Parker, and D. J. Harding. 2002. Lidar Remote Sensing for Ecosystem Studies. BioScience **52**:19-30.

Lesak, A. A., V. C. Radeloff, T. J. Hawbaker, A. M. Pidgeon, T. Gobakken, and K. Contrucci. 2011. Modeling forest songbird species richness using LiDAR-derived measures of forest structure. Remote Sensing of Environment **115**:2823-2835.

Likens, G., C. Driscoll, D. Buso, T. Siccama, C. Johnson, G. Lovett, T. Fahey, W. Reiners, D. Ryan, and C. Martin. 1998. The biogeochemistry of calcium at Hubbard Brook. Biogeochemistry **41**:89-173.

Likens, G. E., C. T. Driscoll, and D. C. Buso. 1996. Long-term effects of acid rain: response and recovery of a forest ecosystem. Science-AAAS-Weekly Paper Edition **272**:244-245.

Lim, K., P. Treitz, M. Wulder, B. St-Onge, and M. Flood. 2003. LiDAR remote sensing of forest structure. Progress in Physical Geography **27**:88-106.

Long, R. P., S. B. Horsley, and P. R. Lilja. 1997. Impact of forest liming on growth and crown vigor of sugar maple and associated hardwoods. Canadian Journal of Forest Research **27**:1560-1573.

MacArthur, R. H. 1958. Population ecology of some warblers of northeastern coniferous forests. Ecology **39**:599-619.

MacArthur, R. H. and H. S. Horn. 1969. Foliage Profile by Vertical Measurements. Ecology **50**:802-804.

MacArthur, R. H. and J. W. MacArthur. 1961. On Bird Species Diversity. Ecology **42**:594-598.

Marquis, R. J. and C. J. Whelan. 1994. Insectivorous birds increase growth of white oak through consumption of leaf-chewing insects. Ecology **75**:2007-2014.

Marqus, D. A. and R. L. Ernst. 1991. The effects of stand structure after thinning on the growth of an Allegheny hardwood stand. Forest Science **37**:1182-1200.

Martinuzzi, S., L. A. Vierling, W. A. Gould, M. J. Falkowski, J. S. Evans, A. T. Hudak, and K. T. Vierling. 2009. Mapping snags and understory shrubs for a LiDAR-based assessment of wildlife habitat suitability. Remote Sensing of Environment **113**:2533-2546.

Montgomery, D. C. 2008. Design and analysis of experiments. Wiley, New York.

Müller, J. and R. Brandl. 2009. Assessing biodiversity by remote sensing in mountainous terrain: the potential of LiDAR to predict forest beetle assemblages. Journal of Applied Ecology **46**:897-905.

Næsset, E. 2007. Airborne laser scanning as a method in operational forest inventory: Status of accuracy assessments accomplished in Scandinavia. Scandinavian Journal of Forest Research **22**:433-442.

Næsset, E. and T. Gobakken. 2008. Estimation of above- and below-ground biomass across regions of the boreal forest zone using airborne laser. Remote Sensing of Environment **112**:3079-3090.

Nelson, R., C. Keller, and M. Ratnaswamy. 2005. Locating and estimating the extent of Delmarva fox squirrel habitat using an airborne LiDAR profiler. Remote Sensing of Environment **96**:292-301.

Nur, N., S. L. Jones, and G. R. Geupel. 1999. Statistical guide to data analysis of avian monitoring programs. US Fish and Wildlife Service.

Pascual, C., A. García-Abril, L. G. García-Montero, S. Martín-Fernández, and W. B. Cohen. 2008. Object-based semi-automatic approach for forest structure characterization using lidar data in heterogeneous Pinus sylvestris stands. Forest Ecology and Management **255**:3677-3685.

Pesonen, A., M. Maltamo, K. Eerikäinen, and P. Packalèn. 2008. Airborne laser scanning-based prediction of coarse woody debris volumes in a conservation area. Forest Ecology and Management **255**:3288-3296.

Polis, G. A. 1999. Why are parts of the world green? Multiple factors control productivity and the distribution of biomass. Oikos:3-15.

Ralph, C. J., S. Droege, and J. R. Sauer. 1995. Managing and Monitoring Birds Using Point Counts: Standards and Applications. General Technical Report, USDA Forest Service, Albany, CA.

Reutebuch, S. E., H.-E. Andersen, and R. J. McGaughey. 2005. Light Detection and Ranging (LIDAR): An Emerging Tool for Multiple Resource Inventory. Journal of Forestry **103**:286-292.

Rhoads, A. G., S. P. Hamburg, T. J. Fahey, T. G. Siccama, E. N. Hane, J. Battles, C. Cogbill, J. Randall, and G. Wilson. 2002. Effects of an intense ice storm on the structure of a northern hardwood forest. Canadian Journal of Forest Research **32**:1763-1775.

Riaño, D., F. Valladares, S. Condés, and E. Chuvieco. 2004. Estimation of leaf area index and covered ground from airborne laser scanner (Lidar) in two contrasting forests. Agricultural and Forest Meteorology **124**:269-275.

Richardson, J. J., L. M. Moskal, and S.-H. Kim. 2009. Modeling approaches to estimate effective leaf area index from aerial discrete-return LIDAR. Agricultural and Forest Meteorology **149**:1152-1160.

Robinson, S. K. and R. T. Holmes. 1982. Foraging Behavior of Forest Birds: The Relationships Among Search Tactics, Diet, and Habitat Structure. Ecology **63**:1918-1931.

Robinson, S. K. and R. T. Holmes. 1984. Effects of Plant Species and Foliage Structure on the Foraging Behavior of Forest Birds. The Auk **101**:672-684.

Roth, R. R. 1976. Spatial heterogeneity and bird species diversity. Ecology **57**:773-782.

Schaberg, P. G., E. K. Miller, and C. Eagar. 2010. Assessing the threat that anthropogenic calcium depletion poses to forest health and productivity. Advances in Threat Assessment and Their Application to Forest and Rangeland Management:37.

Schaberg, P. G., J. W. Tilley, G. J. Hawley, D. H. DeHayes, and S. W. Bailey. 2006. Associations of calcium and aluminum with the growth and health of sugar maple trees in Vermont. Forest Ecology and Management **223**:159-169.

Schmid, K., K. Waters, B. Dingerson, R. M. Hadley, J. Carter, J. Dare, and N. C. S. Center. 2008. LiDAR 101: an introduction to LiDAR technology, data, and applications. Charleston, SC: NOAA Coastal Services Center.

Schwarz, P. A., T. J. Fahey, C. W. Martin, T. G. Siccama, and A. Bailey. 2001. Structure and composition of three northern hardwood–conifer forests with differing disturbance histories. Forest Ecology and Management **144**:201-212.

Schwarz, P. A., T. J. Fahey, and C. E. McCulloch. 2003. Factors controlling spatial variation of tree species abundance in a forested landscape. Ecology **84**:1862-1878.

Sherrill, K. R., M. A. Lefsky, J. B. Bradford, and M. G. Ryan. 2008. Forest structure estimation and pattern exploration from discrete-return lidar in subalpine forests of the central Rockies. Canadian Journal of Forest Research **38**:2081-2096.

Sherry, T. W. 1979. Competitive Interactions and Adaptive Strategies of American Redstarts and Least Flycatchers in a Northern Hardwoods Forest. The Auk **96**:265-283.

Sherry, T. W. and R. T. Holmes. 1988. Habitat selection by breeding American Redstarts in response to a dominant competitor, the Least Flycatcher. The Auk:350-364.

Shure, D. and D. Phillips. 1991. Patch size of forest openings and arthropod populations. Oecologia **86**:325-334.

Smith, K. M., W. S. Keeton, T. M. Donovan, and B. Mitchell. 2008. Stand-level forest structure and avian habitat: scale dependencies in predicting occurrence in a heterogeneous forest. Forest Science **54**:36-46.

Solberg, S., E. Næsset, K. H. Hanssen, and E. Christiansen. 2006. Mapping defoliation during a severe insect attack on Scots pine using airborne laser scanning. Remote Sensing of Environment **102**:364-376.

Speer, J. H. 2010. Fundamentals of tree ring research. University of Arizona Press.

St-Onge, B. and U. Vepakomma. 2004. Assessing Forest Gap Dynamics and Growth Using Multi-temporal Laser Scanner Data. International Archives of Photogrammetry, Remote Sensing and Spatial Information Sciences **36**:173-178.

Stephens, P., P. Watt, D. Loubser, A. Haywood, and M. Kimberley. 2007. Estimation of carbon stocks in New Zealand planted forests using airborne scanning LiDAR. Pages 389-394 *in* ISPRS Workshop on Laser Scanning 2007 and SilviLaser 2007. Citeseer.

Stiling, P. and D. C. Moon. 2005. Quality or quantity: the direct and indirect effects of host plants on herbivores and their natural enemies. Oecologia **142**:413-420.

Stokes, M. A. and T. L. Smiley. 1968. An introduction to tree-ring dating. University of Chicago Press, Chicago, IL.

Strengbom, J., J. Witzell, A. Nordin, and L. Ericson. 2005. Do multitrophic interactions override N fertilization effects on Operophtera larvae? Oecologia **143**:241-250.

Swatantran, A., R. Dubayah, S. Goetz, M. Hofton, M. G. Betts, M. Sun, M. Simard, and R. Holmes. 2012. Mapping Migratory Bird Prevalence Using Remote Sensing Data Fusion. PLoS ONE **7**:e28922.

Swatantran, A., R. Dubayah, D. Roberts, M. Hofton, and J. B. Blair. 2011. Mapping biomass and stress in the Sierra Nevada using lidar and hyperspectral data fusion. Remote Sensing of Environment **115**:2917-2930.

van Aardt, J. A. N., R. H. Wynne, and R. G. Oderwald. 2006. Forest Volume and Biomass Estimation Using Small-Footprint Lidar-Distributional Parameters on a Per-Segment Basis. Forest Science **52**:636-649.

Van Bael, S. A., J. D. Brawn, and S. K. Robinson. 2003. Birds defend trees from herbivores in a Neotropical forest canopy. Proceedings of the National Academy of Sciences **100**:8304-8307.

van Doorn, N. S., J. J. Battles, T. J. Fahey, T. G. Siccama, and P. A. Schwarz. 2011. Links between biomass and tree demography in a northern hardwood forest: a decade of stability and change in Hubbard Brook Valley, New Hampshire. Canadian Journal of Forest Research **41**:1369-1379.

Van Ewjik, K. Y., P. M. Treitz, and N. A. Scott. 2011. Characterizing forest succession in Central Ontario using LiDAR-derived indices. Photogrammetric Engineering and Remote Sensing **77**:261-269.

van Leeuwen, M. and M. Nieuwenhuis. 2010. Retrieval of forest structural parameters using LiDAR remote sensing. European Journal of Forest Research **129**:749-770.

Vierling, K., C. Bässler, R. Brandl, L. Vierling, I. Weiß, and J. Müller. 2011. Spinning a laser web: predicting spider distributions using LiDAR. Ecological Applications **21**:577-588.

Vierling, K. T., C. E. Swift, A. T. Hudak, J. C. Vogeler, and L. A. Vierling. 2014. How much does the time lag between wildlife field-data collection and LiDAR-data acquisition matter for studies of animal distributions? A case study using bird communities. Remote Sensing Letters **5**:185-193.

Wehr, A. and U. Lohr. 1999. Airborne laser scanning—an introduction and overview. ISPRS Journal of Photogrammetry and Remote Sensing **54**:68-82.

Whelan, C. J. 2001. Foliage structure influences foraging of insectivorous forest birds: an experimental study. Ecology **82**:219-231.

White, T. 1984. The abundance of invertebrate herbivores in relation to the availability of nitrogen in stressed food plants. Oecologia **63**:90-105.

Wigley, T., K. Briffa, and P. Jones. 1984. On the average value of correlated time series, with applications in dendroclimatology and hydrometeorology. Journal of Climate and Applied Meteorology **23**:201-213.

Woods, K. D. 1984. Patterns of tree replacement: canopy effects on understory pattern in hemlock-northern hardwood forests. Vegetatio **56**:87-107.

Yamaguchi, D. K. 1991. A simple method for cross-dating increment cores from living trees. Canadian Journal of Forest Research **21**:414-416.

Zimble, D. A., D. L. Evans, G. C. Carlson, R. C. Parker, S. C. Grado, and P. D. Gerard. 2003. Characterizing vertical forest structure using small-footprint airborne LiDAR. Remote Sensing of Environment **87**:171-182.

APPENDIX C – Original study-design – tables, figures and supplemental data

Table 7. Means (± SE) of ground truthing and site factors (% volumetric soil moisture, temperature (°C), and % relative humidity) by LiDAR crown and understory closure category, collected during 2012 at Hubbard Brook Experimental Forest, NH, USA. Significant differences among LiDAR category means are displayed in bold.

Response variable	Significance	LiDAR crown & understory closure category			
		High crown High understory	High crown Low understory	Low crown High understory	Low crown Low understory
Ground truthing					
% Ground-based crown closure	NS	74.85 ± 3.73	82.30 ± 1.41	77.11 ± 3.49	80.37 ± 2.19
% Ground-based understory closure	**	**96.52 ± 1.69^{a}**	**86.81 ± 2.20^{b}**	**95.33 ± 1.32^{a}**	**85.56 ± 3.21^{b}**
Site factors					
% volumetric soil moisture	NS	23.41 ± 1.23	24.99 ± 1.55	22.32 ± 0.98	23.63 ± 1.30
Minimum solar[1] temperature	**	**7.79 ± 0.15^{b}**	**8.17 ± 0.16^{a}**	**7.91 ± 0.15^{ab}**	**7.98 ± 0.14^{ab}**
Minimum solar[1] relative humidity	**	**38.44 ± 0.89^{b}**	**39.75 ± 0.81^{ab}**	**40.77 ± 0.64^{a}**	**38.86 ± 0.72^{ab}**

Means (±SE) with differing letters are statistically significantly different based on a Tukey HSD test

** Significant at $P \leq 0.05$, "NS" denotes no significance

[1] The quarter of the year with the greatest amount of sunshine (June 18th - Aug. 7th for this dataset)

Table 8. Mean (± SE) temperature and relative humidity by LiDAR crown and understory closure category, collected during 2012 at Hubbard Brook Experimental Forest, NH, USA. Significant differences among LiDAR category means are displayed in bold.

Response variable	Significance	LiDAR crown & understory closure category			
		High crown High understory	High crown Low understory	Low crown High understory	Low crown Low understory
Temperature (°C)					
Mean June	NS	17.29 ± 0.14	17.40 ± 0.15	17.36 ± 0.18	17.34 ± 0.17
Mean July	NS	18.14 ± 0.14	18.29 ± 0.13	18.26 ± 0.18	18.27 ± 0.16
Mean August	NS	17.86 ± 0.14	18.01 ± 0.13	17.98 ± 0.17	18.01 ± 0.16
Mean Sept.	NS	12.44 ± 0.13	12.62 ± 0.12	12.54 ± 0.16	12.62 ± 0.16
Mean Oct.	NS	12.58 ± 0.12	12.71 ± 0.11	12.60 ± 0.10	12.71 ± 0.11
Mean Solar[1]	NS	18.07 ± 0.14	18.21 ± 0.13	18.17 ± 0.17	18.19 ± 0.16
Mean Meterological[2]	NS	17.22 ± 0.14	17.37 ± 0.13	17.33 ± 0.17	17.35 ± 0.16
Mean Astronomical[3]	NS	17.05 ± 0.14	17.20 ± 0.13	17.16 ± 0.17	17.18 ± 0.16
Median June	NS	16.84 ± 0.17	17.05 ± 0.16	17.03 ± 0.20	16.91 ± 0.18
Median July	NS	18.08 ± 0.14	18.24 ± 0.13	18.22 ± 0.17	18.20 ± 0.16
Median August	NS	17.90 ± 0.13	18.03 ± 0.12	17.98 ± 0.16	18.04 ± 0.14
Median Sept.	NS	12.41 ± 0.12	12.58 ± 0.13	12.46 ± 0.16	12.56 ± 0.15
Median Oct.	NS	13.03 ± 0.08	13.11 ± 0.07	13.06 ± 0.07	13.11 ± 0.08
Median Solar[1]	NS	18.02 ± 0.14	18.17 ± 0.12	18.16 ± 0.16	18.14 ± 0.14
Median Meterological[2]	NS	17.27 ± 0.12	17.42 ± 0.11	17.39 ± 0.15	17.39 ± 0.14
Median Astronomical[3]	NS	17.18 ± 0.12	17.34 ± 0.11	17.30 ± 0.15	17.29 ± 0.14
Min. June	*	**7.87 ± 0.16**[b]	**8.17 ± 0.16**[a]	**7.91 ± 0.15**[ab]	**8.08 ± 0.12**[ab]
Min. July	NS	9.83 ± 0.43	9.89 ± 0.31	10.30 ± 0.27	9.92 ± 0.37
Min. August	NS	9.03 ± 0.27	9.50 ± 0.21	9.42 ± 0.22	9.48 ± 0.31
Min. Sept.	NS	3.40 ± 0.33	3.59 ± 0.26	3.91 ± 0.21	3.65 ± 0.30
Min. Oct.	*	**7.52 ± 0.16**[ab]	**7.67 ± 0.15**[a]	**7.42 ± 0.12**[b]	**7.64 ± 0.16**[ab]

Table 8. (Cont.)

Response variable	Significance	LiDAR crown & understory closure category			
		High crown High understory	High crown Low understory	Low crown High understory	Low crown Low understory
Temperature (°C – Cont.)					
Min. Meterological[2]	NS	40.42 ± 0.61	41.22 ± 0.43	41.64 ± 0.27	41.01 ± 0.55
Min. Astronomical[3]	NS	38.22 ± 0.60	38.58 ± 0.52	39.11 ± 0.37	38.56 ± 0.55
Max. June	NS	28.43 ± 0.18	28.29 ± 0.23	28.08 ± 0.33	28.63 ± 0.33
Max. July	NS	26.87 ± 0.15	26.88 ± 0.20	26.80 ± 0.30	27.15 ± 0.34
Max. August	NS	26.58 ± 0.18	26.75 ± 0.16	26.56 ± 0.30	26.64 ± 0.27
Max. Sept.	NS	22.58 ± 0.17	23.02 ± 0.44	22.33 ± 0.38	23.37 ± 0.88
Max. Oct.	NS	19.55 ± 0.50	19.62 ± 0.63	19.45 ± 0.59	20.27 ± 0.63
Max. Solar[1]	NS	28.43 ± 0.18	28.29 ± 0.23	28.08 ± 0.33	28.63 ± 0.33
Max. Meterological[2]	NS	28.43 ± 0.18	28.29 ± 0.23	28.08 ± 0.33	28.63 ± 0.33
Max. Astronomical[3]	NS	28.43 ± 0.18	28.29 ± 0.23	28.08 ± 0.33	28.63 ± 0.33
Relative humidity (%)					
Mean June	NS	82.77 ± 0.70	83.20 ± 0.45	82.64 ± 0.61	83.46 ± 0.66
Mean July	NS	81.82 ± 0.85	82.29 ± 0.50	81.75 ± 0.67	82.13 ± 0.80
Mean August	NS	87.28 ± 0.89	88.01 ± 0.54	87.39 ± 0.71	87.55 ± 0.76
Mean Sept.	NS	89.60 ± 0.70	89.99 ± 0.52	89.83 ± 0.67	89.64 ± 0.63
Mean Oct.	NS	97.11 ± 0.45	97.50 ± 0.26	97.39 ± 0.24	97.25 ± 0.31
Mean Solar[1]	NS	84.72 ± 0.76	85.28 ± 0.42	84.74 ± 0.59	85.11 ± 0.68
Mean Meterological[2]	NS	85.03 ± 0.81	85.57 ± 0.47	85.05 ± 0.64	85.35 ± 0.73
Mean Astronomical[3]	NS	85.07 ± 0.83	85.64 ± 0.49	85.11 ± 0.65	85.39 ± 0.73
Median June	NS	84.54 ± 1.34	84.85 ± 0.74	83.79 ± 0.74	85.64 ± 1.07
Median July	NS	83.49 ± 1.35	83.83 ± 0.74	82.64 ± 0.86	83.78 ± 1.29

Table 8. (Cont.)

Response variable	Significance	LiDAR crown & understory closure category			
		High crown High understory	High crown Low understory	Low crown High understory	Low crown Low understory
Relative humidity (% - Cont.)					
Median August	NS	89.87 ± 1.31	90.60 ± 0.73	89.36 ± 0.91	90.12 ± 1.11
Median Sept.	NS	93.05 ± 1.18	93.36 ± 0.87	92.57 ± 0.83	93.05 ± 0.95
Median Oct.	NS	99.66 ± 0.34	99.97 ± 0.03	100 ± < 0.01	100 ± < 0.01
Median Solar[1]	NS	87.83 ± 1.15	88.31 ± 0.59	87.25 ± 0.75	88.21 ± 1.02
Median Meterological[2]	NS	87.71 ± 1.29	88.21 ± 0.68	87.22 ± 0.86	88.08 ± 1.10
Median Astronomical[3]	NS	87.83 ± 1.32	88.40 ± 0.71	87.36 ± 0.88	88.22 ± 1.11
Min. June	**	**40.08 ± 0.99^{ab}**	**40.50 ± 0.84^{ab}**	**42.30 ± 0.53^{a}**	**39.58 ± 0.75^{b}**
Min. July	**	**39.05 ± 0.84^{b}**	**41.04 ± 0.55^{a}**	**40.87 ± 0.65^{a}**	**39.91 ± 0.79^{a}**
Min. August	*	**44.45 ± 0.84^{ab}**	**46.07 ± 2.06^{ab}**	**48.31 ± 1.65^{a}**	**43.26 ± 1.20^{b}**
Min. Sept.	NS	51.43 ± 0.99	50.63 ± 1.74	51.45 ± 1.14	47.94 ± 1.98
Min. Oct.	NS	67.79 ± 1.69	68.90 ± 3.04	68.44 ± 2.57	65.36 ± 2.63
Min. Solar[1]	**	**38.44 ± 0.89^{b}**	**39.75 ± 0.81^{ab}**	**40.77 ± 0.64^{a}**	**38.86 ± 0.72^{a}**
Min. Meterological[2]	**	**38.44 ± 0.89^{b}**	**39.63 ± 0.84^{ab}**	**40.77 ± 0.64^{a}**	**38.63 ± 0.81^{b}**
Min. Astronomical[3]	**	**38.44 ± 0.89^{b}**	**39.63 ± 0.84^{ab}**	**40.77 ± 0.64^{a}**	**38.63 ± 0.81^{b}**

Means (±SE) with differing letters are statistically significantly different based on a Tukey HSD test

* Significant at $P \leq 0.10$, ** Significant at $P \leq 0.05$

[1] The quarter of the year with the greatest amount of sunshine (~May 7th - Aug. 7th, 2012)

[2] The quarter of the year with the warmest temperatures (~June 18th - Sept. 18th, 2012)

[3] Summer solstice (June 20th, 2012) through fall equinox (Sept. 21st, 2012)

Table 9. Sub-plot and micro-plot basal area (m^2/ha) and micro-plot stems/ha by tree species at Hubbard Brook Experimental Forest, NH, USA

Sub-plot (trees > 12.5 cm)			Micro-plot (trees 2.5 - 12.5 cm)			Micro-plot (≤ 12.5 cm)		
Species	Total BA	Percent	Species	Total BA	Percent	Species	Total Stems	Stems/Ha
Betula alleghaniensis	428.9	35.5	*Fagus grandifolia*	64.8	63.1	*Fagus grandifolia*	123	21964.3
Acer saccharum	394.8	32.6	*Acer saccharum*	15	14.6	*Viburnum lentago*	111	19821.4
Fagus grandifolia	203.5	16.8	*Acer pensylvanicum*	8.1	7.9	*Acer pensyvanicum*	92	16428.6
Fraxinus americana	74.7	6.2	*Picea rubens*	7	6.8	*Acer saccharum*	66	11785.7
Acer rubrum	46.1	3.8	*Tsuga Canadensis*	5	4.8	*Picea rubens*	33	5892.9
Picea rubens	36.3	3	*Abies balsamea*	2.5	2.4	*Acer spicatum*	26	4642.9
Abies balsamea	10	0.8	*Acer spicatum*	0.2	0.2	*Betula alleghaniensis*	20	3571.4
Tsuga canadensis	5.7	0.5	*Betula alleghaniensis*	0.1	0.1	*Acer rubrum*	17	3035.7
Betula papyrifera	4.9	0.4	*Acer rubrum*	0	0	*Abies balsamea*	10	1785.7
Acer pensylvanicum	4.6	0.4	*Betula papyrifera*	0	0	*Fraxinus americana*	10	1785.7
Unknown	0.3	0	*Fraxinus americana*	0	0	*Sorbus americana*	3	535.7
						Tsuga Canadensis	3	535.7
						Lonicera sp.	2	357.1
Conifer	52	4.3	Conifer	14.5	11.6	*Cornus alternifolia*	1	178.6
Deciduous	1157.9	95.7	Deciduous	88.3	88.4	*Quercus rubra*	1	178.6
Total BA	1209.8	100	Total BA	102.7	100	Total Stems	519	92678.6

Table 10. Mean (± SE) foliar cation concentrations of sunlit/upper canopy and mid-canopy sugar maple and yellow birch foliage by LiDAR crown and understory closure category, collected during 2012 at Hubbard Brook Experimental Forest, NH, USA. Significant differences among LiDAR category means are displayed in bold.

Species & cation/molar ratio	Significance	LiDAR crown & understory closure category			
		High crown High understory	High crown Low understory	Low crown High understory	Low crown Low understory
Foliar cation concentration - sunlit/upper canopy ($mg \cdot kg^{-1}$)					
Sugar maple:					
Ca	NS	4965.89 ± 565.79	5534.03 ± 192.17	5650.07 ± 626.43	5214.28 ± 429.92
Al	NS	69.85 ± 10.95	63.48 ± 9.13	70.85 ± 11.66	72.39 ± 10.33
K	NS	7470.56 ± 366.76	8152.25 ± 481.53	8311.45 ± 452.42	7911.42 ± 454.05
P	NS	1455.37 ± 175.26	1546.09 ± 222.51	1347.03 ± 136.33	1598.29 ± 215.66
Mg	NS	976.82 ± 107.59	1045.7 ± 50.46	1035.3 ± 107.52	972.79 ± 89.55
Mn	NS	1307.39 ± 192.33	1020.60 ± 104.65	1324.35 ± 169.05	989.51 ± 108.72
Ca:Al Molar Ratio	NS	55.71 ± 8.91	70.41 ± 11.09	70.14 ± 18.9	55.91 ± 8.49
Ca:Mn Molar Ratio	NS	6.17 ± 1.21	8.19 ± 1.07	6.83 ± 1.22	7.66 ± 0.75
Mg:Mn Molar Ratio	NS	1.97 ± 0.35	2.64 ± 0.45	2.08 ± 0.36	2.36 ± 0.25
Yellow birch:					
Ca	**	**7966.97 ± 489.31^{b}**	**10122.90 ± 667.88^{a}**	**7969.18 ± 384.25^{b}**	**8757.82 ± 472.02^{ab}**
Al	NS	68.13 ± 8.32	59.01 ± 9.34	61.31 ± 9.24	51.73 ± 6.93
K	NS	9653.69 ± 748.75	11814.4 ± 972.45	11776.79 ± 714.89	11289.71 ± 974.94
P	NS	1425.87 ± 108.95	1479.61 ± 79.13	1291.43 ± 80.48	1729.22 ± 226.74
Mg	NS	2347.36 ± 140.4	2479.96 ± 132.97	2197.16 ± 88.13	2323.18 ± 125.26
Mn	NS	1794.31 ± 259.1	1727.24 ± 200.49	1522.94 ± 251.59	1322.55 ± 126.98
Ca:Al Molar Ratio	*	**85.06 ± 8.35^{b}**	**132.98 ± 16.67^{a}**	**101.31 ± 13.83^{ab}**	**130.84 ± 18.4^{ab}**
Ca:Mn Molar Ratio	NS	7.10 ± 1.02	8.70 ± 0.98	8.96 ± 1.51	9.88 ± 1.19
Mg:Mn Molar Ratio	NS	3.42 ± 0.49	3.59 ± 0.50	4.18 ± 0.81	4.29 ± 0.48

Table 10. (Cont.)

Cation/molar ratio	Significance	LiDAR crown & understory closure category			
		High crown High understory	High crown Low understory	Low crown High understory	Low crown Low understory
Foliar cation concentration - mid-canopy ($mg \cdot kg^{-1}$)					
Sugar maple:					
Ca	NS	6745.85 ± 863.16	9075.61 ± 956.57	6457.17 ± 1017.12	6734.93 ± 866.16
Al	NS	29.44 ± 5.79	34.77 ± 6.65	32.64 ± 6.38	29.07 ± 5.33
K	NS	1302.36 ± 132.09	1947.85 ± 321.95	1236.20 ± 49.96	1319.76 ± 173.28
P	NS	1284.30 ± 351.01	1186.91 ± 261.22	1526.68 ± 370.01	866.56 ± 131.75
Mg	**	**1199.88 ± 56.48^{ab}**	**1233.81 ± 61.89^{a}**	**1106.6 ± 42.75^{b}**	**1120.23 ± 56.42^{ab}**
Mn	NS	11281.88 ± 2097.91	13435.27 ± 2696.83	7755.81 ± 392.7	9959.02 ± 1689.64
Ca:Al Molar Ratio	NS	331.46 ± 130.67	280.33 ± 82.31	213.33 ± 62.46	216.1 ± 53.56
Ca:Mn Molar Ratio	NS	12.58 ± 3.58	36.76 ± 21.35	8.03 ± 1.58	14.78 ± 4.48
Mg:Mn Molar Ratio	NS	4.18 ± 1.31	16.44 ± 11	2.83 ± 0.58	4.67 ± 1.4
Yellow birch:					
Ca	NS	13370.39 ± 2708.15	14288.63 ± 3033.39	9677.17 ± 568.67	10051.40 ± 881.92
Al	NS	33.53 ± 5.31	36.76 ± 5.09	35.06 ± 4.95	36.99 ± 5.74
K	NS	4058.83 ± 818.80	3493.98 ± 656.53	2673.96 ± 152.71	2559.17 ± 239.52
P	NS	1528.99 ± 370.02	1671.71 ± 304.80	1962.49 ± 377.69	1260.77 ± 150.37
Mg	NS	1396.42 ± 111.03	1385.27 ± 79.10	1251.45 ± 54.54	1220.05 ± 70.07
Mn	NS	17365.71 ± 3175.19	18199.24 ± 4228.39	12189.46 ± 465.62	13194.72 ± 1253.79
Ca:Al Molar Ratio	NS	369.25 ± 99.81	345.05 ± 114.83	254.71 ± 64.85	231.95 ± 44.53
Ca:Mn Molar Ratio	NS	23.67 ± 10.16	30.64 ± 20.08	8.09 ± 1	14.24 ± 4.04
Mg:Mn Molar Ratio	NS	11.73 ± 5.1	11.81 ± 7.38	3.75 ± 0.56	6.09 ± 1.87

Means (±SE) with differing letters are statistically significantly different based on a Tukey HSD test

* Significant at $P \leq 0.10$, ** Significant at $P \leq 0.05$, "NS" denotes no significance

Table 11. Mean (± SE) arthropod and avian factors by LiDAR crown and understory closure category, collected during 2012 at Hubbard Brook Experimental Forest, NH, USA.

Response variable	Significance	LiDAR crown & understory closure category			
		High crown High understory	High crown Low understory	Low crown High understory	Low crown Low understory
Arthropod measures					
Arthropod mass	NS	5.94 ± 2.47	12.13 ± 4.77	7.89 ± 3.25	3.08 ± 2.19
Lepidopteran larvae mass	NS	6.66 ± 2.51	13.03 ± 4.79	10.17 ± 3.24	4.21 ± 2.21
Avian measures					
Shannon diversity index	NS	1.96 ± 0.08	1.90 ± 0.09	1.87 ± 0.07	2.00 ± 0.05
Ecological species diversity	NS	7.29 ± 0.62	6.91 ± 0.56	6.63 ± 0.53	7.43 ± 0.32
Evenness	NS	0.87 ± 0.01	0.90 ± 0.01	0.89 ± <0.01	0.89 ± 0.01
Total # of individuals	NS	34.67 ± 2.86	30.33 ± 1.89	31.89 ± 2.12	32.22 ± 2.14
Mean # of individuals	NS	8.67 ± 0.71	7.58 ± 0.47	7.97 ± 0.53	8.06 ± 0.53
Cumulative species richness	NS	9.78 ± 0.81	8.56 ± 0.73	8.44 ± 0.77	9.67 ± 0.53

"NS" denotes no significance

Table 12. Linear relationships between total arthropod mass, Lepidopteran adult mass, Lepidopteran larval mass and various measures of foliar nutrition for both upper and mid canopy sugar maple and yellow birch foliage, collected during 2012 at Hubbard Brook Experimental Forest, NH, USA. Significance, beta values (β; i.e., effect size) and standard errors (SE) are reported. Significant differences among LiDAR category means are displayed in bold.

	Upper/sunlit canopy			Mid-canopy		
	Significance	β	SE	Significance	β	SE
Sugar maple						
Total arthropod mass						
N	N/A	N/A	N/A	**	**22.2290**	**8.13400**
P	NS	0.00190	0.00360	*	**0.02595**	**0.01121**
K	NS	0.00079	0.00153	NS	0.00013	0.00034
C	N/A	N/A	N/A	NS	1.23700	1.22300
Lepidopteran mass (adult)						
N	N/A	N/A	N/A	NS	-0.22940	0.83540
P	NS	-0.00024	0.00033	NS	-0.00132	0.00110
K	NS	0.00003	0.00001	NS	-0.00003	0.00003
C	N/A	N/A	N/A	NS	-0.16000	0.11220
Lepidopteran mass (larvae)						
N	N/A	N/A	N/A	*	**21.6470**	**8.15900**
P	NS	0.00224	0.00359	*	**0.02733**	**0.01109**
K	NS	0.00056	0.00153	NS	0.00017	0.00034
C	N/A	N/A	N/A	NS	1.37300	1.21600
Yellow birch						
Total arthropod mass						
N	N/A	N/A	N/A	**	**20.1900**	**6.97000**
P	NS	0.00020	0.00470	NS	0.01124	0.00791
K	NS	0.00081	0.00075	NS	0.00015	0.00024
C	N/A	N/A	N/A	NS	0.64520	1.21470
Lepidopteran mass (adult)						
N	N/A	N/A	N/A	NS	0.66310	0.71560
P	NS	-0.00002	0.00054	NS	-0.00065	0.00075
K	NS	0.00002	0.00007	NS	-0.00001	0.00002
C	N/A	N/A	N/A	NS	-0.14080	0.11100
Lepidopteran mass (larvae)						
N	N/A	N/A	N/A	**	**19.9610**	**6.97100**
P	NS	0.00034	0.00469	NS	0.01264	0.00783
K	NS	0.00075	0.00075	NS	0.00017	0.00024
C	N/A	N/A	N/A	NS	0.80820	1.20920

"NS" denotes not significant, "N/A" denotes not applicable due to no significance

* $P \leq 0.05$, ** $P \leq 0.01$

Table 13. Comparisons between continuous values (minimum, maximum, and range) of ground-based and LiDAR-derived crown and understory closure at Hubbard Brook Experimental Forest, NH, USA.

		LiDAR classifications			
	Ground-based	4 ha scale original routine	50m scale original routine	4 ha scale & no refinement	50m scale & no refinement
Crown closure					
Min	57.67	89.89	87.02	72.02	82.56
Max	96.67	98.08	99.71	97.50	98.57
Range	39.00	8.20	12.69	25.48	16.01
Understory closure					
Min	67.67	43.00	35.42	43.00	35.42
Max	100.00	78.15	83.98	78.15	83.98
Range	32.33	35.15	48.56	35.15	48.56

Table 14. The influence of LiDAR re-classification (by scale and refinement) on the significance of response variables by LiDAR crown and understory closure category.

Response variable	4 ha original routine	LiDAR re-classification		
		Scale	No refinement	Scale & no refinement
Ground truthing				
% crown closure	NS**	No Δ**	No Δ**	No Δ**
% understory closure	S	+ S	- S	- S
Site measures				
% volumetric soil moisture	NS	No Δ	+ S*	+ S**
Min. Solar temp. (°C)	S**	NS**	+ S**	- S**
Min. Solar rel. humidity (%)	S**	NS**	NS**	NS**
Stand-based measures				
Sub-plot basal area (m^2/ha)				
Standing dead	NS	No Δ	No Δ	+ S
Micro-plot basal area (m^2/ha)				
All crown positions	S	NS	NS	NS
Suppressed	NS	No Δ	No Δ	No Δ
Stem Counts				
Stems/ha - 1-4.9"	S	NS	- S	NS
Decline				
Crown vigor index	NS**	+ S**	No Δ*	+ S**
% branch dieback	S	+ S*	NS	+ S*
Tree-based measures				
Sugar maple BAI (cm^2)				
2009 (year of LiDAR acquisition)	S**	NS**	NS**	NS**
Post-ice storm/pre-LiDAR (1999-2008)	S**	NS**	NS**	NS**
Pre-ice storm (1988-1997)	S**	NS**	- S*	NS*
Yellow birch BAI (cm^2)				
2009 (year of LiDAR acquisition)	NS	No Δ	No Δ	No Δ
Post-ice storm (1999-2008)	NS	No Δ	No Δ	No Δ
Pre-ice storm (1988-1997)	NS	No Δ	No Δ	No Δ

Table 14. (Cont.)

Response variable	4 ha original routine	LiDAR re-classification		
		Scale	No refinement	Scale & no refinement
Foliar nutrition - sunlit/upper canopy ($mg \cdot kg^{-1}$)				
Sugar maple:				
Ca	NS**	No Δ**	No Δ**	No Δ**
Mn	NS**	+ S**	No Δ*	No Δ*
Ca:Al molar ratio	NS**	No Δ**	No Δ**	No Δ**
Ca:Mn molar ratio	NS**	No Δ**	+ S**	No Δ**
Yellow birch:				
Ca	S**	+ S**	- S**	- S**
Mn	NS	No Δ	No Δ	No Δ
Ca:Al molar ratio	S	+ S	+ S	+ S
Ca:Mn molar ratio	NS*	No Δ*	No Δ	No Δ
Foliar nutrition - mid-canopy ($mg \cdot kg^{-1}$)				
Sugar maple:				
Mg	S	+ S	NS	NS
Yellow birch:				
Mg	NS	No Δ	No Δ	No Δ
Arthropod measures				
Mean arthropd mass	NS	No Δ	No Δ	No Δ
Mean Lep. larvae mass	NS	No Δ	No Δ	No Δ
Avian measures				
Shannon diversity index	NS	No Δ	No Δ	No Δ
Ecological species diversity	NS	No Δ	No Δ	No Δ
Evenness	NS	No Δ	No Δ	No Δ
Total # of individuals	NS	No Δ	No Δ	No Δ
Mean # of individuals	NS	No Δ	No Δ	No Δ

"S" denotes a significant p-value ($\alpha=0.05$, unless otherwise noted)

"NS" denotes a p-value that is not significant ($\alpha=0.05$, unless otherwise noted)

"No Δ" = No change in significance from the 4 ha original routine classification

"+" denotes an improved p-value, "-" denotes a worse p-value

* Block significant at $P \leq 0.10$, ** Block significant at $P \leq 0.05$

Table 15. Non- significant response variables at the 4 ha original classification routine, and unchanged by scale and refinement.

Response variable	4 ha original routine	LiDAR re-classification		
		Scale	No refinement	Scale & no refinement
Site measures				
Temperature (°C)				
Mean solar temp.	NS**	No Δ**	No Δ**	No Δ**
Median solar temp.	NS**	No Δ**	No Δ**	No Δ**
Max. solar temp.	NS**	No Δ**	No Δ**	No Δ**
Relative humidity (%)				
Mean solar rel. humidity	NS**	No Δ**	No Δ**	No Δ**
Median solar rel. humidity	NS**	No Δ**	No Δ**	No Δ**
Stand measures				
Sub-plot basal area (m^2/ha)				
D, CD, I, S, Dead & Unclassified	NS	No Δ	No Δ	No Δ
D, CD, I, & S	NS	No Δ	No Δ	No Δ
D, CD, & I	NS	No Δ	No Δ	No Δ
D & CD	NS	No Δ	No Δ	No Δ
S & I	NS**	No Δ**	No Δ**	No Δ**
Stem counts				
Total stems/ha	NS	No Δ	No Δ	No Δ
Viburnam alnifolium stems/ha	NS*	No Δ*	No Δ**	No Δ**
Stems/Ha < 1"	NS	No Δ	No Δ	No Δ
Tree-based measures				
Sugar maple BAI (cm^2)				
Δ BAI (%) - 1970's & 2000's	NS**	No Δ**	No Δ**	No Δ**
Δ BAI (%) - 1970's & 2000-2012	NS**	No Δ**	No Δ**	No Δ**
BAI - Post LiDAR (2010-2012)	NS**	No Δ**	No Δ**	No Δ**
BAI - 2008-2010	NS**	No Δ**	No Δ**	No Δ**
Yellow birch BAI (cm^2)				
Δ BAI (%) - 1970's & 2000's	NS	No Δ	No Δ	No Δ
Δ BAI (%) - 1970's & 2000-2012	NS	No Δ	No Δ	No Δ
BAI - post-LiDAR (2010-2012)	NS	No Δ	No Δ	No Δ
BAI - 2008-2010	NS	No Δ	No Δ	No Δ

Table 15. (Cont.)

Species & cation/molar ratio	4 ha original routine	LiDAR re-classification		
		Scale	No refinement	Scale & no refinement
Foliar nutrition - sunlit/upper canopy ($mg \cdot kg^{-1}$)				
Sugar maple:				
Al	NS**	No Δ**	No Δ**	No Δ**
Mg	NS**	No Δ**	No Δ**	No Δ**
P	NS**	No Δ**	No Δ**	No Δ**
K	NS**	No Δ**	No Δ*	No Δ**
Mg:Mn molar ratio	NS**	No Δ**	No Δ**	No Δ**
Yellow birch:				
Al	NS*	No Δ*	No Δ*	No Δ*
Mg	NS**	No Δ	No Δ**	No Δ*
P	NS*	No Δ**	No Δ	No Δ*
K	NS	No Δ	No Δ	No Δ
Mg:Mn molar ratio	NS*	No Δ*	No Δ*	No Δ*
Foliar nutrition - mid-canopy ($mg \cdot kg^{-1}$)				
Sugar maple:				
Ca	NS*	No Δ*	No Δ*	No Δ**
Al	NS**	No Δ**	No Δ**	No Δ**
Mn	NS	No Δ	No Δ	No Δ
N	NS	No Δ	No Δ	No Δ
P	NS**	No Δ**	No Δ	No Δ
K	NS	No Δ	No Δ	No Δ
C	NS	No Δ	No Δ	No Δ
Ca:Al molar ratio	NS**	No Δ**	No Δ**	No Δ**
Ca:Mn molar ratio	NS	No Δ	No Δ	No Δ
Mg:Mn molar ratio	NS	No Δ	No Δ	No Δ

Table 15. (Cont.)

Species & cation/molar ratio	4 ha original routine	LiDAR re-classification		
		Scale	No refinement	Scale & no refinement
Foliar nutrition - mid-canopy ($mg \cdot kg^{-1}$)				
Yellow birch:				
Ca	NS	No Δ	No Δ	No Δ
Al	NS**	No Δ**	No Δ**	No Δ**
Mn	NS	No Δ	No Δ	No Δ
N	NS**	No Δ*	No Δ**	No Δ**
K	NS	No Δ	No Δ	No Δ
P	NS*	No Δ*	No Δ*	No Δ
C	NS**	No Δ**	No Δ**	No Δ**
Ca:Al molar ratio	NS	No Δ	No Δ*	No Δ*
Ca:Mn molar ratio	NS	No Δ	No Δ	No Δ
Mg:Mn molar ratio	NS	No Δ	No Δ	No Δ

"NS" denotes a p-value that is not significant, "No Δ" = No change in significance

* Block significant at $P \leq 0.10$, ** Block significant *at* $P \leq 0.05$

"D" = Dominant, "CD" = Co-dominant, "I" = Intermediate, & "S" = Suppressed

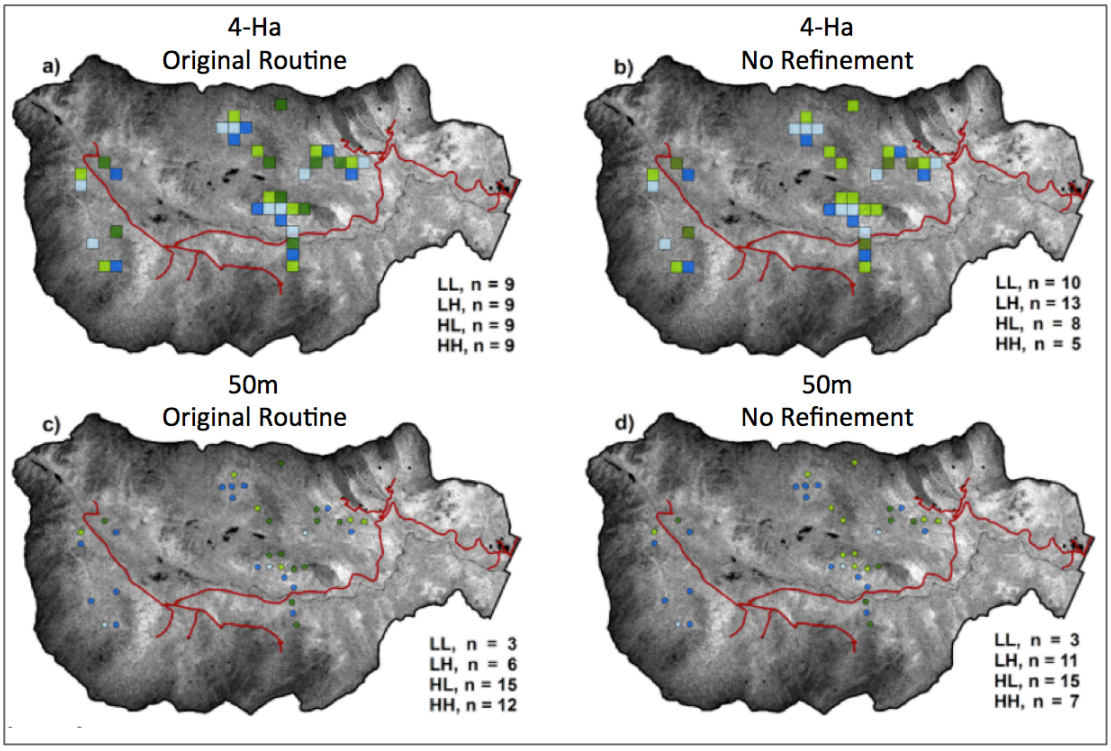

Figure 4. Hubbard Brook Experimental Forest, NH, USA – LiDAR classification schemes: a) 4 ha scale & original routine, b) 4 ha scale with no crown refinement, c) 50m scale & original routine, and d) 50m scale with no crown refinement.

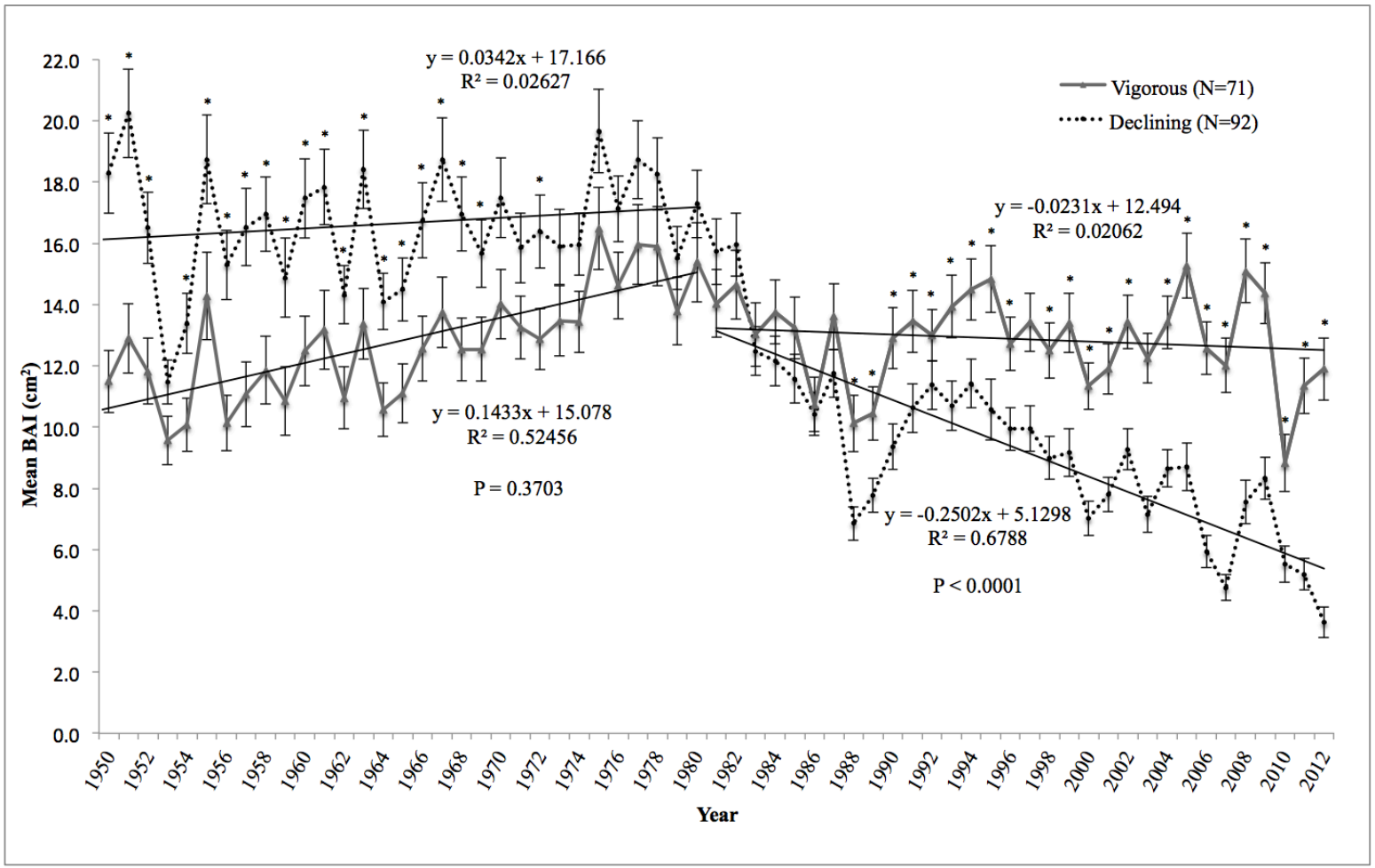

Figure 5. Mean basal area increment (BAI; ± SE) for sugar maple trees by crown vigor index at Hubbard Brook Experimental Forest, NH, USA. Individual years that are significantly different between vigor categories are indicated by an asterisk (based on an orthogonal contrast between categories with $P \leq 0.05$). Slope analyses indicate different growth trajectories for each vigor category and its significance between categories in the years 1950 – 1980 and 1981 – 2012.

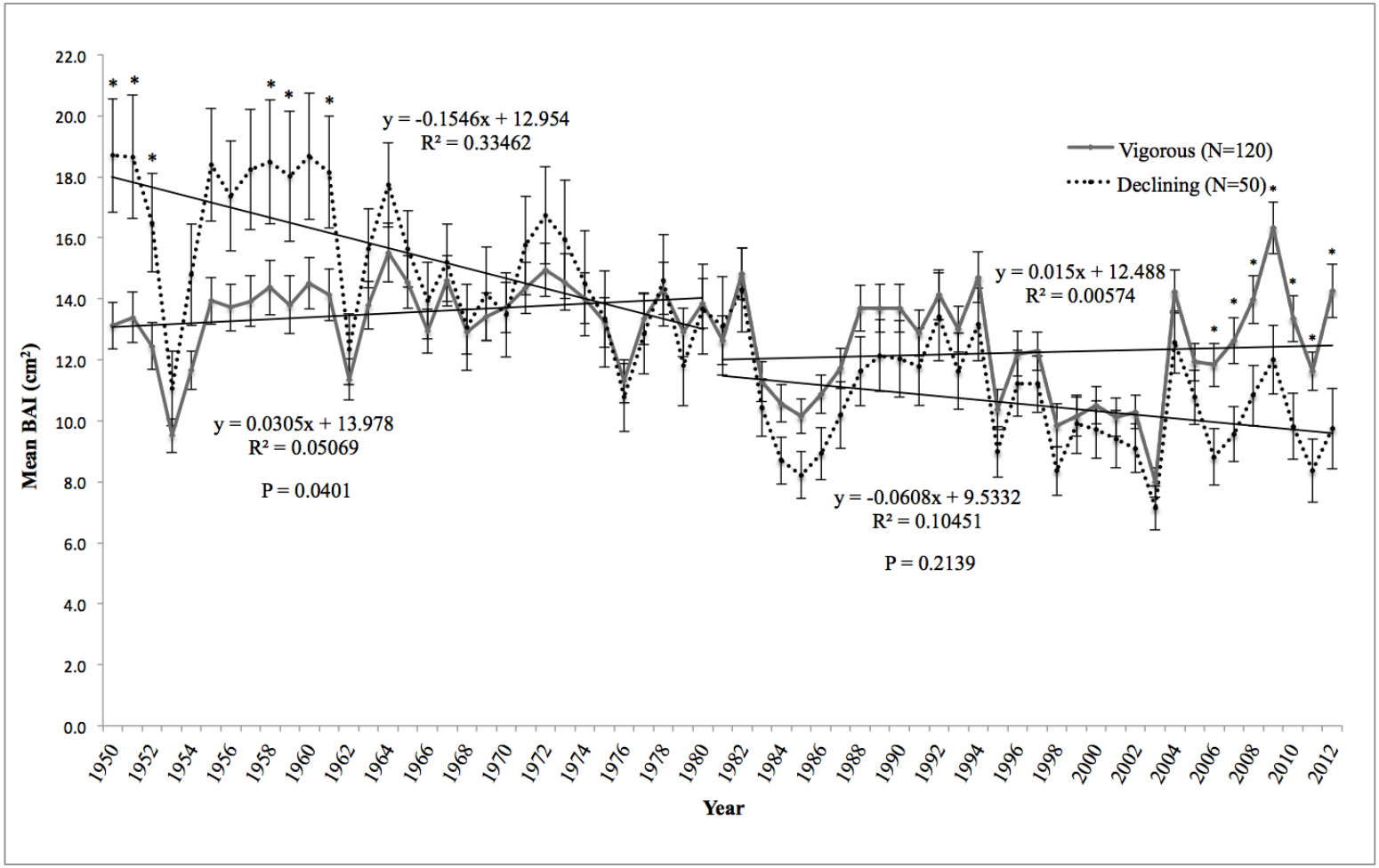

Figure 6. Mean basal area increment (BAI; ± SE) for yellow birch trees by crown vigor index at Hubbard Brook Experimental Forest, NH, USA. Individual years that are significantly different between vigor categories are indicated by an asterisk (based on an orthogonal contrast between categories with $P \leq 0.05$). Slope analyses indicate different growth trajectories for each vigor category and its significance between categories in the years 1950 – 1980 and 1981 – 2012.

Table 16. Dendrochronological statistics for sugar maple (*Acer saccharum*) and yellow birch (*Betula alleghaniensis*) radial xylem increment measurements from 36 plots at Hubbard Brook Experimental Forest, NH, USA. Years in parentheses indicate at which point EPS values were at or above 0.80; the threshold used in this study for our chronology to remain a reliable indicator of stand-level response (Speer 2010).

Sugar maple							
Plot	Length of Chronology	Series inter-correlation[a]	Avg. mean sensitivity[a]	Auto-correlation[a]	N trees	EPS[b] (2012)	EPS[b] (0.80)
96	1824-2012	0.478	0.221	0.698	10	0.9015	0.8207 (1923)
97	1920-2012	0.545	0.299	0.723	10	0.9229	0.8273 (1925)
110	1880-2012	0.546	0.257	0.801	9	0.9154	0.8279 (1922)
135	1844-2012	0.620	0.291	0.789	10	0.9422	0.8304 (1916)
143	1829-2012	0.510	0.228	0.770	9	0.9035	0.8063 (1923)
158	1921-2012	0.637	0.262	0.888	8	0.9335	0.8404 (1923)
169	1894-2012	0.461	0.277	0.786	8	0.8725	0.8105 (1925)
181	1917-2012	0.572	0.274	0.849	8	0.9145	0.8004 (1922)
202	1877-2012	0.607	0.292	0.832	8	0.9251	0.8225 (1888)
220	1912-2012	0.410	0.283	0.812	8	0.8475	0.8066 (1915)
221	1916-2012	0.425	0.254	0.871	7	0.8380	0.8160 (1950)
222	1913-2012	0.557	0.298	0.873	10	0.9263	0.8341 (1915)
223	1816-2012	0.455	0.292	0.837	9	0.8825	0.8067 (1900)
224	1793-2012	0.510	0.294	0.805	8	0.8928	0.8063 (1919)
241	1840-2012	0.523	0.337	0.838	10	0.9164	0.8143 (1913)
242	1866-2012	0.600	0.396	0.817	8	0.9231	0.8182 (1913)
258	1910-2012	0.497	0.239	0.701	10	0.9081	0.8317 (1913)
279	1834-2012	0.513	0.271	0.715	9	0.9046	0.8082 (1913)
281	1880-2012	0.496	0.261	0.808	8	0.8873	0.8311 (1913)
288	1940-2012	0.625	0.295	0.865	8	0.9302	0.8333 (1941)
292	1815-2012	0.443	0.268	0.836	10	0.8883	0.8267 (1941)
304	1916-2012	0.531	0.257	0.814	10	0.9188	0.8191 (1920)
310	1889-2012	0.558	0.343	0.760	9	0.9191	0.8347 (1918)
314	1915-2012	0.574	0.274	0.784	10	0.9309	0.8017 (1917)
316	1917-2012	0.629	0.270	0.844	8	0.9313	0.8357 (1920)
317	1892-2012	0.518	0.379	0.854	10	0.9149	0.8113 (1920)
318	1883-2012	0.543	0.314	0.786	10	0.9224	0.8262 (1911)
338	1897-2012	0.479	0.236	0.767	10	0.9019	0.8213 (1922)
343	1910-2012	0.601	0.282	0.770	8	0.9234	0.8188 (1917)
344	1903-2012	0.513	0.245	0.867	6	0.8634	0.8082 (1922)
365	1883-2012	0.522	0.280	0.790	8	0.8973	0.8137 (1913)
380	1914-2012	0.489	0.259	0.790	10	0.9054	0.8271 (1922)
381	1911-2012	0.617	0.263	0.809	8	0.9280	0.8286 (1914)
382	1915-2012	0.566	0.267	0.855	9	0.9215	0.8391 (1949)
391	1913-2012	0.565	0.233	0.813	8	0.9122	0.8386 (1920)
404	1910-2012	0.481	0.259	0.700	11	0.9107	0.8225 (1943)

Table 16. (Cont.)

Yellow Birch							
Plot	Length of Chronology	Series inter-correlation[a]	Avg. mean sensitivity[a]	Auto-correlation[a]	N trees	EPS[b] (2012)	EPS[b] (0.80)
96	1889-2012	0.403	0.269	0.806	10	0.8710	0.8020 (1900)
97	1915-2012	0.481	0.241	0.809	9	0.8929	0.8225 (1933)
110	1868-2012	0.584	0.310	0.778	10	0.9335	0.8081 (1893)
135	1916-2012	0.764	0.332	0.775	8	0.9628	0.8662 (1917)
143	1823-2012	0.459	0.305	0.717	10	0.8946	0.8092 (1897)
158	1870-2012	0.607	0.317	0.836	10	0.9392	0.8225 (1882)
169	1816-2012	0.522	0.272	0.815	10	0.9161	0.8137 (1890)
181	1919-2012	0.469	0.279	0.802	10	0.8983	0.8154 (1925)
202	1810-2012	0.478	0.314	0.865	8	0.8799	0.8207 (1918)
220	1902-2012	0.428	0.341	0.732	10	0.8821	0.8178 (1917)
221	1896-2012	0.491	0.292	0.835	9	0.8967	0.8283 (1913)
222	1890-2012	0.500	0.279	0.784	10	0.9091	0.8000 (1921)
223	1811-2012	0.532	0.372	0.769	10	0.9191	0.8197 (1914)
224	1915-2012	0.505	0.318	0.768	12	0.9245	0.8032 (1917)
241	1915-2012	0.374	0.313	0.810	8	0.8270	0.8070 (1936)
242	1912-2012	0.627	0.340	0.695	10	0.9439	0.8345 (1915)
258	1740-2012	0.499	0.295	0.769	9	0.8996	0.8328 (1919)
279	1767-2012	0.405	0.292	0.809	8	0.8449	0.8033 (1923)
281	1893-2012	0.661	0.356	0.737	8	0.9398	0.8540 (1908)
288	1866-2012	0.567	0.284	0.848	7	0.9016	0.8397 (1876)
292	1917-2012	0.480	0.304	0.754	10	0.9023	0.8219 (1942)
304	1887-2012	0.633	0.298	0.738	10	0.9452	0.8380 (1916)
310	1892-2012	0.484	0.318	0.708	10	0.9037	0.8243 (1915)
314	1918-2012	0.553	0.310	0.803	10	0.9252	0.8319 (1920)
316	1844-2012	0.596	0.365	0.798	10	0.9365	0.8157 (1916)
317	1851-2012	0.463	0.295	0.772	10	0.8961	0.8117 (1942)
318	1858-2012	0.384	0.331	0.725	8	0.8330	0.8136 (1918)
338	1889-2012	0.524	0.266	0.725	10	0.9167	0.8149 (1893)
343	1900-2012	0.394	0.312	0.789	10	0.8667	0.8199 (1927)
344	1918-2012	0.562	0.305	0.786	8	0.9112	0.8369 (1923)
365	1883-2012	0.505	0.281	0.775	10	0.9107	0.8032 (1913)
380	1911-2012	0.539	0.272	0.696	9	0.9132	0.8238 (1918)
381	1911-2012	0.479	0.277	0.789	9	0.8922	0.8213 (1919)
382	1826-2012	0.464	0.272	0.686	8	0.8738	0.8123 (1913)
391	1914-2012	0.460	0.291	0.777	6	0.8364	0.8099 (1941)
404	1913-2012	0.488	0.248	0.629	8	0.8841	0.8266 (1944)

[a] From COFECHA output (Holmes 1983)

[b] Expressed population signal (EPS) = $(t * r_{bt})/(t * r_{bt} + (1–r_{bt}))$

Where t is the number of trees in the series and r_{bt} is the mean series inter-correlation